**DYNAMIC MODELING OF THE HYDROLOGIC PROCESSES IN AREAS OF DISCONTINUOUS PERMAFROST**

By

William Robert Bolton

RECOMMENDED:

_____

_____

_____

_____

Advisory Committee Chair

_____

Chair, Department of Civil Engineering

APPROVED:

_____

Dean, College of Engineering and Mines

_____

Dean of the Graduate School

_____

Date

# DYNAMIC MODELING OF THE HYDROLOGIC PROCESSES IN AREAS OF DISCONTINUOUS PERMAFROST

A

DISSERTATION

Presented to the Faculty

of the University of Alaska Fairbanks

in Partial Fulfillment of the Requirements

for the Degree of

DOCTOR OF PHILOSOPHY

By

William Robert Bolton, B.A., M.S.

Fairbanks, Alaska

August 2006

**Abstract**

The presence or absence of permafrost is the defining hydrologic characteristic in the sub-arctic environment. Discontinuous permafrost introduces very distinct changes in soil hydraulic properties, which introduce sharp discontinuities in hydrologic processes and ecosystem characteristics. The variation in hydraulic properties vary over short and long time scales as the active layer thaws over the course of a summer or with changes in permafrost extent. The influence of permafrost distribution, active layer thaw depth, and wildfire on the soil moisture regime and stream flow were explored through a combination of field-based observations and computer simulation. Ice-rich conditions at the permafrost table do not allow significant percolation of surface waters, which result in near saturated soils and limited subsurface storage capacity, compared to well-drained non-permafrost sites. As the active layer thaws, the storage capacity of the soils is increased, influencing the hydrologic response to precipitation events. The removal of vegetation by wildfire result in short-term ($<$10 years) increases in moisture content through reduced evapotranspiration demand. Long-term ($>$10 years) drying of soils in moderate to severe wildfire sites is the result of an increased active layer depth and storage capacity. A spatially-distributed, process-based hydrologic model, TopoFlow, was modified to allow spatial and temporal variation in the hydraulic conductivity and porosity of soils. By continual variation of the hydraulic conductivity (proxy for permafrost distribution and active layer thaw depth) and porosity (proxy for storage capacity), the dynamic soil properties found in the sub-arctic environment are adequately represented. The hydrologic response to changes in permafrost condition, vegetation regime, and climate is analyzed. Results from this analysis suggest if the climate system continues to warm as expected, the total amount of summer runoff will be decreased as every scenario tested, with the very important exception of precipitation, resulted in a decreased runoff. The net result of the field observations and computer simulations conducted in this research suggest the presence or absence of permafrost is the dominant influence on soil moisture dynamics and has an important, but secondary role in the stream flow processes.

## Table of Contents

## List of Figures

## List of Tables

**Acknowledgements**

I'd like to thank my third grade teacher for making this all possible. Oh, and the person who told me that going to graduate school was a good idea. And lastly, I want to "thank" my committee, without whose ridiculous demands, I would have graduated so, so, very much faster.

*"If at first you do not succeed, quit."*

—Jo Momma

*"The goal of research is to be the first kid on your block to know something."*

—Joe Ford, Curmudgeon of Complexity

# Chapter 1
# Introduction: Soil moisture and climate change in the Alaskan boreal forest

## 1.1 Climate change in the high latitudes

The body of evidence is mounting that the arctic, including Alaska, is now experiencing an unprecedented degree of environmental change [*Chapman and Walsh*, 1993; *Serreze et al.*, 2000; *IPCC*, 2001; *ACIA*, 2005; *Hinzman et al.*, 2005]. The arctic has warmed $0.098^oC$ per decade from 1861-2000. More recently, the arctic has warmed $0.364^o$C per decade for the 1977-2001 time period [*Jones and Moberg*, 2003] (both rates are statistically significant at the 95% level). In Alaska, the mean annual surface air temperature (Figure 1.1) has increased $2-3^oC$ over the past half century, with greater warming ($3-5^oC$) occurring during the winter (December - February) months [*Chapman and Walsh*, 1993; *Serreze et al.*, 2000; *ACIA*, 2005]. Widespread changes in precipitation, particularly during the winter months, have also been documented [*Anisimov and Fitzharris*, 2001; *Kattsov and Walsh*, 2000]. In Alaska and Western Canada, the annual precipitation has generally increased over the past 50 years [*Hinzman et al.*, 2005].

The mean global air temperature for the 2005 calendar year is the warmest on record (using instrumented data) for the past century – largely attributed to the anomalous warm temperatures experienced throughout the Arctic [*Hanson et al.*, 2006]. With the six warmest years now occurring in the past eight years, coupled with a significant decrease in the Arctic Ocean ice cover [*Stroeve et al.*, 2005; *Overpeck et al.*, 2005], increases in the length of snow-free days [*Hinzman et al.*, 2005; *Chapin et al.*, 2005], and an expanding tree-line into the arctic [*Chapin et al.*, 2005], it appears more likely than not this warming trend will continue into the foreseeable future.

Associated with increases in surface temperature, the permafrost temperatures in boreal forest region of Alaska have also increased [*Osterkamp and Romanovsky*, 1999; *Osterkamp*, 2003]. The permafrost condition in this region is now unstable, as the permafrost temperature is very close to the melting point of ice, often $-1^oC$ or warmer [*Yoshikawa et al.*, 2002]. Increased surface temperatures in combination with an unstable thermal regime has resulted in a reduction in areal permafrost coverage and an increase in active layer depth (the layers of soil above the permafrost that freezes and thaws seasonally) [*Jorgenson et al.*,

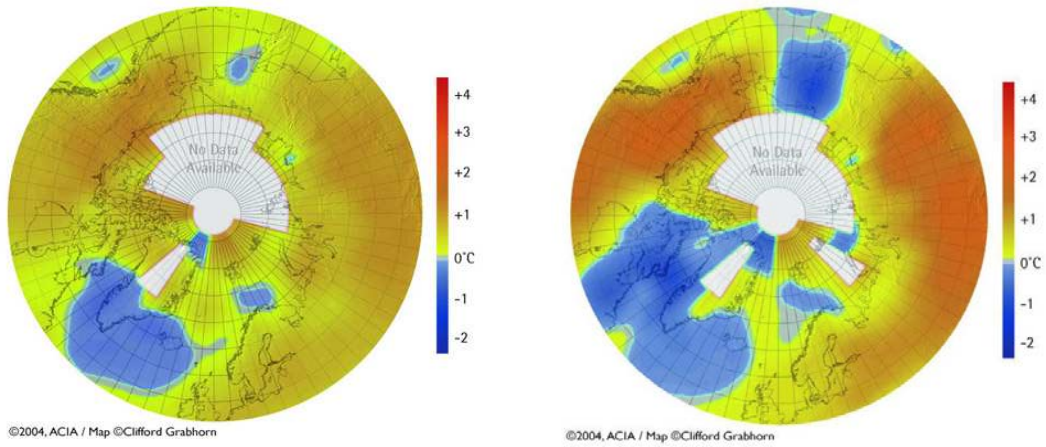


Figure 1.1. Observed air temperature change in the Arctic from 1954-2003. The left panel shows the annual change in air temperature. The right panel shows the winter (December - February) change in air temperature. Figures from *ACIA* [2005].

2001; *Serreze et al.*, 2002; *Yoshikawa et al.*, 2003; *Zhang*, 2005]. The observed change in the climate and thermal regimes have been reflected in the arctic hydrologic system, including later freeze-up and earlier break-up dates of rivers [*Magnuson et al.*, 2000], increased arctic river runoff [*Peterson et al.*, 2002], increased river baseflow in Russian rivers [*Peterson et al.*, 2002; *Yang et al.*, 2002], shrinking (or draining) of lakes [*Smith et al.*, 2005], and an increase in thermokarst development [*Osterkamp and Romanovsky*, 1999; *Osterkamp et al.*, 2000; *Jorgenson et al.*, 2001]. As the thermal and hydrologic systems are fully coupled systems, it is not surprising the hydrologic system has responded to the changes in thermal regime [*Hinzman et al.*, 1991, 2005; *Walsh et al.*, 2005].

Compared to more temperate regions, the northern latitudes are more sensitive to a changing climate. This is due to several factors, including the reduction of surface albedo. The surface albedo is expected to be reduced through a decrease in sea ice cover, temporal and spatial reductions in snow cover, and a northward expansion of the boreal forest [*ACIA*, 2005; *Chapin et al.*, 2005]. General circulation models (GCMs) predict increases in air temperature (particularly winter) and precipitation (both summer and winter) are expected to continue into the next century (Figure 1.2)[*IPCC*, 2001; *ACIA*, 2005].

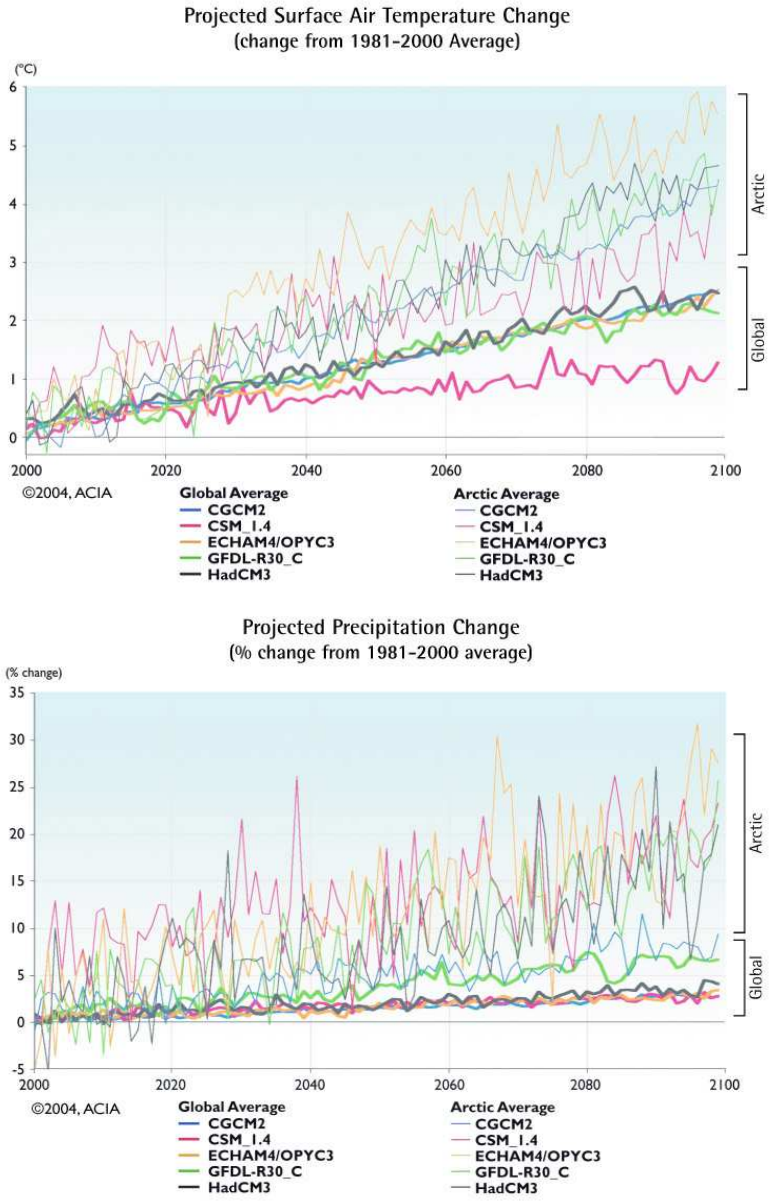


Figure 1.2. Average projected surface air temperature (upper panel) and precipitation (lower panel) from the five Arctic Climate Impact Assessment models. Heavy lines indicate global averages while light lines represent the projected change in the arctic region. Figures from *ACIA* [2005].

## 1.2 Importance of soil moisture and stream flow

The soil moisture regime plays an important role in a number of processes related to climate change including land-atmosphere interactions, soil respiration, permafrost distribution, and the frequency and severity of wildfires.

### 1.2.1 Land-atmosphere interaction

The energy exchange between the land, the sea ice, and atmosphere controls the Earth's climate system on local, regional, and global scales [*Eugster et al.*, 2000]. Soil moisture is the single most important terrestrial factor controlling the surface energy balance after the presence or absence of snow cover. The partitioning of available energy (net radiation minus the ground heat flux) into sensible and latent heat is largely controlled by the soil moisture content [*Betts et al.*, 1999]. Furthermore, soil moisture also has a control on the net solar (short wave) radiation as the albedo of bare soils, lichen, and *Sphagnum* increase with decreasing moisture content [*Eugster et al.*, 2000].

The role of soil moisture on the climate system has recently received increased attention. *Chapin et al.* [2000] recently suggested the relationship between the climate and soil moisture is a major knowledge gap in arctic and boreal forest research in North America. The global climate modeling community has also identified soil moisture as a significant factor in the land surface energy flux and these fluxes show steep gradients on both the regional and sub-grid scales in part due to the heterogeneous distribution of soil moisture *Douville* [2003].

### 1.2.2 Soil respiration

In the sub-arctic environment, soil respiration is typically slow due to low ground temperatures [*French et al.*, 1997]. As a result, the boreal forest is a net sink of carbon, sequestering more than 37% of the total terrestrial carbon [*Smith et al.*, 1993; *Kasischke et al.*, 1995]. If surface temperatures increase as expected, the rate of soil respiration will increase. Soil moisture is important to this process as either carbon dioxide ($CO_2$) or methane ($CH_4$) are produced as a by-product in the soil respiration process [*Moore*, 1983; *Callaghan and Jonasson*, 1996; *Friborg et al.*, 2003]. In soils that are well drained (low soil moisture), aerobic

decomposition of organic matter produces $CO_2$. In poorly-drained soils, anaerobic conditions prevail, which promotes the production of $CH_4$. Increasing the flux of either $CO_2$ or $CH_4$, both strong greenhouse gases, will result in a positive feedback, with increased emissions of either $CO_2$ or $CH_4$, resulting in increased surface temperatures. This will in turn further promote increases in the soil respiration process.

### 1.2.3 Permafrost distribution

Soil moisture is a major component in permafrost aggradation and degradation due to the thermal properties of water. Permafrost distribution is influenced by a number of factors such as landscape, soil types, and vegetation [*Haugen et al.*, 1982]. The presence and thickness of an organic layer overlying permafrost is one of the most important factors in the aggradation and degradation of permafrost [*Viereck*, 1982]. The thermal conductivity of soil is a function of moisture content, soil density, and temperature. Although an increase in soil moisture increases thermal conductivity of the soils (enhancing degradation of permafrost in a warming climate), an increase in soil moisture also results in increased evaporation from the soil surface. Increases in the latent heat flux (from increased evaporation) will result in a decreasing soil temperature and a condition of permafrost maintenance or possible aggradation.

### 1.2.4 Wildfire

The frequency and severity of wildfires primarily depend upon the moisture condition (in part, soil moisture) of the fire fuels [*Rowe and Scotter*, 1973]. Wildfires have been a natural part of the boreal forest ecosystem history [*Rowe and Scotter*, 1973]. Fires in the boreal forest have both immediate and long-term impacts on the ecosystem due to effects on the surface energy balance, the water balance, and underlying permafrost. The effect of wildfire on soil moisture is dependent upon the severity of fire, the soil types, and the presence of permafrost. Due to the fragile state of the permafrost regime, slight changes in either the energy or water balance may lead to threshold changes in the permafrost condition or ecosystem function (i.e. changing vegetation and soil moisture condition).

In the boreal forest, the fire return interval has been estimated to be between 50-500

years [*Yarie*, 1981; *Dyrness et al.*, 1986; *Kasischke et al.*, 1995]. Under a warming climate scenario, it has been hypothesized the frequency and severity of wildfires will increase due to warmer and drier conditions [*Van Wagner*, 1988; *Flannigan and Van Wagner*, 1991]. The total area burned in the North American boreal forest has more than doubled (10-year averages) from the 1960s through the 1990s, while the area burned in the continuous United States has remained at nearly the same level over the same time period [*Kasischke et al.*, 2006]. However, this trend is not evident in Alaska. This may be in part due to reporting methods or fire suppression policy and techniques.

### 1.2.5 Stream flow

The Arctic Ocean is the only ocean in the world in which its terrestrial contributing area is greater than the surface area of the ocean itself [*Vörösmarty et al.*, 2000]. Changes in the freshwater contribution (amount and timing) to the Arctic Ocean may affect the sea-ice formation process and alter the thermohaline circulation pattern [*Arnell*, 2005; *Walsh et al.*, 2005], potentially changing the climate system on local, regional, and global scales.

The boreal forest has an important role in the freshwater discharge to the Arctic Ocean, as the majority of the terrestrial contributing area originates within the boreal forest [*McGuire and Chapin*, 2006]. The timing and amount of precipitation, changes in permafrost dynamics, ecosystem changes (moving treeline, vegetation shifts), and disturbance (natural such as wildfire or man-made such as the building of dams) have all been identified as potential mechanisms leading to a shift in the freshwater budget of the Arctic Ocean [*McGuire and Chapin*, 2006]. *McGuire and Chapin* [2006] claim a major challenge to the research community is "to establish the link between permafrost changes of the boreal forest in response to a warming climate and changes in the discharge of freshwater into the Arctic Ocean." As mentioned earlier, increases in runoff and baseflow from the major Russian rivers to the Arctic Ocean have already been documented [*Peterson et al.*, 2002; *Yang et al.*, 2002].

## 1.3 Research hypothesis

The overarching hypothesis for this research is ***'in the sub-arctic environment, the presence or absence of permafrost is the dominant influence on watershed hydrological processes'***. The sub-arctic is located in the transition zone between the Arctic and more temperate

environments. As such, most of the current or expected changes to the hydrologic system, due to a changing climate, will be be experienced most dramatically and first in this region. For this reason, this study focuses on the hydrologic processes throughout the sub-arctic region.

The primary goal of this research is to develop a spatially-distributed, process-based numerical model, which is able to describe, simulate, and predict the hydrological processes everywhere throughout a sub-arctic watershed. To my knowledge, this has never been accomplished. The aim of this model is to explore the effects of vegetation and soil type, distribution of permafrost, and amount and timing of precipitation on the hydrologic processes in this region. More specifically, the following research objectives are explored in this research:

- To analyze field-based soil moisture patterns in areas underlain with permafrost and in permafrost free areas
- To analyze stream flow patterns in watersheds underlain with differing proportions of permafrost
- To analyze the water balance components in the sub-arctic region and identify the important hydrologic processes in watersheds with varying permafrost extent
- To analyze the short- and long-term impacts of wildfire on the soil moisture regime in Interior Alaska
- To describe and apply a spatially-distributed, process-based hydrologic model in order to simulate spatial and temporal water balance components in the (sub-)arctic environment, including stream flow, snowmelt, evapotranspiration, infiltration & percolation, and groundwater flow.

### 1.4 Research questions

Based upon the objectives of this research, a number of research questions were formulated with the purpose of identifying a number of important issues.

1. *What are the differences in the soil moisture regime in areas underlain with permafrost compared to areas free of permafrost?* In the sub-arctic environment, understanding and

being able to make accurate predictions of the soil moisture regime is essential to linking the terrestrial system to the local and regional climatic processes. The relationship between the climate system and the soil moisture distribution and active layer development has been identified by *Chapin et al.* [2000] as a major gap in boreal forest research.

2. *What are the important hydrologic processes in the sub-Arctic environment?* In light of the expected increases in both temperature and precipitation, it is important to understand and predict the feedback mechanisms of the water cycle [*Kane and Hinzman*, 2004]. In the sub-arctic, small changes in the natural system may lead to dramatic threshold changes to many of the hydrologic processes including stream flow and soil moisture dynamics.

3. *Does vegetation type influence the soil moisture regime and stream flow patterns?* In the boreal forest, deciduous vegetation show latent fluxes which correspond to the equilibrium evaporation rate, while the latent heat flux of coniferous vegetation only approaches 25-50% of the equilibrium evaporation rate [*Baldocchi et al.*, 2000; *Eugster et al.*, 2000]. Are the differences in vegetation types, through differences in evapotranspiration rates, translated to differences in the soil moisture and stream flow regimes?

4. *What are the short- and long-term impacts of wildfire on the soil moisture regime on in Interior Alaska?* In the North American boreal forest, the area burned has more than doubled in the last 40 years [*Kasischke et al.*, 2006]. It has been hypothesized that in a warmer climate in the boreal forest, the frequency and severity of wildfires will continue to increase [*Hinzman et al.*, 2003]. What is the effect of fire severity over time on the soil moisture regime, and by extension, what are (if any) the local and regional impacts to the climate?

5. *By spatially and temporally varying hydraulic conductivity and porosity of the soils, it is possible to simulate the hydrologic response in an area of discontinuous permafrost?* Simulation of the hydrologic processes is challenging due to rapidly changing thermal (permafrost versus non-permafrost, active layer development) and hydrologic (hy-

draulic conductivity and storage capacity) conditions in both time and space (x, y, and z-dimensions). Is it possible to accurately represent the permafrost regime, in hydrologic terms, by simply varying (both spatially and temporally) the hydraulic conductivity (proxy for permafrost distribution) and porosity (proxy for storage capacity) with active layer development?

6. *What are the consequences of climate change for both the hydrologic response in the sub-arctic environment?* Once a hydrologic model is able to adequately simulate the hydrologic processes, it can be used to explore the impacts of a changing climate through applying different climate scenarios (via permafrost distribution, active layer development, air temperature, and precipitation).

I address these questions in two parts: 1) an extensive field data collection program, and 2) adaptation and application of a process-based, spatially-distributed numerical model to the sub-arctic environment. Three sub-basins of the Caribou-Poker Creeks Research Watershed (CPCRW), located 48 km north of Fairbanks, Alaska, have been the primary focus of this research. These sub-basins vary in areal permafrost extent from approximately 3-53% [*Haugen et al.*, 1982; *Yoshikawa et al.*, 1998]. Formal descriptions (including site maps) of CPCRW are found in Sections 2.1, 3.2, and 5.2.

### 1.5 Outline of Chapters

The reoccurring theme throughout this thesis (Chapters 2 - 5, Appendix A) is: How does the distribution of permafrost influence the soil moisture regime and hydrologic processes in a sub-arctic environment? The core chapters of this thesis are organized as a series of publications designed to address this question as well as the research questions described above. Each of these publications represent a step toward the development and application of a numerical model capable of simulating the hydrologic processes in regions of discontinuous permafrost.

The sub-arctic environment can be characterized as being located in the zone of discontinuous permafrost. Although the distribution of permafrost in this region is site specific, it dominates the response of many of the hydrologic processes in this region, including stream flow, soil moisture dynamics, and water storage processes. In Chapter 2 of this the-

sis, I analyze the stream flow response to precipitation events over the course of a summer [*Bolton et al.*, 2000]. The objectives of this chapter were to 1) compare the stream flow response to precipitation events in watersheds of varying permafrost coverage, and 2) investigate changes in stream flow composition over the same period using hydrograph separation techniques. Additionally, comparisons of soil moisture dynamics in an area underlain with permafrost and an area free of permafrost are presented.

The permafrost condition in Interior Alaska is warm and unstable (commonly greater than -1$^o$C [*Yoshikawa et al.*, 2002]), as these soils are usually ice-rich. With the expected changes in air temperature and precipitation (Section 1.1), it is important to be able to understand and predict the feedback mechanisms of the water cycle [*Kane and Hinzman*, 2004], where small changes in the natural system may result in dramatic, threshold changes in the hydrology, ecology, and surface energy balance, with subsequent climatological impacts on local and regional (potentially global) scales. In 2004, a workshop was held to collect and synthesize the water balance components from 39 research watersheds located in or near the circumpolar north [*Kane and Yang*, 2004]. In Chapter 3, a long-term (1978-2003) water balance analysis of the three sub-watersheds of CPCRW is presented [*Bolton et al.*, 2004]. The focus of this study was to synthesize the water balance components from watersheds of varying permafrost with the intent of identifying key similarities and differences in these components with permafrost coverage.

In Chapter 4, I describe the structure and formulation of a process-based hydrologic model, TopoFlow [*Bolton et al.*, submitted-b]. TopoFlow is largely based upon the ARHYTHM model [*Hinzman et al.*, 1995; *Zhang et al.*, 2000], which was developed at the Water and Environmental Research Center, University of Alaska Fairbanks. The purpose of TopoFlow is to describe and predict all hydrologic processes everywhere throughout a watershed. In Chapter 5 the model is then applied in CPCRW [*Bolton et al.*, submitted-a]. In order to represent the discontinuous permafrost condition, I vary the soil properties (hydraulic conductivity and porosity) of each model layer as proxies for permafrost distribution and soil storage capacity of the active layer. Different climate scenarios are also tested (changes in air temperature, precipitation, permafrost distribution, active layer development, and vegetation types) to explore potential changes in the stream flow regime.

Wildfires in the boreal forest have been a natural part of ecosystem. Wildfire have

both immediate and long term effects on the ecosystem due to changes in the surface energy balance, water balance, and permafrost regime. The short-term effects of wildfire on soil moisture and thermal regimes, in both cold and temperate regions, have been well documented [*Tiedemann et al.*, 1979; *Klock and Helvey*, 1976; *Moore and Keeley*, 2000]. In Appendix A, the immediate through long-term effects of wildfire to the permafrost regime throughout Interior Alaska are explored [*Yoshikawa et al.*, 2002]. In this paper, soil moisture measurements are collected and analyzed at 11 different wildfires, with dates of ignition ranging from 1924 through 2000 (measurements collected during the active burn). This study was conducted as part of a larger interdisciplinary fire disturbance project called FROSTFIRE [*Hinzman et al.*, 2003].

Figure 2.6 has been modified from the original figure to include statistical information not previously published. Figures A.6 and A.7 were originally prepared for publication, but were not included in the final published manuscript. Other slight modifications have been made in Chapters 2 - A in order to fit the thesis format.

**Bibliography**

ACIA (2005), *Impacts of a warming Arctic: Arctic Climate Impact Assessment*, 1046 pp., Cambridge University Press.

Anisimov, O., and B. Fitzharris (2001), *Polar regions (Arctic and Antarctic)*, chap. *Climate Change 2001: Impacts, Adaptation, and Vulnerability*. Contribution of Working Group II to the Third Assessment report of the Intergovernmental Panel on Climate Change, pp. 801–841, Cambridge University Press.

Arnell, N. (2005), Implications of climate change for freshwater inflows to the Arctic Ocean, *Journal of Geophysical Research*, *110*.

Baldocchi, D., F. M. Kelliher, T. Black, and P. Jarvis (2000), Climate and vegetation controls on boreal zone energy exchange, *Global Change Biology*, *6*(Supplement 1), 69–83.

Betts, A. K., M. Goulden, and S. Wofsy (1999), Controls on evaporation in a boreal spruce forest, *Journal of Climate*, *12*, 1601–1618.

Bolton, W., L. Hinzman, and K. Yoshikawa (2000), Stream flow studies in a watershed underlain by discontinuous permafrost, in *Proceedings Water Resources in Extreme Environments*, edited by D. Kane, pp. 31–36.

Bolton, W., L. Hinzman, and K. Yoshikawa (2004), Water balance dynamics of three small catchments in a sub-arctic boreal forest, in *Northern Research Basins Water Balance (Proceedings of a workshop held at Victoria, Canada, March 2004)*, edited by D. L. Kane and D. Yang, IAHS Series of Proceedings and Reports Number 290, pp. 213 – 223.

Bolton, W. R., L. D. Hinzman, and D. L. Kane (submitted-a), Simulating the hydrologic processes in a watershed dominated by discontinuous permafrost, *Journal of Geophysical Research - Biogeosciences*.

Bolton, W. R., S. D. Peckham, and L. Hinzman (submitted-b), Toward understanding the hydrologic processes in a watershed dominated by discontinuous permafrost, *Journal of Geophysical Research - Biogeosciences*.

Callaghan, T., and S. Jonasson (1996), Arctic terrestrial ecosystems and environmental change, in *The Arctic and Environmental Change*, edited by P. Wadhams, J. Dowdeswell, and A. Schofield, pp. 59–76, Gordon and Breach.

Chapin, F., et al. (2000), Arctic and boreal ecosystems of western North America as components of the climate system, *Global Change Biology*, *6*(Supplement 1), 211–223.

Chapin, F., et al. (2005), Role of land-surface changes in the Arctic summer warming, *Science*, *310*, 657–660.

Chapman, W., and J. Walsh (1993), Recent variations in sea ice and air temperature in high latitudes, *Bulletin American Meteorology Society*, *74*, 33–47.

Douville, H. (2003), Assessing the influence of soil moisture on seasonal climate variability with agcms, *Journal of Hydrometeorology*, pp. 1044–1066.

Dyrness, C., L. Viereck, and K. Van Cleve (1986), *Forest Ecosystems in the Alaskan Taiga*, chap. Fire in taiga communities of interior Alaska, pp. 74–86, Springer-Verlag.

Eugster, W., et al. (2000), Land-atmosphere energy exchange in arctic tundra and boreal forest: available data and feedbacks to climate, *Global Change Biology*, *6*(Supplement 1), 84–115.

Flannigan, M., and C. Van Wagner (1991), Climate change and wildfire in Canada, *Canadian Journal of Forest Research*, *21*, 66–72.

French, N., E. Kasischke, J. Michalek, and L. Bourgeau-Chavez (1997), Monitoring the effects of fire on soil temperature and moisture in boreal forest ecosystems using satellite imagery, in *Proceedings of the International Symposium on Physics, Chemistry, and Ecology in Seasonally Frozen Soils*, edited by I. Iskandar, E. Wright, J. Radke, B. Sharratt, P. Groenevelt, and L. Hinzman, pp. 551–557, Fairbanks, Alaska.

Friborg, T., H. Soegaard, T. Christensen, C. Lloyd, and N. Panikov (2003), Siberian wetlands: Where a sink is a source, *Geophysical Research Letters*, *30*(21), 2129.

Hanson, J., R. Ruedy, M. Sato, and K. Lo (2006), Global temperature trends: 2005 summation, http://data.giss.nasa.gov/gistemp/2005/, Goddard Institute for Space Studies.

Haugen, R., C. Slaughter, K. Howe, and S. Dingman (1982), Hydrology and climatology of the Caribou-Poker Creeks Research Watershed, Alaska, *CRREL Report 82-26*, US Army Corps of Engineers Cold Regions Research and Engineering Laboratory.

Hinzman, L., D. Kane, R. Gieck, and K. Everett (1991), Hydrologic and thermal properties of the active layer in the Alaskan Arctic, *Cold Regions Science and Technology*, *19*, 95–110.

Hinzman, L., D. Kane, and Z. Zhang (1995), A spatially distributed hydrologic model for arctic regions, in *International GEWEX Workshop on Cold-Season/Region Hydrometeorology. Summary Report and Proceedings*, no. 15 in Int. GEWEX Project Office Publication, pp. 236–239.

Hinzman, L., N.D. Bettez, F.S. Chapin, M.B. Dyurgerov, C.L.Fastie, B. Griffith, R.D. Hollister, A. Hope, H.P. Huntington, A.M. Jensen, G.J. Jia, T. Jorgenson, D.L. Kane, D.R. Klein, G. Kofinas, A.H. Lynch, A.H. Lloyd, A.D. McGuire, F.E. Nelson, W.C. Oechel, T.E. Osterkamp, C.H. Racine, V.E. Romanovsky, R.S. Stone, D.A.Stow, M. Sturm, C.E. Tweedie, G.L. Vourlitis, M.D. Walker, D.A. Walker, P.J. Webber, J.M. Welker, K.S. Winker, and K. Yoshikawa (2005), Evidence and implications of recent climatic change in northern Alaska and other arctic regions, *Climatic Change*, *72*, 251–298.

Hinzman, L. D., M. Fukuda, D. V. Sandberg, F. S. Chapin III, and D. Dash (2003), FROST-FIRE: An experimental approach to predicting the climate feedbacks from the changing boreal forest regime, *Journal of Geophysical Research*, *108*(D1), 9–1 – 9–6.

IPCC (2001), Climate change 2001: Synthesis report. summary for policymakers., *Tech. rep.*, Intergovernmental Panel on Climate Change.

Jones, P., and A. Moberg (2003), Hemispheric and large-scale surface air temperature variations: An extensive revision and an update to 2001, *Journal of Climate*, *16*, 206–223.

Jorgenson, M., C. Racine, J. Walters, and T. Osterkamp (2001), Permafrost degradation and ecological changes associated with a warming climate in central Alaska, *Climate Change*, *48*, 551–571.

Kane, D., and L. Hinzman (2004), Monitoring extreme environments: Arctic hydrology in transition, *Water Resources Impact*, *6*(1), 24–27.

Kane, D. L., and D. Yang (Eds.) (2004), *Northern Research Basins Water Balance*, IAHS Publication 190, International Association of Hydrological Sciences.

Kasischke, E., N. Christensen, and B. Stocks (1995), Fire, global warming, and the carbon balance of boreal forests, *Ecological Applications*, *5*, 437–451.

Kasischke, E. S., T. S. Rupp, and D. L. Verbyla (2006), Fire trends in the alaskan boreal forest, in *Alaska's Changing Boreal Forest*, edited by F. S. Chapin, M. W. Oswood, K. Van Cleve, L. A. Viereck, and D. L. Verbyla, Long-Term Ecological Research Network Series, chap. 17, pp. 285–301, Oxford University Press.

Kattsov, V., and J. Walsh (2000), Twentieth-century trends of arctic precipitation from observational data and a climate model simulation, *Journal of Climate*, *13*, 1362–1370.

Klock, G., and J. Helvey (1976), Soil-water trends following wildfire on the Entiat Experimental Forest, in *Annual Proceedings Tall Timbers Fire Ecologic Conference*, 15, pp. 193–200.

Magnuson, J., D. Robertson, B. Benson, R. Wynne, D. Livingstone, T. Arai, R. Assel, R. Barry, V. Card, E. Kuusisto, N. Granin, T. Prowse, K. Steward, and V. Vuglinski (2000), Historical trends in lake and river ice cover in the northern hemisphere, *Science*, *289*, 1743–1746.

McGuire, A. D., and F. S. Chapin (2006), Climate feedbacks in the Alaskan boreal forest, in *Alaska's Changing Boreal Forest*, edited by F. S. Chapin, M. W. Oswood, K. Van Cleve, L. A. Viereck, and D. L. Verbyla, Long-Term Ecological Research Network Series, chap. 19, pp. 309–322, Oxford University Press.

Moore, C., and J. Keeley (2000), Long-term hydrologic response of a forested catchment to prescribed fire, in *Proceedings Water Resources in Extreme Environments*, edited by D. Kane, pp. 37–42, American Water Resources Association, Anchorage, Alaska.

Moore, R. D. (1983), On the use of bulk aerodynamic formulae over melting snow, *Nordic Hydrology*, *14*(4), 193–206.

Osterkamp, T. (2003), A thermal history of permafrost in alaska, in *Proceedings of the Eighth International Conference on Permafrost, 21-25 July 2003*, pp. 863–868, Balkema Publishers.

Osterkamp, T., and V. Romanovsky (1999), Evidence for warming and thawing of discontinuous permafrost in Alaska, *Permafrost and Periglacial Processes*, *10*, 17–37.

Osterkamp, T., L. Viereck, Y. Shur, M. Jorgenson, C. Racine, A. Doyle, and R. Boone (2000), Observations of thermokarst and its impact on boreal forests in Alaska, USA, *Arctic, Antarctic and Alpine Research*, *32*, 303 – 315.

Overpeck, J., et al. (2005), Arctic system on trajectory to new, seasonally ice-fre state, *EOS, Transactions American Geophysical Union*, *86*(34), 309,312–313.

Peterson, B., R. Holmes, J. McClelland, C. Vörösmarty, R. Lammers, A. Shiklomanov, I. Skiklomanov, and S. Rahmstort (2002), Increasing river discharge to the Arctic Ocean, *Science*, *298*, 2171–2173.

Rowe, J., and G. Scotter (1973), Fire in the boreal forest, *Quaternary Research*, *3*, 444–464.

Serreze, M., D. Bromwich, M. Clark, A. Etringer, T. Zhang, and R. Lammers (2002), Large-scale hydro-climatology of the terrestrial arctic drainage system, *Journal Geophysical Research*, *108*(D2), D01,108.

Serreze, M., et al. (2000), Observational evidence of recent change in the northern high latitude environment, *Climate Change*, *46*, 159–207.

Smith, L., Y. Sheng, G. MacDonald, and L. Hinzman (2005), Disappearing arctic lakes, *Science*, *308*, 1429.

Smith, T., W. Cramer, R. Dixon, R. Neilson, and A. Solomon (1993), The global terrestrial carbon cycle, *Water, Air and Soil Pollution*, *70*, 19–37.

Stroeve, J., M. Serreze, F. Fetterer, T. Arbetter, W. Meiser, J. Maslanik, and K. Knowles (2005), Tracking the Arctic's shrinking ice cover: another extreme September minimum in 2004, *Geophysical Research Letters*, *32*, L04,501, doi:10.1029/2004GL021810.

Tiedemann, A., C. Conrad, J. Dieterich, J. Hurnbeck, W. Megahan, L. Viereck, and D. Wade (1979), Effects of fire on water – a state-of-knowledge review, *General Technical Report WO-10*, U.S. Department of Agriculture Forest Service, 28 p.

Van Wagner, C. (1988), The historical pattern of annual burned area in Canada, *Forest Chronicle*, *64*, 182–185.

Viereck, L. (1982), Effects of fire and firelines on active layer thickness and soil temperatures in Interior Alaska, in *Proceedings of the 4th Canadian Permafrost Conference*, pp. 123–134, Ottawa.

Vörösmarty, C., B. Fekete, M. Meybeck, and R. Lammers (2000), A simulated topological network representing the global system of rivers at 30-minute spatial resolution (stn-30), *Global Biogeochemical Cycles*, *14*, 599–621.

Walsh, J. E., O. Anisimov, J.O.M. Hagen, T. Jakobsson, J. Oerlemans, T.D. Prowse, V. Romanovsky, N. Savelieva, M. Serreze, A. Shiklomanov, I. Shiklomanov, S. Solomon, A. Arendt, D. Atkinson, M.N. Demuth, J. Dowdeswell, M. Dyurgerov, A. Glazovsky, R.M. Koerner, M. Meier, N. Reeh, O. Sigurosson, K. Steffen, and M. Truffer (2005) Cryosphere and hydrology, in *Arctic Climate Impact Assessment*, edited by C. Symon, L. Arris, and B. Heal, Chap. 6, pp. 184–242, Cambridge University Press.

Yang, D., D. Kane, L. Hinzman, X. Zhang, T. Zhang, and H. Ye (2002), Siberian Lena River hydrologic regime and recent change, *Journal Geophysical Research*, *107*(D23), 4694, doi:10.1029/2002JD002,542.

Yarie, J. (1981), Forest fire cycles and life tables: A case study from Interior Alaska, *Canadian Journal of Forest Research*, *11*, 554–562.

Yoshikawa, K., L. Hinzman, N. Ishikawa, C. Collins, and V. Lunardini (1998), Air and ground temperature models at Caribou-Poker Creeks Research Watershed, in *Proceedings of the 49th AAAS Arctic Science Conference*, Fairbanks, Alaska.

Yoshikawa, K., W. Bolton, V. Romanovsky, M. Fukuda, and L. Hinzman (2002), Impacts of wildfire on the permafrost in the boreal forest of Interior Alaska, *Journal of Geophysical Research*, *107*(8148: doe:10.1029/2001JD000438), printed 108(D1), 2003.

Yoshikawa, K., D. White, L. Hinzman, D. Goering, K. Petrone, W. Bolton, and N. Ishikawa (2003), Water in permafrost: Case study of aufeis and pingo hydrology in discontinu-

ous permafrost, in *International Conference on Permafrost, Proceedings 8*, vol. 2, edited by M. Phillips, S. Springman, and L. Arenson, pp. 1259–1264.

Zhang, T. (2005), Spatial and temporal variability in active layer thickness over the Russian Arctic drainage basin, *Journal of Geophysical Research*, *110*, D16,101.

Zhang, Z., D. Kane, and L. Hinzman (2000), Development and application of a spatially-distributed Arctic hydrological and thermal process model (ARHYTHM), *Hydrological Processes*, *14*, 1017–1044.

# Chapter 2

## Stream Flow Studies in a Watershed Underlain by Discontinuous Permafrost*

**Abstract**

Permafrost plays an important role in the hydrology of sub-arctic watersheds. Ice-rich conditions at the permafrost table do not allow significant percolation, resulting in increased response time to precipitation events (including snowmelt), limited subsurface storage, and low base flows between precipitation events. The Caribou-Poker Creeks Research Watershed (CPCRW), located 48 km north of Fairbanks, Alaska, is underlain by discontinuous permafrost along north facing slopes and valley bottoms. Spring snowmelt is usually the major hydrologic event of the year but accurate discharge measurements have been difficult to obtain due to extensive aufeis formation at the stream gauging stations. Although spring snowmelt is usually the dominant hydrologic event of the year, maximum stream discharge was recorded during a major rainfall event in June. Comparison of the specific discharges from the C2, C3, and C4 sub-watersheds which are underlain, respectively, with 3.5, 53.2, and 18.8% permafrost show that the C3 sub-watershed had higher peak specific discharges and a lower specific base flow compared to the C2 and C4 sub-watersheds. However, as the active layer depth (the layer of soil above the permafrost the thaws and freezes seasonally) increased throughout the summer, the C3 sub-watershed displayed decreasing peak specific discharges, the result of increased subsurface storage, during precipitation events. Recession analysis show the contribution of subsurface water during precipitation events from the C3 and C4 sub-watersheds increased throughout the summer as the active layer increased in thickness while the contribution from the subsurface flow in the low permafrost basin remained nearly constant.

KEY TERMS: stream flow runoff, permafrost, active layer, research watershed.

### 2.1 Introduction

Permafrost plays an important role in the hydrology of sub-arctic watersheds. Ice-rich conditions at the permafrost table do not allow significant surface percolation, resulting in

*W.R. Bolton, L. Hinzman, and K. Yoshikawa. 2000. Stream flow studies in a watershed underlain by discontinuous permafrost. in D.L. Kane (ed.), Proc. Water Resources in Extreme Environments, American Water Resources Association. pp 31-36.

increased response time to precipitation events (including snowmelt), limited subsurface storage, and low base flows between precipitation events compared to permafrost free areas. Soil moisture content is also important to hydrologic processes. The soil moisture capacity determines the amount of infiltration that can occur during precipitation events. Once the soil is saturated, surface water will not be able to infiltrate into the subsurface, resulting in overland flow. The soil moisture content is affected by many factors including vegetation type, soil type, presence of permafrost, amount and timing of precipitation, and slope.

The Caribou-Poker Creeks Research Watershed is located 48 km north of Fairbanks ($65^o10'$N, $147^o30'$W) and encompasses an area of 101.5 km$^2$ (Figure 2.1). CPCRW was established in 1969 in response to the need for sub-arctic hydrologic information [*Slaughter*, 1971] following the Fairbanks flood in 1967. Permafrost in CPCRW is discontinuous, generally found along north facing slopes and valley bottoms [*Haugen et al.*, 1982; *Nelson*, 1978]. Thickness of organic soils overlying permafrost soils range between 20-50 cm [*Slaughter and Kane*, 1979]. Soils free of permafrost are generally found on south to southwest facing slopes. The organic soils in non-permafrost areas are less than 15 cm thick. The areas of C2 (5.2 km$^2$), C3 (5.7 km$^2$), and C4 (11.4 km$^2$) sub-watersheds of CPCRW are underlain, respectively, with 3.5, 53.2, and 18.8% permafrost [*Haugen et al.*, 1982].

The objectives of this paper are to (1) compare stream flow response to precipitation events in the C2 (LoP), C3 (HiP), and C4 (MedP) sub-watersheds, and (2) using hydrograph separation techniques, investigate the changes in stream flow composition in areas of discontinuous permafrost. Four summer storms in the 1999 field season were used for analysis.

### 2.1.1 Field Methods

Stream stage was recorded at the LoP, HiP, and MedP sub-watersheds using Campbell Scientific CR10X data loggers and a Microswitch 5-psi pressure transducer. Five consecutive measurements were averaged every hour and recorded. Stage measurements were taken at the MedP sub-watershed on a 30-minute interval after 7 July 1999. Parshall flumes were used at each sub-watershed to obtain continuous discharge data. Discharge measurements were made using USGS standard methods at different stage levels to confirm the discharge

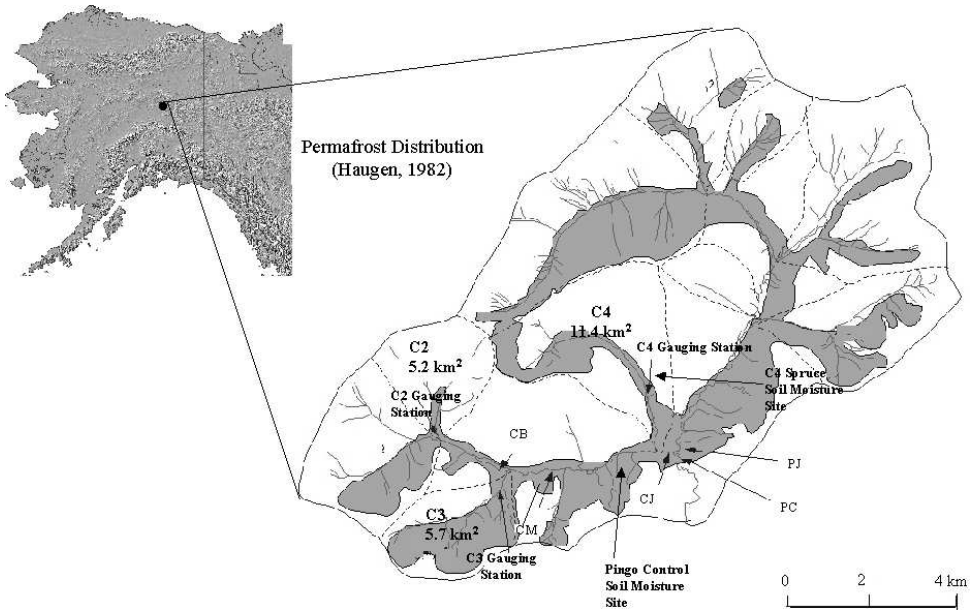


Figure 2.1. Caribou-Poker Creeks Research Watershed Location and Permafrost Distribution

data obtained from the data logger. Point stream flow measurements were conducted from the initiation of snowmelt until late September when freeze-up occurred. Pressure transducers and data loggers were installed immediately following melt from the flumes. Rainfall measurements were collected in the LoP and HiP sub-watersheds (through 24 August 1999) using tipping-bucket rain gauges. In the MedP sub-watershed, a weighing bucket rain gauge was used to record precipitation.

Snow measurements conducted include snow depth, snow water equivalent, and snow ablation. Snow water equivalent measurements were made using an Adirondack snow sampler. At each site, 10 snow water equivalent and 50 snow depth measurements were averaged following the combination technique of *Rovansek et al.* [1993]. Extensive snow surveys were conducted in mid-March, followed by periodic measurements through the completion of snowmelt.

Soil moisture content is measured at 5 locations in CPCRW. At each site, Campbell Scientific CS615 soil moisture probes were installed horizontally into small pits and connected to a Campbell Scientific CR10(X) data logger that recorded on hourly intervals. The data obtained from the CS615 probes were used to calculate the dielectric constant of the

soil. The *Topp et al.* [1980] equation for mineral soils and *Stein and Kane* [1983] equation for organic soils were then applied to obtain the soil moisture content. Four of the soil moisture stations are located within the MedP sub-watershed. These sites are located in a valley bottom, a spruce stand, a birch stand, and along a shrubby ridge. The fifth soil moisture site is located adjacent to Caribou Creek in a mixed birch/spruce stand, which is underlain by permafrost. Factors such as vegetation type, slope, presence of permafrost, and aspect were considered in site locations. The total depth of each soil moisture pit varied between 37 cm and 70 cm, with 4 to 6 soil moisture probes installed at each location. Soil moisture probes were installed in the surface duff layer, the organic soil, and at regular intervals through the mineral soil.

## 2.2 Results

### 2.2.1 Snowmelt

Spring snowmelt is the major hydrological event of the year, although accurate discharge measurements have been difficult to obtain due to extensive aufeis formation at the stream gauging stations and the flow becomes dispersed outside of the normal channels. Snow precipitation accounted for approximately 30-40% of the yearly total of incoming precipitation. Ablation of the snow pack occurred over a 2-3 week period. However, over the final 4-5 days, rapid ablation of the remaining snow pack (over 50% of the maximum snow water equivalent) occurred during a period of sustained temperatures above $0^{o}$C (Figure 2.2).

### 2.2.2 Summer Storms

Comparison of the specific discharge during precipitation events show the HiP sub-watershed consistently displays the highest peak specific discharges while the LoP sub-watershed sub-watershed consistently displays the lowest peak specific discharge (Figure 2.3). Although the spring snowmelt is the major hydrologic event of the year, the maximum stream specific discharge was recorded during a major precipitation event in June (Storm 1). Figure 2.4 indicates that this precipitation event occurred before any significant thawing of the mineral soils of the active layer, a period when the soil storage capacity is near

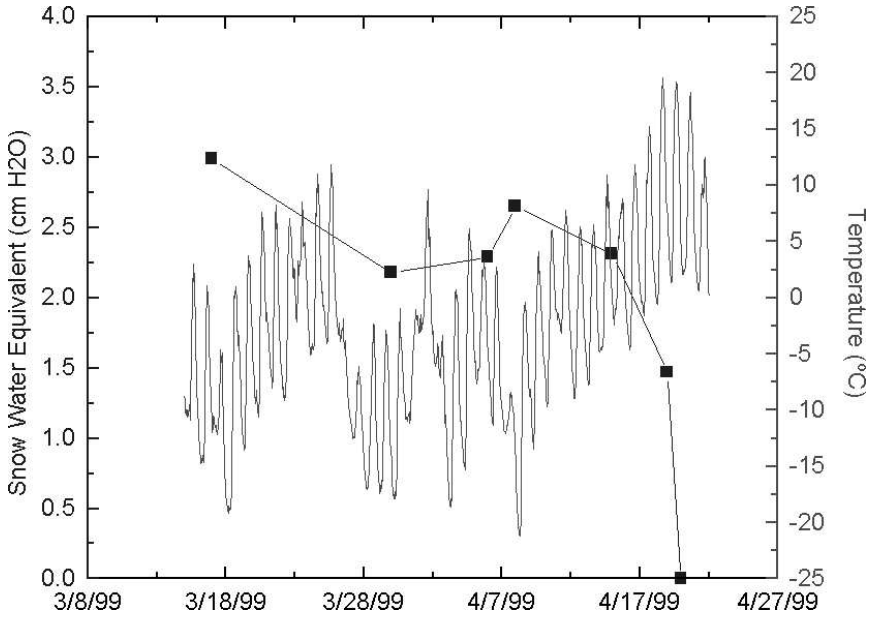


Figure 2.2. Snow Ablation Near the Stream Outlet of the C4 Sub-Watershed.

its minimum. In areas underlain by permafrost, thawing of the active layer throughout the summer potentially increases the soil water capacity (dependent upon whether these soils are saturated or not), resulting in decreasing surface water runoff and lower specific discharges during large precipitation events (Storms 1-4). Between precipitation events, the HiP sub-watershed displayed the lowest specific baseflow while the LoP sub-watershed consistently displayed the highest specific baseflow.

### 2.2.3 Hydrograph Separation

In areas underlain by permafrost, the depth of the active layer limits the amount of subsurface water that eventually contributes to stream flow. As the active layer thaws, the potential storage capacity of the soils increase, resulting in increased subsurface water contributing to stream flow. Using the graphical separation techniques, described by *McNamara et al.* [1997], the fraction of subsurface water contributing to storm events can be determined. This technique is difficult to use on overlapping storm events, which happened frequently during the 1999 field season. Discharge measurements were averaged over 6 hour periods to aid in this analysis. During the 1999 field season, the amount of

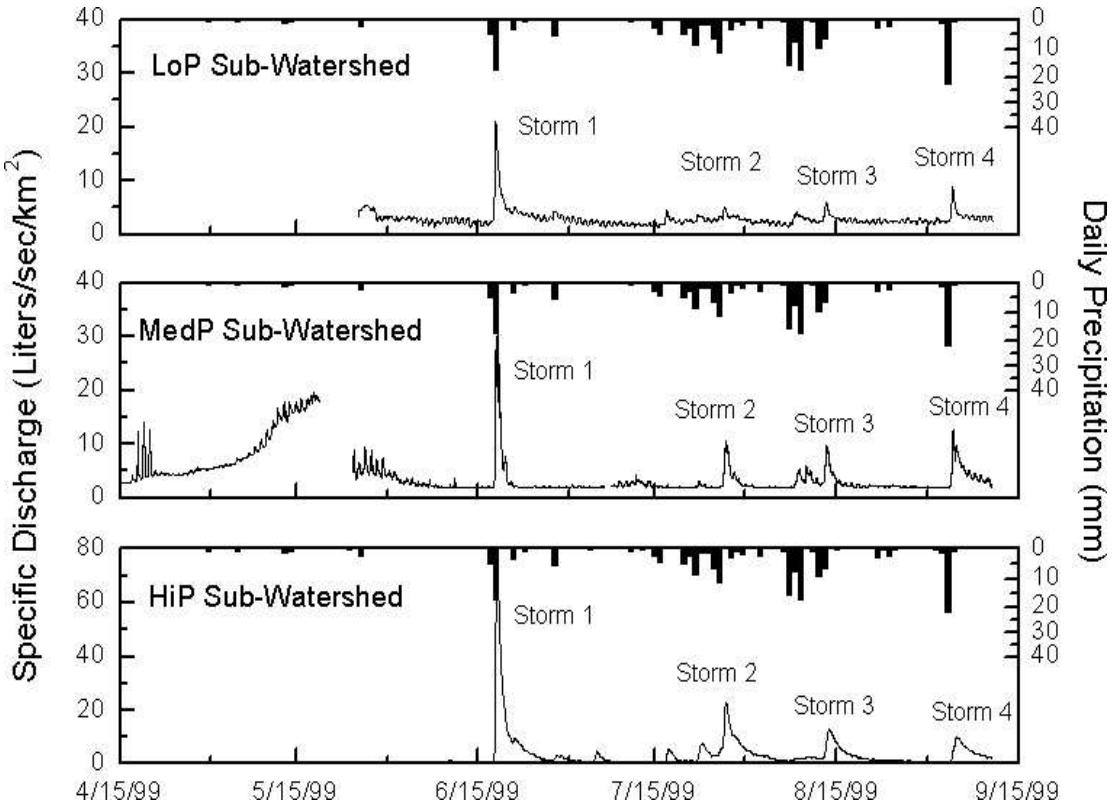


Figure 2.3. Specific Discharge Hydrograph and Precipitation for the LoP, MedP, and HiP Sub-Watersheds. Note the difference in scales.

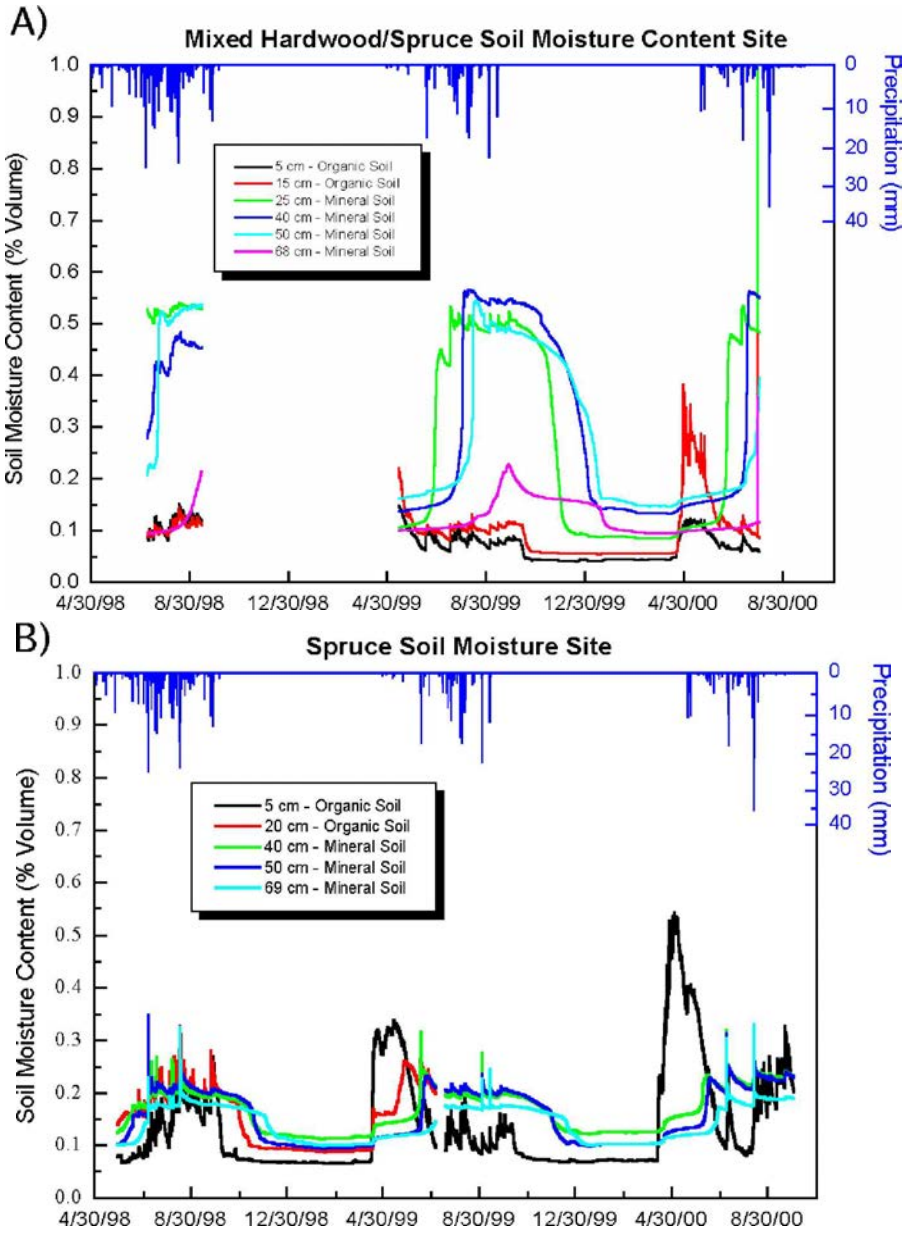


Figure 2.4. Soil Moisture Contents in (a) an Area Underlain by Permafrost and (b) an Area Free of Permafrost.

Table 2.1. Results of Hydrograph Separation.

| Sub-Watershed | Storm Event | Date | Total Discharge ($m^3$) | Subsurface Water |
|---|---|---|---|---|
| LoP | 1 | 6/6 | 15,965 | 68 |
| | 2 | ND | ND | ND |
| | 3 | 8/12 | 4,937 | 76 |
| | 4 | 9/2 | 5,315 | 74 |
| HiP | 1 | 6/6 | 56,555 | 17 |
| | 2 | 7/25 | 27,384 | 46 |
| | 3 | 8/12 | 18,893 | 51 |
| | 4 | 9/2 | 17,147 | 66 |
| MedP | 1 | 6/6 | 35,103 | 25 |
| | 2 | 7/25 | 16,854 | 57 |
| | 3 | 8/12 | 14,980 | 59 |
| | 4 | 9/3 | 35,644 | 88 |

ND, not determined due to complex hydrograph.

old water contributing to the LoP sub-watershed remained fairly consistent, while the amount of subsurface water contributing to both the HiP and MedP sub-watersheds increased throughout the summer (Table 2.1, Figures 2.5,2.6). These results are generally consistent with the results obtained by *McNamara et al.* [1997] in an area of continuous permafrost.

### 2.3 Conclusion

Spring snowmelt is usually the major hydrologic event of the year in these watersheds, although the peak discharges observed in this study were recorded during a major rainfall event in June, before the active layer had thawed substantially. Ice-rich conditions at the permafrost table inhibit significant percolation to the subsurface soils, resulting in a decreased infiltration rate and increased overland flow during rainfall events compared to areas free of permafrost. Soil moisture contents of mineral soils in areas underlain by permafrost remained near saturation throughout the summer, displaying little response to rainfall events, while the soil moisture contents in areas free of permafrost remained drier, displaying a greater response to rainfall events. The C3 sub-watershed [containing the highest amounts of permafrost] displayed higher peak specific discharges (watershed discharge divided by basin area), a lower specific baseflow, and a slower response time

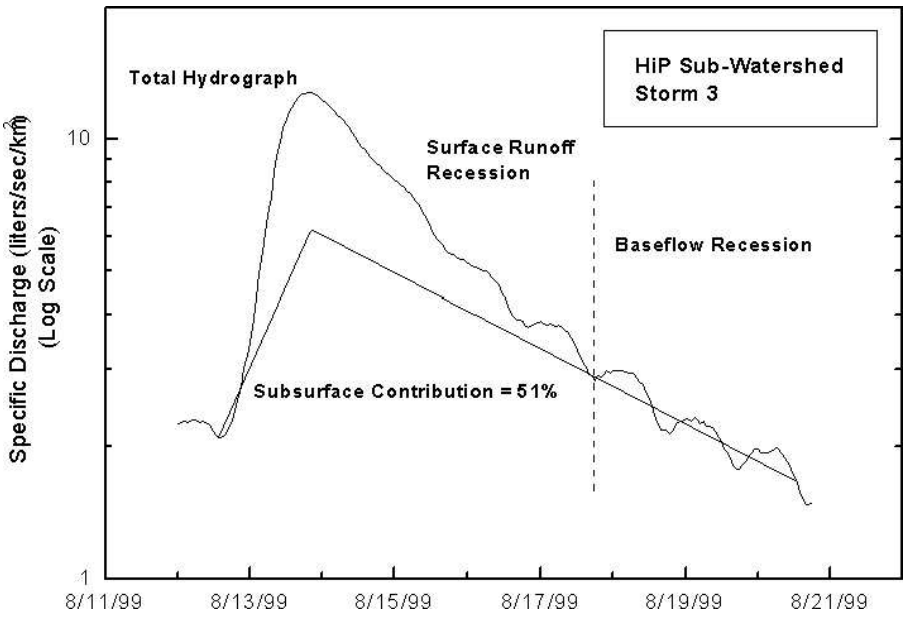


Figure 2.5. Storm 3, HiP Sub-Watershed Graphical Hydrograph Separation.

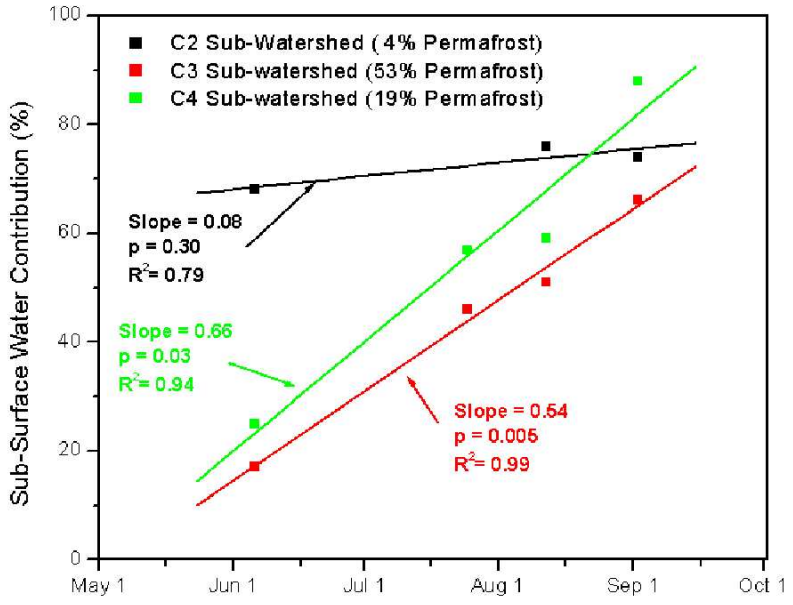


Figure 2.6. Subsurface Water Contribution from the LoP, MedP, and HiP Sub-Watersheds.

during rainfall events compared to the C2 and C4 sub-watersheds. As the active layer began to thaw, increasing the soil water storage capacity, the C3 sub-watershed displayed decreasing peak specific discharges during large rainfall events. Hydrograph separation analysis indicate the subsurface water contribution to the storm hydrographs from the C2 sub-watershed [containing the lowest amount of permafrost] during precipitation events was about 70% throughout the summer. The subsurface water contribution from the C3 and C4 sub-watersheds increased throughout the summer from amounts as low as 17% to those approaching 88%.

### 2.4 Acknowledgements

Support for this research was provided under grants from the National Science Foundation LTER Program (Grant No. DEB-9707461), the Japan Marine Science and Technology Center (JAMSTEC) under the YuWEx program, and the Alaska Section of the American Water Resources Association.

**Bibliography**

Haugen, R., C. Slaughter, K. Howe, and S. Dingman (1982), Hydrology and climatology of the Caribou-Poker Creeks Research Watershed, Alaska, *CRREL Report 82-26*, US Army Corps of Engineers Cold Regions Research and Engineering Laboratory.

McNamara, J., D. Kane, and L. Hinzman (1997), Hydrograph separations in an rctic watershed using mixing model and graphical techniques, *Water Resources Research*, *33*(7), 1707–1719.

Nelson, G. (1978), Hydrologic information for land-use planning, Fairbanks vicinity, Alaska, *Open-File Report 78-959*, U.S. Geological Society.

Rovansek, R., D. Kane, and L. Hinzman (1993), Improving estimates of snowpack water equivalent using double sampling, in *Proceedings of the 50th Eastern Western Snow Conference*, edited by M. Ferrick and T. Pangburn, pp. 157–163.

Slaughter, C. (1971), Caribou-Poker Creeks Research Watershed: Background and current status, *Special Report 157*, CRREL.

Slaughter, C., and D. Kane (1979), Hydrologic role of shallow organic soils in cold climates, in *Canadian Hydrology Symposium: Proceedings, 79-Cold Climate Hydrology*, pp. 380–389.

Stein, J., and D. Kane (1983), Monitoring the unfrozen water content of soil and snow using time domain reflectometry, *Water Resources Research*, *19*(6), 1537–1584.

Topp, G., J. Davis, and A. Annan (1980), Electromagnetic determination of soil water content: measurements in coaxial transmission lines, *Water Resources Research*, *16*(3), 574–582.

# Chapter 3

## Water balance dynamics of three small catchments in a sub-arctic boreal forest*

**Abstract**

Abstract This study examines the water balance components from three small sub-arctic watersheds near Fairbanks, Alaska, U.S.A., which vary in permafrost coverage from 3 to 53%. The results show that the presence or absence of permafrost affects many of the water balance components, particularly stream flow runoff and groundwater storage. The average annual precipitation is 410 mm, 2/3 of which is rain. Evapotranspiration, derived using the Priestley-Taylor method, averages between approximately 200-310 mm. During the snowmelt and summer runoff periods, the presence of poorly-drained permafrost limits infiltration of surface waters, generating higher runoff than in comparable well-drained non-permafrost soils. Lower storm flow, but higher baseflow is consistently observed in the C2 (3% permafrost coverage) and C4 (18% permafrost coverage) sub-basins when compared to the C3 (53% permafrost coverage) sub-basin. In the sub-arctic region, many of the storage processes (subsurface storage, interception, and stream icings) are critically important to the water balance, but are the least well quantified.

KEY TERMS: Alaska; boreal forest; Caribou-Poker Creeks Research Watershed; discontinuous permafrost; water balance

### 3.1 Introduction

The global climate has been warming [*Chapman and Walsh*, 1993] and the northern latitudes are particularly sensitive to climate change, with expected increases in both air temperature, particularly winter, and precipitation (both winter and summer)[*IPCC*, 2001]. Permafrost in Interior Alaska is relatively warm (usually above -3$^o$C) and unstable, as these soils are often ice-rich [*Yoshikawa et al.*, 2002]. In light of a changing climate, it is critically important to collect long-term hydrological data to better understand and predict the feedback mechanisms of the water cycle [*Kane and Hinzman*, 2004]. Hydrological responses in

*W.R. Bolton, L. Hinzman, and K. Yoshikawa, Water balance dynamics of three small catchments in a Sub-Arctic boreal forest, *Northern Research Basins Water Balance* (Proceedings of a workshop held at Victoria, Canada, March 2004), IAHS Publication 290, pp. 213-223, 2004.

Table 3.1. Physical hydrologic characteristics of selected sub-basins of study in the Caribou-Poker Creeks Research Watershed (modified from *Haugen et al.*, 1982).

| **Basin** | **C2** | **C3** | **C4** |
|---|---|---|---|
| Area ($km^2$) | 5.2 | 5.7 | 11.4 |
| Aspect | S | NE | SSE |
| Elevation (m) | 323–738 | 274–770 | 226–686 |
| Total stream length | 2.2 | 2.6 | 5.0 |
| Drainage Density (km $km^2$) | 0.70 | 0.73 | 0.70 |
| Area below 305 m (%) | 0.0 | 0.1 | 5.9 |
| Area between 305 and 488 m | 29.0 | 39.5 | 27.3 |
| Area between 488 and 640 m | 38.0 | 51.4 | 50.9 |
| Area above 640 m | 33.0 | 9.1 | 15.9 |
| Area underlain by permafrost (%) | 3.5 | 53.2 | 18.8 |

watersheds with discontinuous permafrost are particularly important as these regions will display dramatic, threshold changes in hydrology, ecology and surface energy balance as permafrost degrades. The presence or absence of permafrost is a dominant factor controlling surface and groundwater hydrology, with consequent impacts to local biological, ecological and climatological processes. Understanding the controls that permafrost exerts on hydrological processes may improve projections of watershed responses under a warmer climate. The focus of this study is to synthesize the water balance components from three small watersheds of varying permafrost coverage in Interior Alaska.

### 3.2 Watershed Description

The Caribou-Poker Creeks Research Watershed (CPCRW) (Figure 3.1), the site chosen for this study, is located 48 km north of Fairbanks, Alaska ($65^o10'$N, $147^o30'$W). Located in the boreal forest, CPCRW encompasses an area of 101.5 $km^2$ and is underlain with discontinuous permafrost. The three sub-watersheds of CPCRW selected for this study are C2 (5.2 $km^2$), C3 (5.7 $km^2$), and C4 (11.4 $km^2$). Each sub-watershed is underlain, respectively, with approximately 3, 53, and 19% permafrost (Table 3.1) [*Haugen et al.*, 1982; *Yoshikawa et al.*, 1998].

Permafrost in CPCRW is generally found along north facing slopes and valley bottoms [*Haugen et al.*, 1982]. Soils free of permafrost are generally found on south to southwest fac-

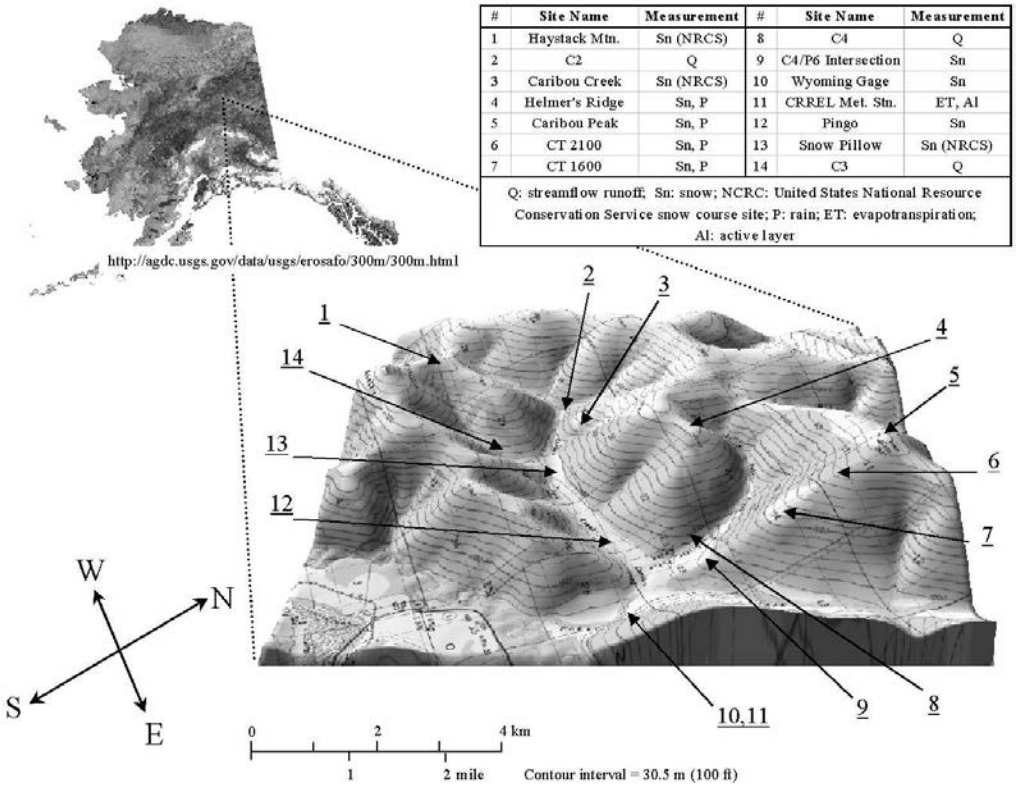


| # | Site Name | Measurement | # | Site Name | Measurement |
|---|---|---|---|---|---|
| 1 | Haystack Mtn. | Sn (NRCS) | 8 | C4 | Q |
| 2 | C2 | Q | 9 | C4/P6 Intersection | Sn |
| 3 | Caribou Creek | Sn (NRCS) | 10 | Wyoming Gage | Sn |
| 4 | Helmer's Ridge | Sn, P | 11 | CRREL Met. Stn. | ET, Al |
| 5 | Caribou Peak | Sn, P | 12 | Pingo | Sn |
| 6 | CT 2100 | Sn, P | 13 | Snow Pillow | Sn (NRCS) |
| 7 | CT 1600 | Sn, P | 14 | C3 | Q |

Q: streamflow runoff; Sn: snow; NCRC: United States National Resource Conservation Service snow course site; P: rain; ET: evapotranspiration; Al: active layer

Figure 3.1. Site location and measurement locations of the Caribou-Poker Creeks Research Watershed

ing slopes. Permafrost distribution is influenced by a number of factors such as landscape, soil type, and vegetation cover [*Haugen et al.*, 1982]. In CPCRW, the thermal condition of the permafrost is unstable, varying from -3 to $0^oC$, with thickness ranging from 0-120 m [*Yoshikawa et al.*, 2003]. The maximum active layer thickness averages 0.52 m (2000 - 2002) at a low elevation point in the center of the watershed (Figure 3.1, Site 11).

Vegetation in CPCRW consists of black spruce (*Picea mariana*), which is typically found along poorly-drained north-facing slopes and valley bottoms. Aspen (*Populus tremuloides*), birch (*Betula papyrifera*), alder (*Alnus crispa*), and sporadic white spruce (*Picea glauca*) are found on the well-drained, south-facing soils [*Haugen et al.*, 1982]. Tussock tundra (*Carex aquatilis*), feather moss (*Hylocomium spp.*), and sphagnum mosses (*Sphagnum sp.*) are also found along the valley bottoms.

### 3.3 Determination of Components

The generalized water balance equation used in this study is,

$$(P_{snow_max} + P_{rain}) - Q - ET + \Delta S = 0 \tag{3.1}$$

where $P_{snow_max}$ is the maximum snow water equivalent just prior to spring melt, $P_{rain}$ is the summer precipitation, $Q$ is stream flow runoff, $ET$ is evapotranspiration, and $\Delta S$ is the change in storage.

*Woo* [1990] notes in permafrost basins, year-to-year changes in storage may be significant. In the boreal forest, many of the storage processes, such as interception storage, stream icings (aufeis), and differences in subsurface storage (due to presence or absence of permafrost) are not well quantified. As we are unable to accurately measure these storage processes, the storage term is calculated as the residual in water balance equation. All water balance components are determined from the time of maximum snow water equivalent (late March to early April) through the fall freeze-up period (late September to early October).

### 3.3.1 Precipitation

**Snow**

Beginning in 1970, the United States National Resource Conservation Service (NRCS, formerly US Soil Conservation Service) has been compiling monthly snow water equivalent and snow depth measurements from three 'snow course' sites in the Caribou Creek basin: Haystack Mtn., Caribou Creek, and Snow Pillow (Figure 3.1, Sites 1, 3, and 13). Beginning in 1998, extensive snow surveys throughout CPCRW have been collected in mid-March (to determine the maximum cumulative snow water equivalent and snow depth), followed by periodic measurements through the ablation period. At each measurement site, a double sampling method [*Rovansek et al.*, 1993] is used to determine the snow water equivalent. The maximum snow water equivalents measured during the basin-wide snow surveys (1998-2003) display little orographic effect (Figure 3.2). Maximum snow pack is usually observed from mid-March to early April as snow typically accumulates all winter, and mid-winter thaw events are uncommon. Ablation measurements at the Wyoming gage (Figure 3.1, Site 10) indicate snowmelt usually occurs over a 2-3 week period, beginning in mid-April. Rapid ablation of the snow pack occurs over the final 4-7 days when the air temperature remains above $0^{o}$C throughout the day and night. No significant redistribution of the snow pack has been observed in CPCRW, except along exposed ridge tops, which occupy a small proportion of the watershed area. The maximum snow water equivalent was determined by averaging the maximum snow water equivalents measured at the three NRCS Snow Course sites (1978-1997) and the basin wide snow surveys, which include the NRCS sites (1998-2003). A high correlation ($r^2 = 0.99$, slope = 0.93, SD = 0.37) exists between snow surveys conducted at the NRCS sites and the basin wide snow surveys conducted during the 1998-2003 period, indicating that historic measurements conducted at these index sites do provide a valid proxy for the estimation of the total watershed snowpack.

**Rain**

Liquid precipitation has been monitored at Helmer's Ridge, Caribou Peak, CT 1600, and CT 2100 meteorological stations located in CPCRW (Figure 3.1, Sites 4, 5, 6, and 7) since

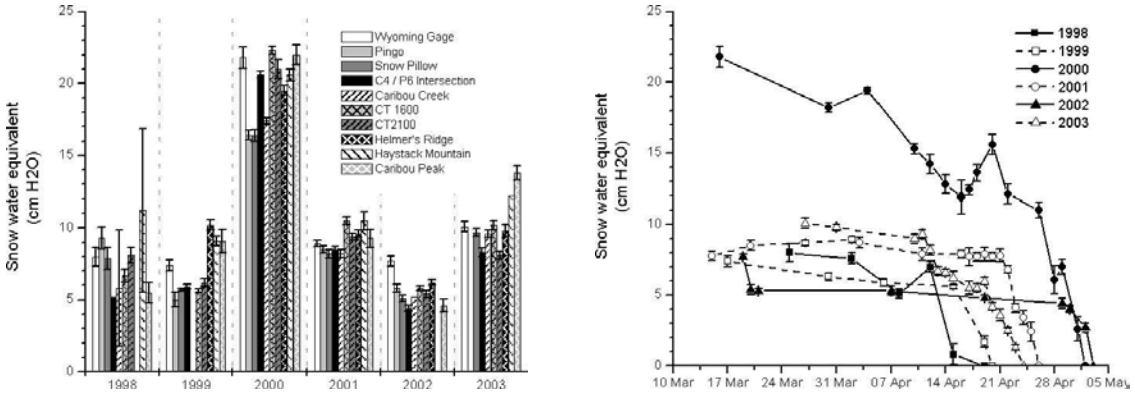


Figure 3.2. (a)Maximum snow water equivalent measured during the mid-March basin-wide sampling event. The sites in the legend are in ascending order of elevation. (b)Snow ablation (1998-2003) near the confluence of Caribou and Poker Creeks. Error bars represent one standard deviation.

1976, with continuous measurements beginning in 1988. Prior to 1988, monthly precipitation data are estimated based upon comparisons with Fairbanks records. As with the maximum snow water equivalent, comparisons of the seasonal cumulative precipitation display little, albeit inconsistent, orographic effects. The rainfall total for each month is determined by averaging the monthly total precipitation for each site in which continuous data are available. The total yearly rainfall is the summation of the monthly averages.

### 3.3.2 Evapotranspiration

For years 2000-03, calculation of the evapotranspiration (ET) is based upon the Priestley-Taylor equation [*Priestley and Taylor*, 1972]. For each sub-basin, the Priestley-Taylor coefficient ($\alpha$), the ratio of actual evapotranspiration to equilibrium evapotranspiration, is determined by multiplying the percentage of each vegetation type (estimated from *Haugen et al.* [1982]) with the appropriate $\alpha$-value for that vegetation (estimated from *Baldocchi et al.* [2000]). The ratios of black spruce ($\alpha = 0.4$) to deciduous vegetation (predominately birch/aspen, $\alpha = 0.9$) are estimated to be 1:3, 4:1, and 1:2 in the C2, C3, and C4 sub-basins. For the C2, C3, and C4 sub-basins, $\alpha$ is assumed to be 0.775, 0.5, and 0.735, respectively. Meteorological data from the CRREL Met. Stn. (Figure 3.1, Site 11) are used in calculating ET. Energy conducted into the ground was calculated using soil temperatures at 2 and

11.5 cm, with a thermal conductivity of 0.3 W $m^{-1}$ $^{o}C^{-1}$ [*Yoshikawa et al.*, 2003]. Although thermal conductivity of the organic soils change with moisture content (0.1 to 0.7 W $m^{-1}$ $^{o}C^{-1}$ for 5-90% soil moisture (by volume), [*Yoshikawa et al.*, 2002]), it should be noted that this thermal conductivity value is probably typical for most periods of the thawed season.

For years prior to 2000, ET is estimated by relating the total daily ET calculated by the Priestley-Taylor Method from 2000-02 to the daily maximum ($T_{max}$), daily minimum ($T_{min}$), daily average air temperature ($T_{ave}$), and Julian day ($JD$) using linear regression. The equations used to estimate ET for the C2, C3, and C4 sub-basins are:

$$\begin{aligned} DailyET(mm)C2 = {} & 1.506 + 0.09878(T_{max}) - 0.00991(JD) \\ & - 0.07632(T_{min}) + 0.0686(T_{ave}) \end{aligned} \tag{3.2}$$

$$\begin{aligned} DailyET(mm)C3 = {} & 0.971 + 0.06373(T_{max}) - 0.00639(JD) \\ & - 0.04924(T_{min}) + 0.04426(T_{ave}) \end{aligned} \tag{3.3}$$

$$\begin{aligned} DailyET(mm)C4 = {} & 1.428 + 0.09369(T_{max}) - 0.00940(JD) \\ & - 0.07230(T_{min}) + 0.06506(T_{ave}) \end{aligned} \tag{3.4}$$

Figure 3.3 shows daily ET for 2003 as calculated by the Priestley-Taylor method and estimated by equations 3.2, 3.3, and 3.4. Temperature data from CPCRW were used when possible. Missing temperature data were estimated using the Fairbanks temperature records by the function (based upon 2000-03 field data)

$$T_{max}[CPCRW] = -0.60736 + 1.08345 * T_{max}[Fairbanks], r^2 = 0.937 \tag{3.5}$$

$$T_{min}[CPCRW] = -5.12049 + 0.89691 * T_{min}[Fairbanks], r^2 = 0.694 \tag{3.6}$$

$$T_{ave}[CPCRW] = -1.82356 + 0.96183 * T_{ave}[Fairbanks], r^2 = 0.925 \tag{3.7}$$

In 1983, evapotranspiration at Ester Creek, located approximately 50 km southwest of

CPCRW, was reported to 229 mm [*Gieck*, 1986], which compares well to the 192-299 mm range estimated for CPCRW.

### 3.3.3 Runoff

Calibrated Parshall flumes were installed in the C2, C3, and C4 sub-basins in 1977, 1978, and 1979, respectively [*Slaughter*, 1981]. Stage measurements were recorded at regular intervals, which in turn were used to generate a continuous discharge record. Periodic manual discharge measurements have been made at various stage levels to verify the calculated discharge data. Stream flow measurements were conducted from the initiation of spring snowmelt until late fall when freeze-up occurs.

Spring snowmelt is usually the major hydrologic event of the year. However, discharge measurements during this period have been difficult to obtain to due to extensive aufeis (icing) formations at the gauging stations, which often disperse the flow outside the main stream channel. As a result, continuous discharge measurements usually begin after the main snowmelt pulse. Although the snowmelt period is the major hydrologic event of the year, the record peak stream flow usually occurs during summer rainstorm events. This is due to the fact that the highest rainfall intensities are greater than the maximum snowmelt rate on a daily time scale [*Kane and Hinzman*, 2004].

Differences in stream flow among watersheds are dramatic and are dependent upon the amount of permafrost underlying each sub-basin. Comparison of the basins show that as the areal extent of permafrost increases, peak specific discharge increases, specific baseflow decreases, and response times to precipitation events increase (Figure 3.4)[*Haugen et al.*, 1982; *Bolton et al.*, 2000]. Comparison of total summer runoff ratios (Q/P) displays little difference between the sub-basins (Table 3.2). In years in which daily streamflow is available before 15 May, the Q/P ratios average 0.24, 0.27, and 0.27 for the C2, C3, and C4 sub-basins, respectively. Although higher permafrost basins have a greater runoff ratios during precipitation events, the lower permafrost basins make up the difference through a higher baseflow between precipitation events. Large amounts of aufeis have been observed in these sub-basins (such as 1992 and 2000). Surface water, generated by melting aufeis increases the Q/P ratio by increasing the runoff with no corresponding increase in the precipitation. This demonstrates the importance of aufeis in northern watersheds and

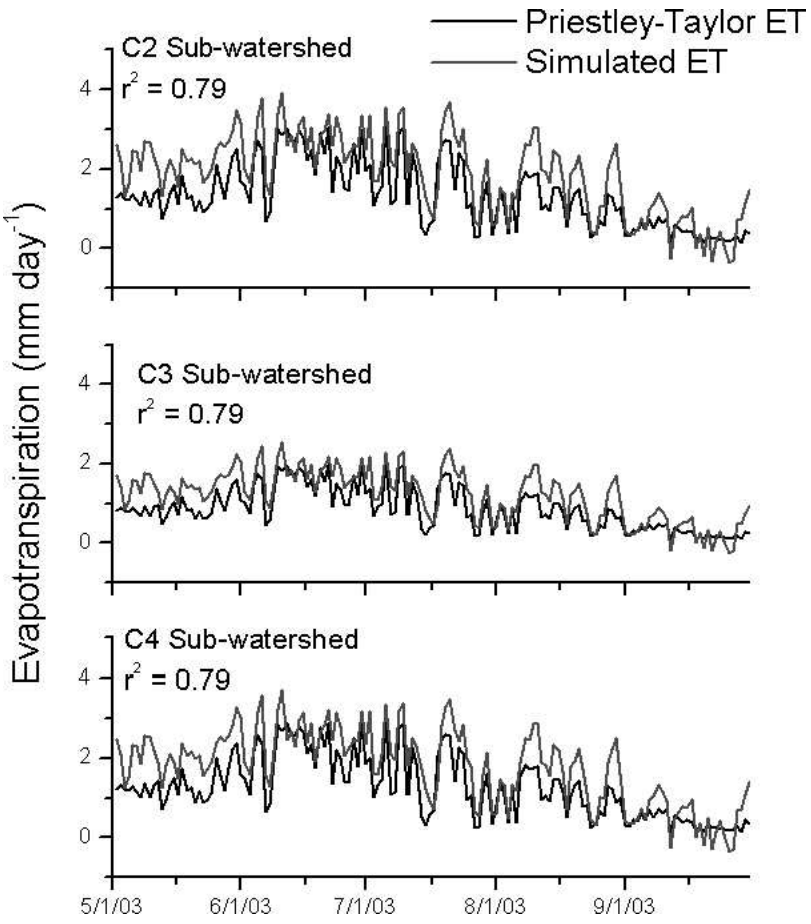


Figure 3.3. Evapotranspiration in the C2, C3, and C4 sub-basins for the 2003 summer. ET calculations were made using the Priestley-Taylor method from 2000-03. Prior to 2000, ET was simulated using min/max/average air temperature and Julian day. Differences in ET reflect varying proportions of vegetation type in each sub-basin.

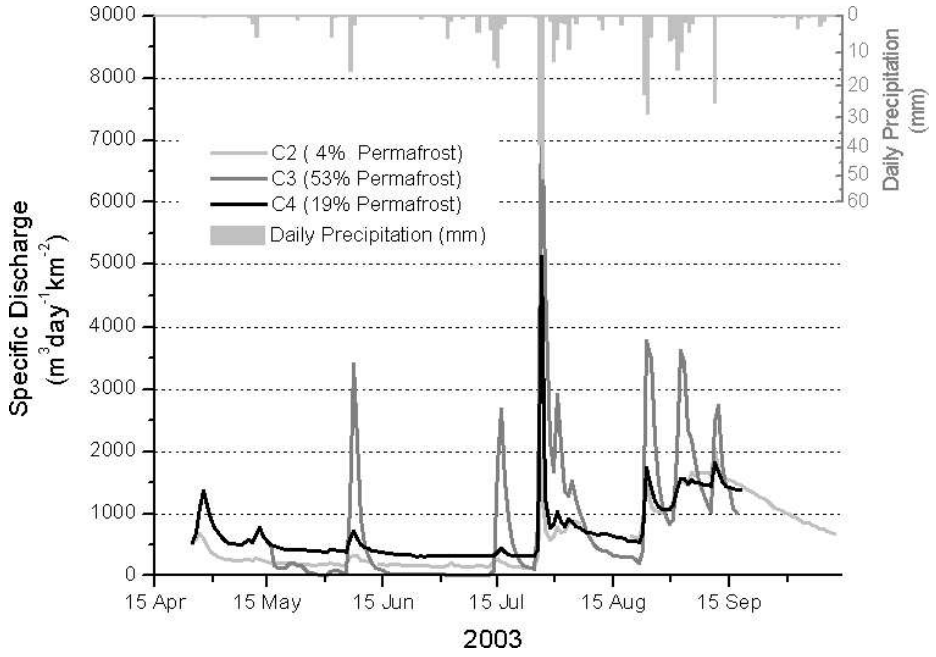


Figure 3.4. Specific discharge of the C2, C3, and C4 sub-watersheds of CPCRW.

in some cases may explain the some of the observed year-to-year variability in the runoff ratio.

### 3.4 Results and Discussion

The Sub-arctic represents an important transitional region from temperate to arctic environments. Spring and summer runoff appears to be increasing in many Siberian rivers [*Yang et al.*, 2002; *Peterson et al.*, 2002]. It has been suggested the increased discharge may be due to a reduction in permafrost or, more likely, to an increase in precipitation [*Berezovskaya et al.*, In Press]. The presence or absence of permafrost significantly impacts many of the hydrologic processes in the Sub-arctic. Ice-rich conditions at the permafrost table inhibit percolation of surfaces waters to subsurface soils, resulting in a decreased groundwater recharge and an increased runoff generation compared to permafrost free areas. During precipitation events, the ice-rich conditions at the permafrost table restricts drainage to the subsurface, allowing surface waters to move relatively quickly downslope through the organic mat and active layer to the stream. In contrast, areas free of permafrost are relatively well drained, allowing infiltration to a deeper subsurface system. In these areas,

Table 3.2. Summer (1 May – 1 October) evapotranspiration and runoff ratios for the C2, C3, and C4 sub-basins, Caribou-Poker Creeks Research Watershed, Interior Alaska, 1978-2003.

| | **C2 Sub-basin** | | **C3 Sub-basin** | | **C4 Sub-basin** | |
|---|---|---|---|---|---|---|
| Year | $ET/P$ | $Q/P$ | $ET/P$ | $Q/P$ | $ET/P$ | $Q/P$ |
| 1978 | 1.36 | – | 0.88 | – | 1.29 | – |
| 1979 | 1.31 | – | 0.84 | – | 1.24 | – |
| 1980 | 1.31 | – | 0.85 | – | 1.24 | – |
| 1981 | 1.07 | – | 0.69 | – | 1.01 | – |
| 1982 | 1.09 | – | 0.70 | – | 1.03 | – |
| 1983 | 1.15 | – | 0.74 | – | 1.09 | – |
| 1984 | 1.26 | – | 0.81 | – | 1.20 | – |
| 1985 | 0.99 | – | 0.64 | – | 0.94 | – |
| 1986 | 1.23 | – | 0.79 | – | 1.16 | – |
| 1987 | 1.43 | – | 0.92 | – | 1.36 | – |
| 1988 | 1.09 | – | 0.70 | – | 1.03 | – |
| 1989 | 1.37 | – | 0.89 | – | 1.30 | – |
| 1990 | 1.01 | – | 0.65 | – | 0.96 | – |
| 1991 | 2.24 | – | 1.44 | – | 2.12 | – |
| 1992 | 0.85 | – | 0.55 | – | 0.80 | – |
| 1993 | 1.09 | – | 0.70 | – | 1.03 | – |
| 1994 | 1.04 | 0.30 | 0.67 | 0.27 | 0.99 | 0.31 |
| 1995 | 1.10 | 0.24 | 0.71 | – | 1.05 | 0.21 |
| 1996 | 1.01 | – | 0.65 | – | 0.95 | – |
| 1997 | 1.65 | – | 1.07 | – | 1.57 | – |
| 1998 | 0.85 | – | 0.55 | – | 0.81 | – |
| 1999 | 1.29 | – | 0.83 | – | 1.22 | 0.29 |
| 2000 | 0.87 | – | 0.56 | – | 0.82 | 0.29 |
| 2001 | 1.11 | 0.24 | 0.72 | 0.26 | 1.05 | – |
| 2002 | 0.96 | – | 0.62 | – | 0.91 | – |
| 2003 | 0.54 | 0.21 | 0.35 | 0.28 | 0.51 | 0.25 |
| Mean | 1.16 | 0.25 | 0.75 | 0.27 | 1.10 | 0.27 |
| Max | 2.24 | 0.30 | 1.44 | 0.28 | 2.12 | 0.31 |
| Min | 0.54 | 0.21 | 0.35 | 0.26 | 0.51 | 0.21 |
| SD | 0.31 | 0.04 | 0.20 | 0.01 | 0.30 | 0.04 |

P: Rain preciptiation; Q C2, C3, C4: Summer streamflow runoff for the C2, C3, and C4 sub-basins; –:< 85% Continuous data. Note: $Q/P$ ratios are only presented for years in which daily meteorological and streamflow data area available before 15 May. $ET/P$ ratios greater than 1.0 are possible as soil moisture derived from snowmelt is not included in these calculations.

the infiltration capacity of these non-permafrost soils must be exceeded before runoff generation can take place. Comparison of the C2 and C3 sub-basins (3 and 53% permafrost extent, respectively), in the years of similar discharge record (1978, 1983, 1987, 1994, 2000, and 2001), show that stream flow in C2 is consistently lower than C3 (Table 3.3), with the exception of 1994 - which is the only year measurements include snowmelt. In general, the ratio of summer runoff to summer precipitation varies little between the sub-basins (Table 3.2). In the C2 and C4 sub-basins, evapotranspiration accounts for a least one-half to nearly all summer precipitation. In the C3 sub-basin, evapotranspiration only accounts for one-third to three-quarters summer precipitation. Differences between the C2 and C3 sub-basin summer runoff are offset by a higher winter discharge (greater depletion rate in groundwater storage) in C2 sub-basin.

In the sub-arctic environment, the storage processes are critically important in calculation of the water balance, but are the least well quantified. If the northern climate continues to warm as expected, we should expect a gradual shift in the water balance. In basins with substantial permafrost now, one should expect a decrease in summer runoff and an increase in winter baseflow as permafrost extent decreases. These results may be unique to watersheds with discontinuous permafrost, perhaps representing an interim between watersheds with no permafrost and those with continuous permafrost. The degree of similarity to basins in more arctic or more temperate regions is dictated by the percentage of permafrost. As the percentage of frozen ground decreases, base flow increases and the specific peak flow decreases. As the summer proceeds and the active layer increases in thickness, the available storage increases, the rates of recession or recession constants decrease (longer recession periods) as water moves more slowly through deeper soil layers toward the stream. Similarly, as the active layer increases in thickness, streams become somewhat less flashy as the peak flows decrease due to greater attenuation of surface runoff in the deeper soil layers.

### 3.5 Acknowledgements

Support for this research was provided by the U.S. National Science Foundation Division of Environmental Biology under the Long Term Ecological Research Program (Grant Number DEB-9211769), NSF Arctic System Science Program (OPP-0229705), a grant from

Table 3.3. Water balance data for the C2, C3, and C4 sub-basins, Caribou-Poker Creeks Research Watershed, Interior Alaska, 1978 – 2003.

| | | | | C2 Sub-basin | | | | C3 Sub-basin | | | | C4 Sub-basin | | | |
|---|---|---|---|---|---|---|---|---|---|---|---|---|---|---|---|
| Year | Snow | Rain | $P_{Total}$ | Q | $Q_{Dates}$ | ET | $\Delta S$ | Q | $Q_{Dates}$ | ET | $\Delta S$ | Q | $Q_{Dates}$ | ET | $\Delta S$ |
| 1978 | 81.3 | 229.3 | 310.5 | 30.5 | 172–275 | 231.3 | -32.3 | 42.9 | 172–274 | 201.5 | 66.1 | – | – | 296.1 | – |
| 1979 | 117.7 | 251.9 | 369.6 | – | – | 329.0 | – | 27.1 | 116–273 | 212.3 | 130.2 | – | – | 311.9 | – |
| 1980 | 93.1 | 227.6 | 320.7 | 24.6 | 169–267 | 298.2 | -2.1 | – | – | 192.4 | – | 32.8 | 142–267 | 282.7 | 5.2 |
| 1981 | 95.7 | 271.1 | 370.8 | 108.0 | 140–280 | 293.4 | -30.6 | 102.4 | 156–266 | 189.3 | 79.1 | 81.0 | 160–280 | 278.2 | 11.6 |
| 1982 | 84.7 | 288.8 | 373.5 | 86.3 | 146–279 | 313.8 | -26.6 | 77.6 | 159–279 | 202.5 | 93.4 | 71.2 | 133–279 | 297.5 | 4.8 |
| 1983 | 143.9 | 260.3 | 404.2 | 123.5 | 130–266 | 298.7 | -18.0 | 137.1 | 130–267 | 192.8 | 74.3 | 81.8 | 131–273 | 283.2 | 39.2 |
| 1984 | 100.8 | 240.7 | 341.5 | 145.1 | 138–284 | 303.7 | -107.3 | – | – | 195.9 | – | 114.7 | 138–274 | 287.9 | -61.1 |
| 1985 | 188.0 | 292.2 | 480.2 | 171.6 | 151–288 | 288.8 | 19.8 | 61.9 | 170–266 | 186.3 | 232.0 | 91.4 | 151–255 | 273.8 | 115.0 |
| 1986 | 97.4 | 257.2 | 354.6 | 70.6 | 175–269 | 315.7 | -31.7 | – | – | 203.7 | – | 101.1 | 141–290 | 299.3 | -45.8 |
| 1987 | 88.1 | 229.0 | 317.1 | 27.7 | 147–286 | 327.7 | -38.3 | 40.1 | 147–279 | 211.4 | 65.6 | 54.0 | 134–286 | 310.7 | -47.6 |
| 1988 | 67.7 | 300.4 | 368.2 | – | – | 326.4 | – | – | – | 210.6 | – | 64.4 | 133–272 | 309.5 | -5.7 |
| 1989 | 171.0 | 239.6 | 410.6 | – | – | 329.3 | – | – | – | 212.5 | – | – | – | 312.3 | – |
| 1990 | 161.7 | 333.5 | 495.2 | 41.9 | 142–268 | 336.1 | 117.2 | – | – | 216.9 | – | 44.5 | 136–269 | 318.7 | 132.0 |
| 1991 | 342.1 | 150.4 | 492.4 | 74.8 | 155–218 | 336.7 | 80.9 | 115.8 | 136–268 | 217.2 | 159.4 | 100.5 | 151–265 | 319.2 | 72.7 |
| 1992 | 153.2 | 346.3 | 499.6 | 79.0 | 155–291 | 293.5 | 127.1 | 64.0 | 155–273 | 189.4 | 246.2 | – | – | 278.3 | – |
| 1993 | 331.6 | 323.5 | 635.1 | – | – | 352.4 | – | – | – | 227.4 | – | – | – | 334.1 | – |
| 1994 | 102.4 | 339.3 | 441.7 | 115.3 | 97–278 | 352.9 | -26.5 | 99.9 | 95–278 | 227.7 | 114.1 | 111.7 | 89–277 | 334.6 | -4.6 |
| 1995 | 163.4 | 325.9 | 489.3 | 89.1 | 101–271 | 359.7 | 40.5 | – | – | 232.1 | – | 36.4 | 108–205 | 341.0 | 111.9 |
| 1996 | 110.9 | 313.4 | 424.3 | – | – | 315.4 | – | 46.5 | 142–268 | 203.5 | 174.3 | 21.4 | 191–270 | 299.1 | 103.8 |
| 1997 | 131.2 | 212.3 | 343.5 | 37.2 | 155–279 | 351.3 | -45.0 | – | – | 226.7 | – | – | – | 331.1 | – |
| 1998 | 75.2 | 345.4 | 420.7 | – | – | 293.7 | – | – | – | 189.5 | – | 72.3 | 141–269 | 278.5 | 69.9 |
| 1999 | 71.6 | 242.1 | 313.6 | 34.2 | 145–275 | 311.7 | -32.3 | – | – | 201.1 | – | 64.6 | 103–253 | 295.6 | -46.6 |
| 2000 | 197.9 | 319.5 | 517.4 | 116.7 | 145–276 | 276.7** | 124.0 | 152.8 | 144–276 | 178.5** | 186.1 | 95.0 | 101–254 | 262.4** | 160.0 |
| 2001 | 91.6 | 271.4 | 363.0 | 76.2 | 113–278 | 301.2* | -14.4 | 83.1 | 113–278 | 194.4* | 85.5 | – | – | 285.7* | – |
| 2002 | 53.2 | 307.2 | 360.4 | 53.0 | 188–294 | 295.8* | 11.6 | 69.4 | 183–295 | 190.8* | 100.2 | 20.5 | 183–289 | 280.5* | 59.4 |
| 2003 | 102.1 | 381.6 | 483.7 | 95.3 | 114–287 | 204.9* | 183.5 | 105.6 | 133–260 | 132.2* | 245.9 | 103.7 | 114–262 | 194.3* | 185.7 |
| Mean | 130.7 | 280.9 | 411.6 | 80.0 | | 312.3 | 15.0 | 83.8 | | 201.5 | 136.8 | 68.1 | | 296.1 | 45.2 |
| Max | 342.1 | 381.6 | 635.1 | 171.6 | | 359.7 | 183.5 | 152.8 | | 232.1 | 246.2 | 114.7 | | 341.0 | 185.7 |
| Min | 53.2 | 150.4 | 310.5 | 24.6 | | 204.9 | -107.3 | 27.1 | | 132.2 | 65.6 | 20.5 | | 194.3 | -61.1 |
| SD | 69.5 | 52.6 | 80.3 | 41.5 | | 31.3 | 74.0 | 36.8 | | 20.2 | 66.0 | 30.1 | | 29.7 | 74.9 |

$P_{Total}$: total precipitation (= snow + rain)(mm); ET: evapotranspiration (mm); Q: streamflow runoff(mm); $Q_{Dates}$: Julian dates of continuous measurement of streamflow runoff; $\Delta S$: change in storage (mm); –: $<$ 85% continuous data; *: ET calculated using Priestley-Taylor Method; **: ET calculated using simulated ET for days 121–146 and Priestley-Taylor Method for remaining days.

the Center of Global Change - University of Alaska Fairbanks, and a fellowship from the Inland Northwest Research Alliance (U.S. Department of Energy contract DE-FG07-02ID14277).

**Bibliography**

Baldocchi, D., F. M. Kelliher, T. Black, and P. Jarvis (2000), Climate and vegetation controls on boreal zone energy exchange, *Global Change Biology*, *6*(Supplement 1), 69–83.

Berezovskaya, S., D. Yang, and L. Hinzman (In Press), Long-term annual water balance analysis of the Lena River, *Global and Planetary Change*.

Bolton, W., L. Hinzman, and K. Yoshikawa (2000), Stream flow studies in a watershed underlain by discontinuous permafrost, in *Proceedings Water Resources in Extreme Environments*, edited by D. Kane, pp. 31–36.

Chapman, W., and J. Walsh (1993), Recent variations in sea ice and air temperature in high latitudes, *Bulletin American Meteorology Society*, *74*, 33–47.

Gieck, R. E. (1986), A water resource evaluation of two subarctic watersheds, Msc thesis, University of Alaska Fairbanks.

Haugen, R., C. Slaughter, K. Howe, and S. Dingman (1982), Hydrology and climatology of the Caribou-Poker Creeks Research Watershed, Alaska, *CRREL Report 82-26*, US Army Corps of Engineers Cold Regions Research and Engineering Laboratory.

IPCC (2001), Climate change 2001: Synthesis report. summary for policymakers., *Tech. rep.*, Intergovernmental Panel on Climate Change.

Kane, D., and L. Hinzman (2004), Monitoring extreme environments: Arctic hydrology in transition, *Water Resources Impact*, *6*(1), 24–27.

Peterson, B., R. Holmes, J. McClelland, C. Vörösmarty, R. Lammers, A. Shiklomanov, I. Skiklomanov, and S. Rahmstort (2002), Increasing river discharge to the Arctic Ocean, *Science*, *298*, 2171–2173.

Priestley, C., and R. Taylor (1972), On the assessment of surface heat flux and evaporation using large scale parameters., *Monthly Weather Review*, *100*(2), 81–92.

Rovansek, R., D. Kane, and L. Hinzman (1993), Improving estimates of snowpack water equivalent using double sampling, in *Proceedings of the 50th Eastern Western Snow Conference*, edited by M. Ferrick and T. Pangburn, pp. 157–163.

Slaughter, C. (1981), Streamflow measurement with pre-fabricated partial flumes in a permafrost dominated watershed., *Research Note 382*, USDA Forest Service PNW Forest and Range Experiment Station.

Woo, M. K. (1990), Permafrost hydrology, in *Northern Hydrology, Canadian Perspectives. Proceedings of the Northern Hydrology Symposium*, edited by T. Prowse, C. Ommanney, and M. Woo, no. 1 in Canadian National Hydrology Research Institute Science Report, pp. 63–76.

Yang, D., D. Kane, L. Hinzman, X. Zhang, T. Zhang, and H. Ye (2002), Siberian Lena River hydrologic regime and recent change, *Journal Geophysical Research*, *107*(D23), 4694, doi:10.1029/2002JD002,542.

Yoshikawa, K., L. Hinzman, N. Ishikawa, C. Collins, and V. Lunardini (1998), Air and ground temperature models at Caribou-Poker Creeks Research Watershed, in *Proceedings of the 49th AAAS Arctic Science Conference*, Fairbanks, Alaska.

Yoshikawa, K., W. Bolton, V. Romanovsky, M. Fukuda, and L. Hinzman (2002), Impacts of wildfire on the permafrost in the boreal forest of interior Alaska, *Journal of Geophysical Research*, *107*(8148: doe:10.1029/2001JD000438), printed 108(D1), 2003.

Yoshikawa, K., D. White, L. Hinzman, D. Goering, K. Petrone, W. Bolton, and N. Ishikawa (2003), Water in permafrost: Case study of aufeis and pingo hydrology in discontinuous permafrost, in *International Conference on Permafrost, Proceedings 8*, vol. 2, edited by M. Phillips, S. Springman, and L. Arenson, pp. 1259–1264.

# Chapter 4
# Toward Understanding the Hydrologic Processes in Watershed Dominated by Discontinuous Permafrost *

**Abstract**

The sub-arctic environment can be characterized by being located in the zone of discontinuous permafrost. Discontinuous permafrost introduces very distinct changes in hydraulic properties, which introduce sharp discontinuities in hydrological processes and ecosystem characteristics. The variation in hydraulic properties vary over short and long time scales as the active layer develops over the course of a summer or as permafrost degrades in response to a changing climate. Although the distribution of permafrost is site specific, it impacts most of the hydrologic processes, including stream flow, soil moisture dynamics, evapotranspiration, groundwater flow, and water storage processes. It is essential to develop a model that can incorporate such temporal and spatial dynamics, both to model watersheds currently situated in discontinuous permafrost and to project future changes in regions underlain by continuous permafrost. This paper describes a spatially-distributed, process-based hydrologic model, TopoFlow, designed to simulate and predict soil moisture dynamics and all other hydrologic processes throughout a sub-arctic watershed. All of the major water balance processes are simulated, including precipitation, snowmelt, evapotranspiration, infiltration, groundwater flow, and overland/channel flow. For every process simulated, a user-specified method and time-step are selected. Each input variable can be a scalar, time-series, grid, or grid sequence. The modular structure of TopoFlow permits implementation of additional processes and methods without altering the functionality of the model. The design and structure of TopoFlow in intended to promote a community-based evolution and serve the broad hydrologic community.

KEY WORDS: Permafrost; Active layer; Modeling; Computational hydrology; Soil moisture.

*W.R. Bolton, S. D. Peckham, and L.D. Hinzman, Submitted to *Journal of Geophysical Research – Biogeosciences*


Figure 4.1. Panarctic Permafrost Distribution. Source: International Permafrost Association, 1998. Circumpolar Active-Layer Permafrost System (CAPS), version 1.0.

### 4.1 Introduction

The Köppen Climate Classification System defines the sub-arctic as the region where the mean monthly air temperature is at least $10^{o}$C between one and three months of the year. However, the sub-arctic environment can also be characterized as the region located in the zone of discontinuous permafrost (Figure 4.1). Permafrost underlies approximately 24% of the exposed land area in the Northern Hemisphere [*Romanovsky et al.*, 2002], of which approximately 22% (or 5.6 X $10^6$ km$^2$) is located in the discontinuous zone [*Anisimov and Nelson*, 1997]. Permafrost in this region can be very warm and unstable [*Yoshikawa et al.*, 2002]. Although the distribution of permafrost in this region is site specific, it dominates the response to many of the hydrologic processes in this region, including stream flow, soil moisture dynamics [*Haugen et al.*, 1982; *Bolton et al.*, 2000], infiltration and percolation [*Kane and Stein*, 1983a,?], evapotranspiration [*Dingman and Koutz*, 1974; *Baldocchi et al.*, 2000; *Hinzman et al.*, 2006], nutrient transport [*Jones et al.*, 2005], sediment transport [*Slaughter et al.*, 1983], and water storage processes.

### 4.1.1 Influence of permafrost on hydrologic processes

In the sub-arctic environment, the presence or absence of permafrost is generally controlled by physiographic features such as aspect, slope, and elevation. Other factors such as soil types, soil moisture, vegetation cover, and disturbance - either anthropogenic or natural (such as wildfire) can also influence the distribution of permafrost [*Haugen et al.*, 1982; *Yoshikawa et al.*, 2002]. In Interior Alaska, permafrost is generally located along north facing slopes and valley bottoms, while areas free of permafrost are generally located on south to southwest facing slopes [*Nelson*, 1978; *Haugen et al.*, 1982]. Hydrologically speaking, the sub-arctic environment is unique in that the thermal and hydrologic regime of the soil (permafrost versus non-permafrost) can vary greatly over short spatial scales (x- and y-direction), with depth into the ground (z-direction), and over time (short- and long-term). It is well documented the hydraulic conductivity of ice-rich permafrost soils can be several orders of magnitude lower than their unfrozen counterpart (e.g. *Kane and Stein* [1983]; *Burt and Williams* [1976]; *Freeze and Cherry* [1979]). Ice-rich soils are common at the permafrost table as surface water, which percolates to the permafrost, refreeze [*Woo*, 1986]. The ice-rich condition at the permafrost table significantly reduces the permeability of the soil, effectively creating an aquiclude, dividing the groundwater system into a sub- and supra-permafrost components [*Dingman*, 1975; *Woo*, 1990].

In areas underlain with permafrost, the active layer, the thin layer of soil above the permafrost, which annually thaws and freezes, is the zone where most hydrologic, biologic, ecologic, and geomorphic processes occur [*Kane et al.*, 1991; *Hinzman et al.*, 1998; *Woo*, 2000]. The thawing of the active layer begins immediately upon the completion of snowmelt [*Boike et al.*, 1998] and is dependent upon a number of factors including soil material, duration of snow cover, soil moisture and ice-content, and convection of heat by ground water [*Woo*, 1986]. As a result, the depth of the active layer is spatially and temporally variable. In Interior Alaska, the active layer depth is thinner on north-facing slopes than south-facing slopes due to differences in vegetative cover and a late lying snow cover [*Brown*, 1973; *Washburn*, 1979]. The active layer zone is hydrologically dynamic where both the hydraulic conductivity and storage capacity increase throughout the summer. As the position of the active layer is both spatially and temporally variable, the storage capacity and hydraulic conductivity of these near surface soils are also variable in both space and

time [*Woo and Steer*, 1983].

The difference in hydraulic properties between areas underlain with permafrost and non-permafrost areas result in markedly different runoff patterns [*Slaughter and Kane*, 1979]. In permafrost areas, ice-rich soil pores inhibit percolation of surface waters (either snowmelt or rainfall) at the permafrost table. This results in movement of surface waters relatively quickly downslope through the organic mat and near surface soils. In contrast, the relatively well-drained non-permafrost soils allow percolation of surface waters to a deep subsurface groundwater system without significant lateral flow [*Slaughter and Kane*, 1979]. Movement of water through this deep groundwater system is relative slow compared to the water movement through the near surface soils in the permafrost region [*Hinzman et al.*, 1991; *Bolton et al.*, 2004]. Stream flow in permafrost dominated watersheds can be characterized by a larger contributing area, higher specific discharge (discharge normalized by basin area), rapid rise to peak flow (often described as 'flashy'), rapid decline following peak flow, prolonged recession, and a lower specific baseflow compared to catchments of lesser permafrost coverage [*Dingman*, 1973; *Slaughter and Kane*, 1979; *Haugen et al.*, 1982; *Chacho and Bredthauer*, 1983; *McNamara et al.*, 1998; *Bolton et al.*, 2000; *Petrone et al.*, 2000]. Over the course of a summer season, the thawing of the active layer increases the water holding capacity of the soil, resulting in a decreasing surface water contribution during precipitation events and a steadily increasing baseflow contribution [*Hinzman and Kane*, 1991; *Bolton et al.*, 2000].

Large differences in the soil moisture regime also exist between areas underlain with permafrost and soils free of permafrost. As the ice-rich conditions at the permafrost table restrict percolation to the deeper sub-surface, a near surface water table (perched on top of the permafrost table) results in soils that are relatively wet (at or near saturation) compared to the well-drained non-permafrost soils. Soils underlain with permafrost display little response to precipitation events as these soils are typically near saturation. Changes in the soil moisture during precipitation events are rapid in non-permafrost soils indicating a high infiltration rate and rapid percolation to the deeper sub-surface soils [*Bolton et al.*, 2000]

### 4.1.2 System response to a warming climate

Temperatures in the western portion of the high northern latitudes are rising at an unprecedented rate [*Chapman and Walsh*, 1993; *Serreze et al.*, 2000]. The permafrost condition in Interior Alaska is warm and unstable, with temperatures often $-1^oC$ or warmer [*Yoshikawa et al.*, 2002]. Recent studies indicate the permafrost temperature in this region is warming [*Osterkamp and Romanovsky*, 1999; *Osterkamp*, 2003]. The warmer climate in combination with an unstable permafrost regime has led to shrinking permafrost coverage and an increased active layer depth [*Jorgenson et al.*, 2001; *Serreze et al.*, 2002; *Zhang*, 2005]. These changes to the permafrost regime and increased atmospheric temperatures have led to observed changes in the hydrologic regime, including later freeze-up and earlier break-up dates of rivers [*Magnuson et al.*, 2000], increased arctic river runoff [*Peterson et al.*, 2002], shrinking lakes [*Smith et al.*, 2005], and thermokarst development [*Osterkamp and Romanovsky*, 1999; *Osterkamp et al.*, 2000; *Jorgenson et al.*, 2001]. As the sub-arctic thermal and hydrologic systems are fully coupled, it is not surprising that changes in the permafrost regime have led to these observed changes in the hydrologic system [*Hinzman et al.*, 2005; *Walsh et al.*, 2005].

Increases in air temperature (particularly winter) and precipitation (both summer and winter) are expected to continue into the future [*IPCC*, 2001]. If the northern environment continues to warm as predicted, one should expect a shifting change in the water balance corresponding to a thinner and spatially reduced permafrost condition. In watersheds with significant permafrost coverage, it is likely that a decreasing summer and an increasing winter discharge will be observed [*Bolton et al.*, 2004; *Hinzman et al.*, 2005]. Changes in the quantity and timing of relatively warm freshwater into the Arctic Ocean may have profound impacts on the thermohaline circulation pattern, potentially changing the regional climate system [*ACIA*, 2005; *Arnell*, 2005].

In the (sub-)arctic environment, soil respiration is typically slow due to low ground temperatures [*French et al.*, 1997], making this region a carbon sink (carbon input $<$ carbon output). Currently, the boreal forest accounts for about one-third of the carbon sequestered in terrestrial ecosystems [*McGuire et al.*, 1995]. Projected increases in the surface temperature may lead to enhanced degradation of this stored organic matter to either carbon dioxide ($CO_2$) or methane ($CH_4$), dependent upon a lowering (aerobic condition) or rising

(anaerobic condition) of the water table [*Callaghan and Jonasson*, 1996; *Moore et al.*, 1998; *Friborg et al.*, 2003]. An increase in the rate of either $CO_2$ or $CH_4$, both strong greenhouse gases, into the atmosphere would serve as a positive feedback to further warming of the atmosphere.

### 4.1.3 Modeling need

In light of these predicted changes and potential feedbacks, it is important to be able to understand and predict the feedback mechanisms of the water cycle [*Kane and Hinzman*, 2004]. At this point, a good understanding of many of the (sub-)arctic hydrologic processes exists at the plot and hillslope scales. However, the understanding we have gained from these plot-scale studies have not been adequately or systematically incorporated into process based meso-scale hydrologic models [*Vörösmarty et al.*, 1993]. Furthermore, the land-surface parameterizations used in global climate models do not adequately resolve the soil conditions [*Walsh et al.*, 2005], which often rely on either point measurements or on information derived from satellite data. It is clear a meso-scale physically-based hydrologic model is needed to bridge the gap between our plot-scale understanding to regional- (or global-) scale climate models by capturing the hydrologic behavior and variation of individual watersheds. Currently, there is a lack of process-based hydrologic models that adequately simulate the soil moisture dynamics at the watershed scale and also include a realistic land-atmosphere exchange in permafrost dominated regions.

Several hydrologic models have been developed to simulate the spatial distribution and variation of physical processes. The approach and design of these models varies with the problem being studied, with each emphasizing a specific process, hydrologic regime, or spatial/temporal scale. The TOPMODEL (TOPography based hydrological MODEL, *Bevin and Kirkby* [1979]) and its variants (e.g. STOPMODEL [*Walter et al.*, 2002], Dynamic TOPMODEL [*Bevin and Freer*, 2001]) rely on a statistical method of hydrologic similarity, based upon a topography index. The topographic index is defined as $\ln(a/\tan\beta)$, where $a$ is the area draining through a point upslope and $\beta$ is the local slope angle. All points with the same index value are assumed to respond in a hydrologically similar way, requiring calculations only for different index values. Similarly, lumped parameter models such as the PRMS (Precipitation-Runoff Modeling System, [*Leavesley et al.*, 1983]), HSPF (Hydrologic

Simulation Program - Fortan, [*Bicknell et al.*, 1997]), SWAT (Soil and Water Assessment Tool, [*Arnold et al.*, 1993]), VIC (Variable Infiltration Capacity, [*Liang et al.*, 1994]), and the SLURP (Simple Lumped Reservoir Parametric Model [*Kite*, 1978, 1989]) rely on sub-dividing watersheds based upon similar soil, hydrologic, and land use properties, called hydrologic response units (HRUs), reducing the number of variables and and calculations required during simulations. The SHE (Systéme Hydrologique Européen, [*Jonch-Clausen*, 1979; *Abbott et al.*, 1986]) and MIKE-SHE [*DHI*, 1998] models are a spatially-distributed, physically-based models that simulating many of the hydrologic processes including precipitation, evapotranspiration, overland flow, channel flow, vadose zone flow, and groundwater flow. The physically-based processes of these models require a substantial set of high quality data, often not available in the (sub-)arctic environment. The KINEROS2 (Kinematic Runoff and Erosion Model [*Goodrich et al.*, 2000]), $DR_3M$ (Distributed Routing Rainfall-Runoff Model, [*Alley and Smith*, 1982]), and the CASC2D (CASCade 2-Dimensional, [*Julian and Saghafian*, 1991]) are single event based models, emphasizing a specific process. *Wigmosta et al.* [1994] presents a model (Distributed Hydrology Vegetation Model, DHVM) that focusses on vegetation - hydrology relationships with the inclusion of a two-layer canopy model for evapotranspiration and a two-layer rooting zone model. The models described above generally developed for specific applications particular to a specific hydrologic regime. None of these models is suited to handle the rapidly changing thermal (permafrost versus non-permafrost and active layer development) and hydraulic (hydraulic conductivity and storage capacity) conditions in the x-, y-, and z-directions typical of the sub-arctic hydrologic regime.

### 4.1.4 Objective

The main purpose of the model we are developing, TopoFlow, is to describe, simulate, and predict all (sub-)arctic hydrologic processes at the meso-scale using energy and climate forcings. The main objective of this paper is to describe and document the TopoFlow numerical model which is able to reproduce all the hydrological processes while reflecting the spatial and temporal varying properties that are ubiquitous in both the arctic and sub-arctic environments.

## 4.2 Model development

### 4.2.1 TopoFlow overview

TopoFlow is a process-based, spatially-distributed hydrologic model based upon the ARHYTHM (Arctic Region HYdrologic and THermal Model, (*Hinzman et al.* [1995]; *Zhang et al.* [2000])). TopoFlow utilizes an user friendly graphical user interface (GUI), incorporating point-and-click functionality and context specific help dialogs. TopoFlow is designed to evolve into a hydrologic model that is utilized and enhanced by all disciplines within the hydrologic community. Well documented open-source code (available for download from the TopoFlow website (http://instaar.colorado.edu/topoflow/) and structured in a modular fashion, members of the hydrologic community are able (and encouraged) to develop and incorporate new hydrologic methods without altering the overall structure or functionality of TopoFlow. Other features of TopoFlow include pre- and post-processing tools which aid in the preparation of spatially-distributed input files and rapid visualization and analysis of output files. Written in IDL (Interface Data Language), TopoFlow is portable across the Windows, MacIntosh, and Unix computing environments.

Numerically, TopoFlow is based upon the conservation of mass principal,

$$Inputs - Outputs \pm \Delta Storage = 0 \tag{4.1}$$

where: *Inputs*, *Outputs*, and $\Delta Storage$ are, respectively, the amount of water over a time period, $\Delta t$. Using the continuity principal, the water balance is calculated for each element in the model domain for each time step,

$$P_T + GW_{in} - (Q_{CH} + ET + GW_{out}) = \Delta Storage \tag{4.2}$$

where: $P_T$ is precipitation (rain and snowmelt), $GW_{in,out}$ is groundwater inflow and outflow, $Q_C$ is overland and channel flow, $ET$ is evapotranspiration, and $\Delta Storage$ is the change in storage (all forms of water).

The structure of TopoFlow is divided into three components: model input, process simulation, and model output. Each of these components are described below.

### 4.2.2 Model input

The model input component of TopoFlow consists of two parts: 1) digital elevation model (DEM) analysis, and 2) determination of the model time step. Both the DEM analysis and determination of the model time-step must be completed before the process simulation can begin. However, once the DEM analysis has been completed for the model domain, it does not need to be repeated.

#### DEM analysis and flow routing

In order to run TopoFlow, input files that define the model domain, the topography, the direction of lateral water movement, the Horton-Strahler order number, and an information file, describing the structure of the model domain, must be generated. Although not necessary to complete this step, commercial software such as RiverTools$^{TM}$, are able to efficiently generate each of these files. An example of the required information file can be found on the TopoFlow website, (http://instaar.colorado.edu/topoflow).

Implementation of DEMs to aide in hydrologic analysis has become commonplace due to the increased availability and quality of DEMs, and rapid growth in computing power. In hydrologic analysis, the most common form of the DEM is the square-grid network. The square-grid network is computationally simple to setup and efficient, and overlying other spatial information is relatively simple compared to other networks such as those created using contours or triangular irregular network (TINs) [*Moore et al.*, 1993; *Grayson and Blöschel*, 2000]. For each TopoFlow simulation, the model domain and topography are defined by a square-grid network DEM, which encompasses the catchment area. Each TopoFlow element has dimensions of the DEM pixel resolution (x- & y-directions) with up to ten user specified layers of variable thickness in the z-direction (Figure 4.2).

The slope between two TopoFlow elements is defined as the difference in the land surface elevation between two elements divided by the straight-line distance between the centers of the elements [dimensionless value]. Each TopoFlow element is assigned a 'local slope', which is the defined as the steepest (largest positive value) slope between an element and its eight neighboring elements (Figure 4.3b).

The horizontal water direction for each TopoFlow element is based upon the D8 method

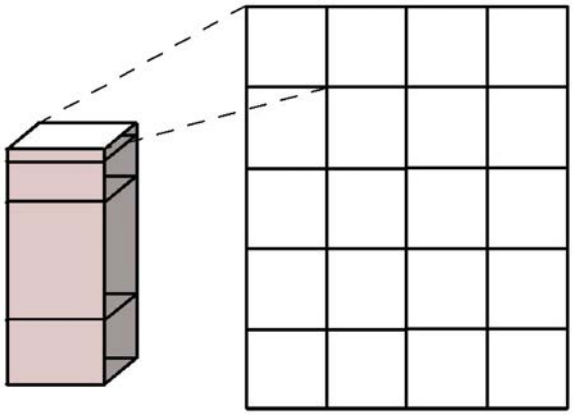

Figure 4.2. Rectangular elements used in TopoFlow. The dimensions of each element corresponds to the DEM pixel resolution in the x- & y-directions. Up to 10 user defined layers of variable thickness represent the z-direction. Elements are labeled sequentially in calendar fashion (by rows) from the upper left (NW corner) to the lower right (SE corner).

[*O'Callaghan and Mark*, 1984]. Flow directions are defined as moving from one element to an adjacent element in the direction of the 'local slope.' In the case of flat areas, where the steepest slope is equal to zero, the flow direction is forced in the direction from higher surrounding topography to lower topography [*Garbrecht and Martz*, 1997]. Each element within the model domain is assigned a flow direction based on one of the eight primary compass directions [NE, E, SE, S, SW, W, NW, N] corresponding to the eight surrounding neighbor elements. Flow directions for each element are coded with corresponding values of [1, 2, 4, 8, 16, 32, 64, 128]. Flow directions for edge elements of the DEM are not assigned a flow direction and are not considered part of the TopoFlow model domain (Figure 4.3c). The decision to move from the triangular elements used in ARHYTHM [*Hinzman et al.*, 1995; *Zhang et al.*, 2000] model to rectangular elements was in part due to difficulties in routing flow through flat regions, such as those found on the North Slope of Alaska. Although the triangular elements are the most efficient method of representing topographic features [*Grayson and Blöschel*, 2000], the ability to efficiently route water through these flat regions was determined to be more critical.

Each TopoFlow element is assigned an order number based upon the Horton-Strahler classification [*Horton*, 1945; *Strahler*, 1957]. Each 'headwater' element is designated as first-order. An element in which the flow direction of two first-order elements join together

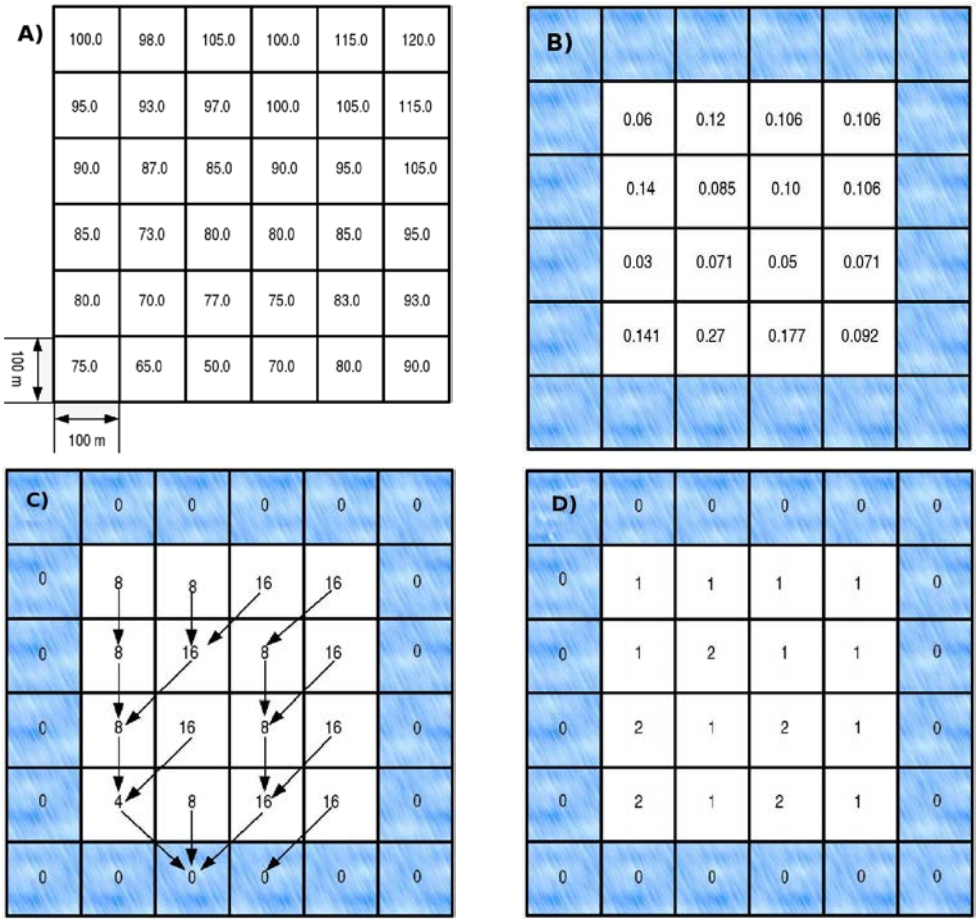


Figure 4.3. Digital Elevation Analysis. A) An example of a 100-meter DEM. Numerical values in each element represent the land surface elevation. B) The 'local slope' of each interior element. The 'local slope' is defined as the steepest (largest positive value) slope between an element and its eight neighboring elements. C) Flow routing. Each element is assigned a numerical value which designates the direction in which water from one element flows one of the adjacent eight elements. Arrows indicate direction of flow determined by the direction of the local slope. D) Order number. Each of these four files (DEM, Local Slope, Flow Direction, and Order Number) and an Information file must be generated prior to running TopoFlow. Note: Elements on the edge of the DEM (shaded elements) are not considered part of the model domain.

form a second-order element. An element in which the flow directions of two second-order elements meet forms a third-order element, and so on (Figure 4.3d). Only when two elements of the same order flow into another element, does the flow order increase, meaning that numerous lower-order elements can flow into a larger-order element without changing the order number of the larger-order element. *Peckham* [1995] observed that by 'pruning' (or removing) lower-order elements from the flow network tree, the remaining 'un-pruned' branches closely resemble the natural channel pattern of the drainage network. Conceptually, the 'pruned' lower-order element represent elements in which overland flow would occur (if either the water table elevation exceeds the land surface elevation or if the infiltration capacity of the soils is exceeded by either the snowmelt or precipitation rate). Higher-order, 'non-pruned' branches are elements in which channel flow occurs.

**Model timestep**

In order to maintain numerical stability, the maximum distance traveled by a parcel of water in one time step must be less than one pixel width, i.e. the Courant condition:

$$(vmax \cdot \Delta t) \leq dx \tag{4.3}$$

where: $vmax$ is the estimated maximum velocity a particle of water can travel, [m/s]; $\Delta t$ is the model time step, [s]; and $dx$ is the width of an element, [m]. In order to satisfy the Courant condition, the time step used in the channel flow process must be $\leq dx/vmax_{chan}$, where $vmax_{chan}$ is the maximum velocity a particle of water travels within a channel segment. This is the maximum model time-step possible for simulations.

**TopoFlow input tools**

TopoFlow has a number of features to aide in the model input and simulation process. TopoFlow features an user friendly point-and-click GUI (Figure 4.4). The wizard-style GUI is designed to ensure all required input files or variables are input correctly. For each process, the formulas used for each selected method is available with a click of a button. Additionally, context specific 'Help' dialogs are also available with a click of a button.

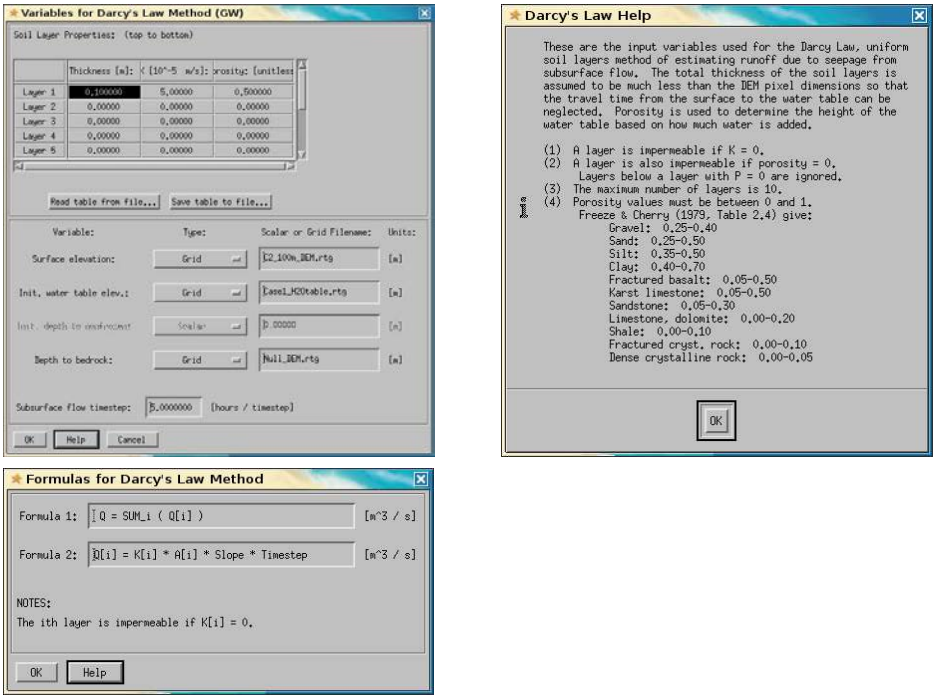


Figure 4.4. TopoFlow Graphical User Interface. TopoFlow features an user friendly point-and-click GUI with method specific Help and Formulas dialogs.

A number of pre-processing tools are available to aide in the creation of spatially-distributed input files. Three of the pre-processing tools relate to the creation of spatially and temporally distributed meterological data. Using the Inverse Distance Method, the first tool creates spatial and temporal meteorologic data (grid sequence file) from point measurements. The second tool calculates the clear sky short-wave radiation flux (grid sequence file) for a specified period (Day A to Day B) and interval (i.e. hour, minute, day). Direct, diffuse, and backscatter radiation components are calculated based upon topographic/surface features, such as slope and aspect angle and albedo, and atmospheric properties, such as air temperature and relative humidity. The third pre-processing tool creates a grid sequence file for fractal rain events. Fractal rain events are localized rain events which follow power-law distributions of several decades [*Dickman*, 2004]. Tools which create the channel geometry grids (based upon either the order or area grids), a profile smoothed DEM, and a steady state initial flow depth grid are also available.

### 4.2.3 Process simulation

The sub-Arctic lies in the transition zone between the continuous permafrost region of the Arctic and the sporadic/non-permafrost region of the temperate environment. As a result, the thermal and hydrologic characteristics of both the Arctic and temperate region occur in the sub-Arctic, and are reflected with permafrost distribution. Many of the sub-arctic hydrologic processes are highly variable in both space and time. For example, groundwater flow in this region occurs in the deep subsurface system (in permafrost free areas, sub-permafrost groundwater) or in the shallow surface soils within the active layer (in permafrost areas, supra-permafrost groundwater). The supra-permafrost groundwater flow is also strongly influenced by the active layer depth, which is in a continuous state of change (either thawing or freezing). Other hydrologic processes such as evapotranspiration (reflected in vegetation distribution and surface energy balance), infiltration, percolation, overland & channel flow, as well as soil moisture dynamics (all reflected in permafrost distribution) exhibit a high spatial and temporal variability. Additionally, many of the hydrologic processes take place on different time scales - channel flow in seconds, infiltration and percolation in minutes to hours, groundwater flow and snowmelt in hours to days.

In the northern region, the number of data collection stations (stream discharge, meteorological stations) is sparse for a number of reasons (lack of funding, harsh and remote environment, etc) [*Shiklomanov et al.*, 2002]. As a result, spatial and/or temporal data sets may not be justified to use as model input. TopoFlow addresses this issue by allowing the user to select a specific data type for nearly every input variable. The format for each input variable can take one of the following forms: 'scalar' - constant value in both time and space; 'time series' - spatially constant data, variable in time; 'grid' - spatially variable data, constant with time; and 'grid sequence' - both spatial and temporally variable data.

The structure of TopoFlow is such that a method is specified for each hydrologic process. For each process, the option of 'None' exists, meaning that specific process will not be used in the simulation. For those hydrologic processes simulated, a physically-based method of simulation is available. However, many of these physically-based methods are extremely data intensive. Given the overall lack (and declining) number of meteorologic stations [*Shiklomanov et al.*, 2002] located in the northern regions, process simulations using (semi-)empirical methods, having fewer data requirements, are also available (Figure 4.5).

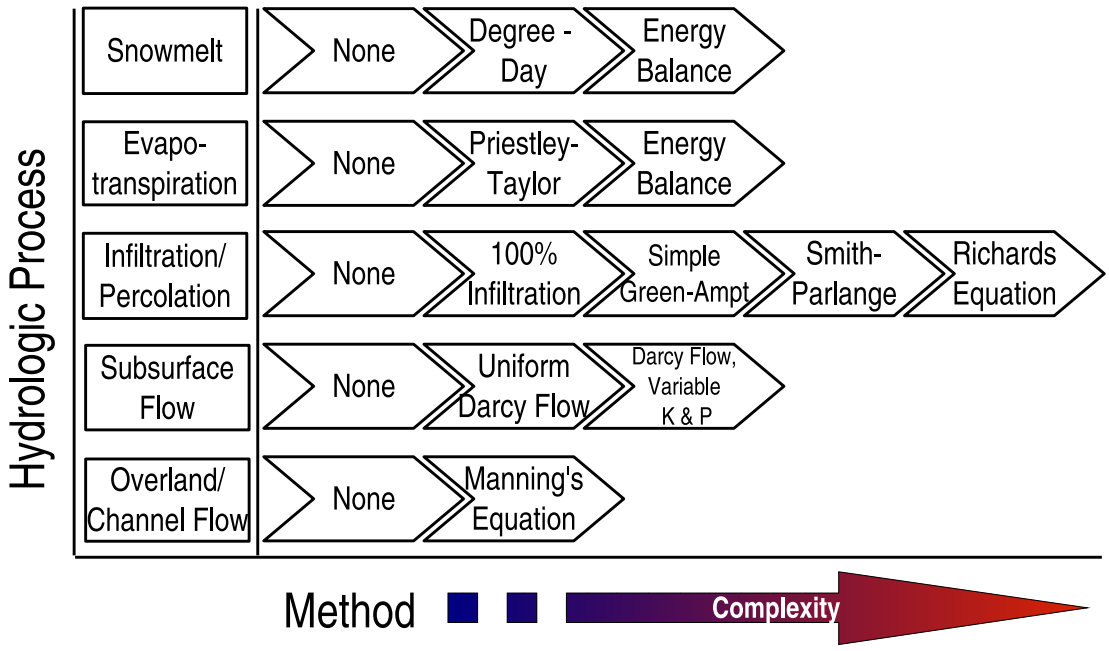


Figure 4.5. Hydrologic processes and methods simulated using TopoFlow. For each model simulation, any combination of processes (including 'None') maybe employed.

As the complexity of the method used to simulate processes increase, the data and computational requirements increase proportionately (Section 4.2.3). The time step used for each process simulated is user specified and is independent of the other processes simulated.

The TopoFlow model is a modification (second generation) of the ARHYTHM model. As such, many of the hydrologic processes simulated are formulated in the exact manner as ARHYTHM and are documented in *Zhang et al.* [2000]. The hydrologic processes currently supported include precipitation, snowmelt, evapotranspiration, infiltration, overland/channel flow, and groundwater flow. The governing equations for all the hydrologic processes and methods currently used in TopoFlow are listed in Table 4.4. Significant changes in the infiltration and overland & channel flow processes have been made in TopoFlow and are described in detail below. The energy and hydrologic processes considered in the model development are shown in Figure 4.6.

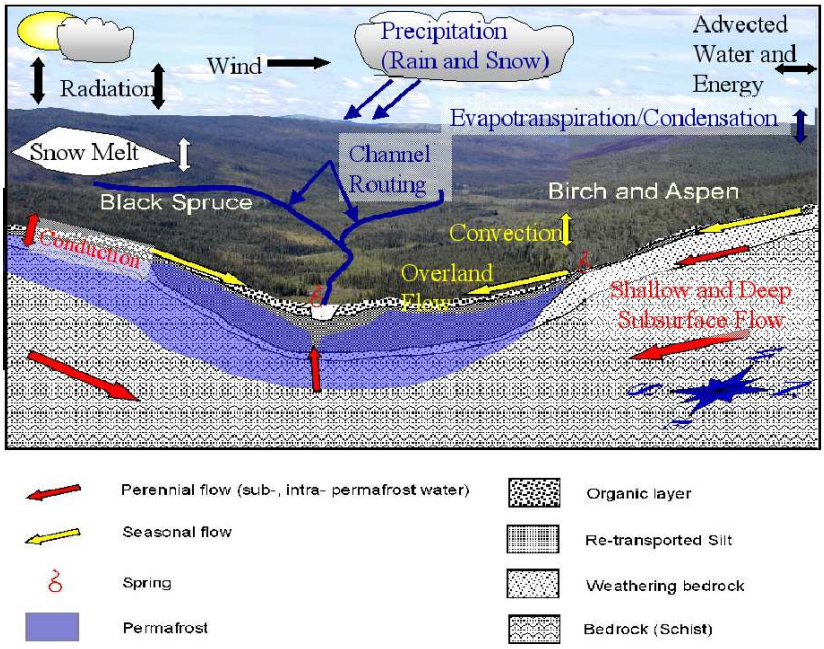


Figure 4.6. Energy and hydrologic processes simulated in TopoFlow. Figure modified from *Hinzman et al.* [2006].

### Infiltration and percolation

There is a high degree of spatial and temporal variability in the infiltration and percolation processes in the sub-arctic environment. In the sub-Arctic, the presence or absence of permafrost controls the pathways of groundwater flow, either limiting it to the near surface active layer (in areas underlain with permafrost) or allowing percolation to a deep (sub-permafrost) groundwater system [*Hinzman et al.*, 2000]. As a result, runoff patterns between permafrost and permafrost free slopes are markedly different [*Slaughter and Kane*, 1979; *Bolton et al.*, 2000] (Section 4.1.1). The distribution of water in the soil column is an important factor in determination of the runoff response to precipitation events. As moisture content increases, the amount of water storage available in the soils is reduced. *Dingman* [1973] suggested that the wetter the watershed prior to a rainfall event, a higher percentage of runoff would occur (compared to similar magnitude rainfall events). Percolation of surface waters to the deep groundwater system is not only dependent upon the distribution of permafrost, but also the time of year. The snowmelt period in most high latitude regions

is typically the major hydrologic event of the year [*Kane and Yang*, 2004; *Bolton et al.*, 2004] as 6-8 months of precipitation, held in storage as the winter snowpack, is released into the system over a relatively short 2-3 week period. *Kane and Stein* [1983a,?] have indicated the snowmelt period is of particular importance as most groundwater recharge occurs during this period, as evapotranspiration demands are typically very low. Groundwater recharge occasionally occurs during prolonged precipitation events [*Kane and Stein*, 1983] following the snowmelt period.

TopoFlow currently uses four different methods to simulate the infiltration and percolation processes. Three of the methods are primarily based upon Darcy's Law and the principal of conservation of mass: 1) Finite-Difference Solution of the Richards Equation; 2) Green-Ampt, Single Event; and 3) Smith-Parlange, Single Event. A forth method, Instantaneous Infiltration, was used in the ARHYTHM model and can be used in areas of continuous permafrost. As with the other processes, the amount of input data and computational resources required is proportional to the complexity of the method used. Discussion of the four different methods used to simulation the infiltration and percolation process follows below.

*Finite-Difference Solution of the Richards Equation.* The Richards Equation [*Richards*, 1931] for infiltration is:

$$\frac{\partial \theta}{\partial t} = \frac{\partial}{\partial x}\left[K\frac{\partial \psi}{\partial x} - K\right] \tag{4.4}$$

where $\theta$ is the soil water content [by volume]; $z$ is vertical depth into the soil, positive downward from the surface, [$m$]; $K$ is the hydraulic conductivity of the soil, [$m/s$]; $\psi$ is the soil water capillary head, [$m$]; and $t$ is time, [$sec$]. The Richards equation is solved using the finite difference solution as described in *Smith* [2002]. The finite difference formulation of the Richards Equation (Equation 4.4) can be rewritten (following *Smith* [2002]) as:

$$\frac{\left[\theta^{j} - \theta^{j-1}\right]}{\Delta t} = \frac{-2}{(x_{\iota+1} - x_{\iota-1})} \left\{ \begin{array}{c} \omega\left[\overline{K}_{\iota,\iota+1}\left(\frac{(\psi_{\iota+1}-\psi_{\iota})}{\Delta x_{\iota,\iota+1}} - p_g\right) - \overline{K}_{\iota,\iota-1}\left(\frac{(\psi_{\iota}-\psi_{\iota-1})}{\Delta x_{\iota,\iota-1}} - p_g\right)\right]^{j} + \\ (1-\omega)\left[\overline{K}_{\iota,\iota+1}\left(\frac{(\psi_{\iota+1}-\psi_{\iota})}{\Delta x_{\iota,\iota+1}} - p_g\right) - \overline{K}_{\iota,\iota-1}\left(\frac{(\psi_{\iota}-\psi_{\iota-1})}{\Delta x_{\iota,\iota-1}} - p_g\right)\right]^{j-1} \end{array} \right\} \tag{4.5}$$

where ι are individual points (or nodes) that represent a soil layer (conceptually at the center of the soil layer); $p$ is the gravitational term (=1 for vertical infiltration); ω is a weighing factor (when ω = 1.0, the equation is fully implicit requiring an iterative solution, when ω=0.0, an explicit solution at time step $j$ is allowed, dependent only on known values from the previous time step,$j-1$); $\overline{K}$ is the mean hydraulic conductivity of the soil layer; and $\Delta x$ is the spatial distance between the specified nodes. Assuming vertical infiltration and ω=0.0 (explicit solution), Equation 4.5 reduces to:

$$\frac{\theta^j - \theta^{j-1}}{\Delta t} = \frac{-2}{(x_{\iota+1} - x_{\iota-1})} \left[ \overline{K}_{\iota,\iota+1} \left( \frac{\psi_{\iota+1} - \psi_\iota}{\Delta x_{\iota,\iota+1}} - 1.0 \right) - \overline{K}_{\iota,\iota-1} \left( \frac{\psi_\iota - \psi_{\iota-1}}{\Delta x_{\iota,\iota-1}} - 1.0 \right)^{j-1} \right] \tag{4.6}$$

A complication with this formulation is that the left side of Equation 4.6 has the unknown value $\theta^j$ and the right side has unknown terms ψ at ι, $\iota-1$, and $\iota+1$. Using the Brooks-Corey [1964] relation, the pressure head, ψ can be found as a function of soil moisture, θ:

$$\psi(\theta) = \psi_b \cdot \theta_e^{-1.0/\lambda} \tag{4.7}$$

where $\psi_b$ is the air entry tention, $\theta_e$ is the effective saturation, and λ is the pore size distribution coefficient. The effective saturation is determined using transitional Brooks and Corey (TB-C) relationship [*Smith*, 1990; *Smith et al.*, 1993]:

$$\theta_e = \left[ 1 + \left( \frac{\psi + \psi_a}{\psi_b} \right)^c \right]^{-\frac{\lambda}{c}} \tag{4.8}$$

Here, $c$ is a curvature parameter and $\psi_a$ is a small shift parameter to approximate the hysteresis. Similarly, the unsaturated hydraulic conductivity of the soil can be found as a function of the pressure head,

$$K(\psi) = K_{sat} \cdot K_r \tag{4.9}$$

where $K_{sat,r}$ are the saturated and relative hydraulic conductivities of the soil. The relative hydraulic conductivity is defined as:

$$K_r \equiv \frac{K}{K_s} = \left( \frac{\psi}{\psi_b} \right) \tag{4.10}$$

Combining Equations 4.8 and 4.10 results in,

$$K_r(\psi) = \left[ 1 + \left( \frac{\psi + \psi_a}{\psi_b} \right)^c \right]^{-\frac{\eta}{c}} \tag{4.11}$$

where $\eta$, is the conductivity exponent parameter, is related to $\lambda$, the pore-size distribution parameter.

$$\eta = 2.0 + (3.0 \cdot \lambda) \tag{4.12}$$

Typical values of $\lambda$ for a number of soils are listed in Table 4.1. Given the established relationships between soil moisture, pressure head, and hydraulic conductivity, the kinematic wave approximation can be used to determine the rate of the moisture wave front through the vadose zone.

$$u_s(\theta_u, \theta_l) = \frac{K(\theta_u) - K(\theta_l)}{\theta_u - \theta_l} \tag{4.13}$$

where $u_s$ is the kinematic shock velocity and the subscripts $u$ and $l$ indicate the upper and lower boundaries of the soil layer.

*Green-Ampt, Single Event.* The Green-Ampt equation [*Green and Ampt*, 1911] was the first physically-based attempt to simulate the infiltration process. Based upon Darcy's Law and the principal of conservation of mass, the Green-Ampt model assumes idealized conditions - a single homogeneous soil layer of infinite depth, a horizontal surface, constant surface ponding depth, uniform antecedent soil moisture content, and no evapotranspiration occurs during the rain event. The Green-Ampt method assumes a piston-type water content profile, meaning the soil profile is assumed saturated down to the wetting front, where it abruptly drops to the antecedent moisture conditions. As the model formulation assumes a sharp wetting front, the actual distribution of soil moisture cannot be realistically simulated [*Ravi and Williams*, 1998]. The TopoFlow formulation of the Green-Ampt equation is only valid for simulations of a single precipitation event. The infiltration rate using the Green-Ampt equation is as follows:

$$IN = \frac{(K_{sat} - K_i) \cdot (G \cdot (\theta_s - \theta_i) + I')}{I'} + K_i \tag{4.14}$$

where $K_{sat}$ and $K_i$ are the saturated and initial hydraulic conductivities of the soil, $[m/s]$; and $\theta_s$ and $\theta_i$ are the saturated and initial soil moisture content, [*unitless*].

*Rawls et al.* [1992] estimated the capillary drive parameter, $G$, as:

$$G = \frac{2 \cdot b + 3}{2 \cdot b + 6} \cdot \psi_b \tag{4.15}$$

where $b$ is the pore size distribution index, [*unitless*], and $\psi_b$ is the air entry tension, $[m]$. Estimates of $b$ and $\psi_b$ for different soil types are listed in Table 4.1.

The incremented infiltration depth, $I'$ $[m]$, is defined as:

$$I' = I - K_i t \tag{4.16}$$

where $I$ is the cumulative infiltration depth, $[m]$, and $t$ is time, [*sec*].

$$I = \frac{(K_s - K_i) \cdot (\theta_s - \theta_i) \cdot G}{IN} \tag{4.17}$$

*Smith-Parlange 3-parameter infiltration.* Based upon Darcy's Law and conservation of mass principal, a two-branch model for ponding time and infiltration is based on two assumptions regarding the behavior of the unsaturated hydraulic conductivity near saturation. The first assumption is that hydraulic conductivity varies slowly near saturation. The second assumption is the unsaturated hydraulic conductivity varies exponentially near saturation and includes an estimate of ponding time [*Smith and Parlange*, 1978]. As with the Green-Ampt formulation, a number of simplifying assumptions are made - uniform, homogeneous soil of infinite depth, horizontal surface, and a uniform antecedent soil moisture profile. The TopoFlow formulation of the Smith-Parlange infiltration model describes the total infiltrated depth of the soil profile, but does not provide the actual soil moisture distribution. Like the Green-Ampt formulation, the Smith-Parlange 3-parameter infiltration model is valid only for simulating the infiltration of a single precipitation event. The Smith-Parlange 3-parameter [*Smith and Parlange*, 1978] infiltration model is:

$$IN = K_s + \frac{\zeta \cdot (K_s - K_i)}{exp\left(\frac{\zeta \cdot I'}{G \cdot (\theta_s - \theta_i)}\right)} \tag{4.18}$$

where $\zeta$ is a weighting factor, ranging between 0 - 1. The $\zeta$-value of most soils ranges between 0.8 and 0.85 [*Smith*, 2002].

*Instantaneous Infiltration.* In the Arctic, ice-rich permafrost restricts hydrologic processes to the shallow depth of the active layer. Near surface arctic organic soils are typically very porous and have a large hydraulic conductivity, readily absorbing and releasing snowmelt and summer precipitation waters. Underlying these organic soils, a lower conductivity mineral soil is present. The vertical flow rate of snowmelt or rain water to reach the near surface groundwater table is significantly faster than the lateral flow through the mineral soils [*Zhang et al.*, 2000]. As a result the assumption is made that in the area of continuous permafrost, surface waters (derived from either snowmelt or rainfall) instantaneously percolate to the groundwater table upon reaching the ground surface. In using this method of infiltration, overland flow only occurs once the groundwater table rises above the surface elevation. The formulation for this process is as follows:

$$IN = (SM + P) \tag{4.19}$$

where $IN$ is the infiltration rate, $[m/s]$; $SM$ is the snowmelt rate $[m/s]$; and $P$ is the rainfall rate $[m/s]$.

**Overland and channel Flow**

The integral form of the mass balance for surface flows can be written as

$$\frac{\partial}{\partial t}\int_{\Omega} \rho_w R dA_c = \int_{\Omega} \rho_w dA_c - \int_{\partial\Omega} (\hat{n} \cdot \rho_w \langle \underline{v} \rangle d) d(wb) \tag{4.20}$$

where $\rho_w$ is the density of water, $A_c$ is the cross-sectional area, $\langle v \rangle$ denotes the vertically-averaged downstream velocity, $d$ is the flow depth, $wb$ is the characteristic channel width, and $R$ is the effective rainrate. The effective rainrate is the net sum of all vertical hydrologic processes to an element

Table 4.1. Representative values parameters used in the finite difference solution of the Richards equation and Green-Ampt equation for a variety of soils. Values of porosity, saturated hydraulic conductivity, air entry tension, and pore size distribution indexes. Values in parentheses are standard deviations. Table modified from *Dingman* [2002] and *Williams et al.* [1998]. Data from *Clapp and Hornberger* [1978]; *Brakensiek et al.* [1981]; *Panian* [1987]; *Carsel and Parrish* [1988].

| **Soil Texture** | **Porosity** | $K_{sat}$ $[m/s]$ | $\psi_b$ $[m]$ | **b** | $\lambda$ |
|---|---|---|---|---|---|
| Sand | 0.395 (0.056) | 1.76E-4 | 12.1 (14.3) | 4.05 (1.78) | 0.4 - 1.68 |
| Loamy Sand | 0.410 (0.068) | 1.56E-4 | 9.0 (12.4) | 4.38 (1.47) | 0.46 -1.28 |
| Sandy Loam | 0.435 (0.086) | 3.47E-5 | 21.8 (31.0) | 4.90 (1.75) | 0.40 - 0.89 |
| Silt Loam | 0.485 (0.059) | 7.20E-6 | 78.6 (51.2) | 5.30 (1.96) | 0.22 - 0.42 |
| Loam | 0.451 (0.078) | 6.95E-6 | 47.8 (51.2) | 5.39 (1.87) | 0.26 -0.56 |
| Sandy clay loam | 0.420 (0.059) | 6.30E-6 | 29.9 (37.8) | 7.12 (2.43) | 0.37 - 0.48 |
| Silty clay loam | 0.477 (0.057) | 1.70E-6 | 35.6 (37.8) | 7.75 (2.77) | 0.18 - 0.36 |
| Clay loam | 0.476 (0.053) | 2.45E-6 | 63.0 (51.0) | 8.52 (3.44) | 0.28 -0.4 |
| Sandy clay | 0.426 (0.057) | 2.17E-6 | 15.3 (17.3) | 10.4 (1.64) | – |
| Silty clay | 0.492 (0.064) | 1.03E-6 | 49.0 (62.1) | 10.4 (4.45) | 0.09 - 0.38 |
| Clay | 0.482 (0.050) | 1.28E-6 | 40.5 (39.7) | 11.4 (3.70) | 0.09 - 0.41 |

$K_{sat}$: Saturated hydraulic conductivity; $\psi_b$: Air entry tension; b: Pore size distribution index
$\lambda$: Brooks-Corey pore size distribution coefficient.

$$R = (P + S) - (ET + I) \tag{4.21}$$

where, $P$, $S$, $ET$, and $I$ are respectively, the precipitation (rain and liquid water), subsurface flow, evapotranspiration, and infiltration rates, $[m/s]$. Applying a discretized version of Equation 4.20 to element $i$ in a TopoFlow flow grid (Figure 4.3c) the following results:

$$\frac{\Delta d(i,t)}{\Delta t}(\Delta x \Delta y) = R(i,t)(\Delta x \Delta y) + \sum_{k \in N} Q(k,t) - Q(i,t) \tag{4.22}$$

where $\Delta x$ and $\Delta y$ are the element dimensions, $\Delta t$ is the time step, and $N$ is the set of elements that have element $i$ as their parent.

$$Q(i,t) = \nu(i,t) d(i,t) \Delta w(i) \tag{4.23}$$

is the discharge from element $i$ to its "parent" element just downstream, $\nu$ is the fluid velocity, and $\Delta w(i)$ is the "differential" width of flow away from element $i$, which may be approximated with $\Delta x$ or $\Delta y$. Solving for $\Delta d$ yields

$$\Delta d(i,t) = \Delta t \left\{ \left[ \frac{\sum_{k \in N} Q(k,t) - Q(i,t)}{\Delta x \Delta y} \right] + R(i,t) \right\} \tag{4.24}$$

For a vertically-integrated hydrostatic flow, the momentum balance can be written

$$\frac{\partial}{\partial t} \int_\Omega \rho_w \langle \underline{\nu} \rangle d \, dA_c = \int_\Omega -\rho_w g d \nabla h dA_c + \int_\Omega \underline{\tau_b} (1 + \nabla b \cdot \nabla b)^{1/2} dA_c - \int_{\partial \Omega} d \langle \underline{\nu} \rangle (\hat{n} \cdot \rho_w \langle \underline{\nu} \rangle) d(wb) \tag{4.25}$$

where $\langle \nu \rangle$ is the vertically-integrated horizontal velocity, $d$ is the depth, $b$ is the height of the bed above an arbitrary datum, and $h = (d + b)$ is the free-surface height. The quantity $\tau_b$ is the horizontal component of the (total) shear stress of the bed, which include all of the momentum loss mechanisms in the problem, including skin friction due to grain roughness, and form (or pressure) drag due to bedforms, bars, and any other topographic elements. The factor $(1 + \nabla b \cdot \nabla b)^{1/2} dA_c$ is the differential surface area of the bed, $b$, which can be appreciably greater than $dA_c$ near the banks of the channel.

Applying a discretized (and channel-fitted) version of equation 4.25 to an element, $i$, in a TopoFlow flow grid, we get

$$\left[\frac{\Delta v(i,t)}{\Delta t}d(i,t) + \frac{\Delta d(i,t)}{\Delta t}v(i,t)\right](\Delta x \Delta y) = \sum_{k \in N} v(k,t)Q(k,t) - v(i,t)Q(i,t) + g d(i,t) S_{FS}(i,t)(\Delta x \Delta y) - f(i,t)v^2(i,t)(\Delta x \Delta y) \quad (4.26)$$

where $S_{FS}(i,t)$ is strictly the free-surface slope between element $i$ and its parent element. The drag coefficient, $f$, is given by

$$f = \left[\frac{\kappa}{\ln(\varpi d / z_0)}\right]^2 \quad (4.27)$$

where $z_0$ is the roughness parameter, $(z_0/\varpi d)$ is the relative roughness, $\kappa \approx 0.408$ is von Karman's constant, and $\varpi$ is an integration constant equal to 0.476.

Solving Equation 4.26 for $\Delta v(i,t)$ we get

$$\Delta v(i,t) = -\left[\frac{v(i,t)}{d(i,t)}\right] + \left(\frac{\Delta t}{d(i,t)}\right)\left\{\left[\frac{\sum_{k \in N} v(k,t)Q(k,t) - v(i,t)Q(i,t)}{\Delta x \Delta y}\right] + g d(i,t) S(i,t) - f(i,t)v^2(i,t)\right\} \quad (4.28)$$

Substituting $\Delta d(i,t)$ from Equation 4.24, Equation 4.28 simplifies to

$$\Delta v(i,t) = \left(\frac{\Delta t}{d(i,t)}\right)\left\{\frac{\sum_{k \in N}[v(k,t) - v(i,t)]Q(k,t)}{\Delta x \Delta y}\right\} + \left(\frac{\Delta t}{d(i,t)}\right)[-R(i,t)v(i,t) + g d(i,t) S_{FS}(i,t) - f(i,t)v^2(i,t)] \quad (4.29)$$

Using Equation 4.23, $Q(i,t)$ can be eliminated from Equations 4.24 and 4.29 resulting in the flow depth and downstream velocity change for each element in a time increment, $\Delta t$, as a function of the velocity and depth at time, $t$.

$$\nu(i, t + \Delta t) = \nu(i, t) + \Delta\nu(i, t) \tag{4.30}$$

$$d(i, t + \Delta t) = d(i, t) + \Delta d(i, t) \tag{4.31}$$

Given the flow depth, the kinematic wave solution is used to calculate both channel and overland flow when flow depth, $d$, in an element is positive. A positive flow depth occurs when either the water table exceeds the land surface elevation or when the infiltration capacity of the soils is exceeded by the precipitation rate. Using the kinematic wave assumption, the friction slope ($S_f$) and the bed slope ($S_o$) are equal. The Manning equation can then be used to express the relationship between flow and depth:

$$q = \nu \cdot A_c = \frac{A_c}{N} R_H^{2/3} \sqrt{S_f} \tag{4.32}$$

where $q$ is the rate of lateral flow per unit length [$m^3/s/m$]; $\upsilon$ is the fluid velocity, [$m/s$]; $R_H = A_c/PW$ is the hydraulic radius, [$m$]; $PW$ is the wetted perimeter, [$m$]; $N$ is the Manning's roughness coefficient, [unitless]; and $A_c$ is the cross-section area, $wb \cdot d$, [$m^2$].

A characteristic channel width ($wb$), bank angle ($\theta_{rad}$), and Manning's roughness coefficient ($n$) are assigned for each Horton-Strahler Order number (or rank) number (see Section 4.2.2). A characteristic channel cross-section is defined for each stream segment having a specific order number. A channel cross section can be defined as a trapezoid, a triangle, or a rectangle (Figures 4.7a-c). We further assume that overland flow occurs as a sheet flow. Using this assumption, $R_H \approx d$. For elements in which overland flow will occur (i.e. lower-order Horton-Strahler elements which have been 'pruned' from the channel network tree), the characteristic channel width is set to the width of the element (the DEM dimension) (Figure 4.7d).

**Model performance**

A process simulation analysis was conducted to compare the model performance characteristics when the process time interval, process methods, and data types are varied. The analysis was performed on a 64-bit Linux work station equipped with an Advanced Micro

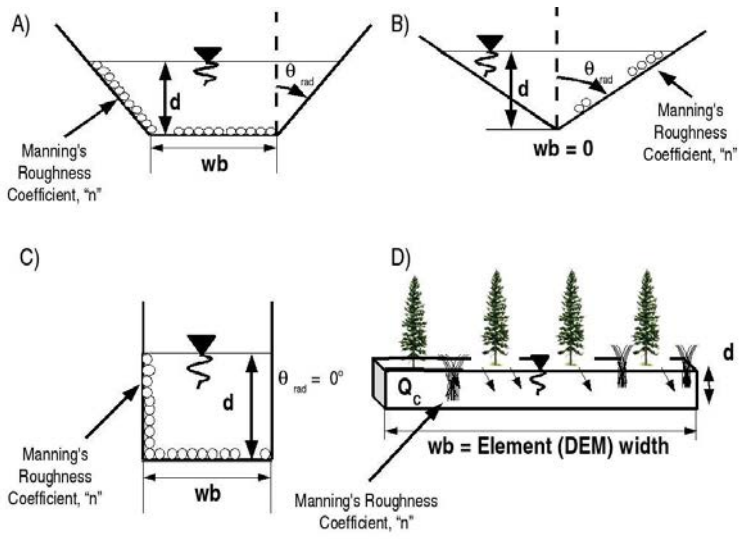


Figure 4.7. Overland and Channel Flow components.

Devices (AMD) Opteron 250 CPU and 2 gigabytes RAM. The model domain used in this analysis has dimensions of 29 columns by 38 rows by 3 soil layers.

Six simulations were conducted in this analysis. The duration of each simulation was 200,000 time-steps (20 seconds per time-step). For each simulation, the following processes were simulated: overland/channel flow, snowmelt, evapotranspiration, infiltration, soil moisture content (derived from soil characteristic curves, see Section 4.2.4), and groundwater flow. Output was limited to a single element and the overland/channel flow process every 180 time-steps (60 minutes).

The time interval used in Tests 1, 3, 5, and 6 are user specified and vary for each process. For overland/channel flow, the time interval is 20 seconds (the model time-step). The snowmelt, evapotranspiration, infiltration, and soil moisture content processes each use a time-step of 60 minutes. The time step for groundwater flow is set at 24 hours. For Tests 2 and 4, a 20-second time-step is used for every process. In order to maintain model stability, the maximum allowable model time-step is limited by the Courant condition. For model domain used in this analysis, the maximum allowable-time step that satisfies the Courant condition is 20 seconds.

The effect of method complexity of model performance was tested varying the snowmelt

and evapotranspiration processes. In Tests 1, 2, and 5, the more relatively complex Energy Balance method of snowmelt and evapotranspiration were simulated. In Tests 3, 4, and 6, the relatively less complex methods of Degree-day method for snowmelt and the Priestley-Taylor method for evapotranspiration were simulated.

The model performance using different types of input data was explored. In Tests 1-4, data input consisted of grid sequences, binary files that vary in both time and space. For Test 5 and 6, input data consisted of time series files, ASCII files that are only temporally variable. Uniform soil properties are used for the groundwater flow process, with values read from an input table. A summary of the test simulations is presented in Table 4.2.

Results from this analysis display the advantage of an independent time-step for each hydrologic process simulated. In order to maintain model stability, the maximum allowable model time-step is limited by the Courant condition. As the vast majority of hydrologic processes operate on at a much slower time scale, defining the appropriate time-step for each process (based upon either the hydrologic process or resolution of the input data) is computationally advantageous. Comparison of the total simulation times for Tests 1-4 show that utilization of process specific time-steps results in approximately a factor of five reduction in total computational time. The computational efficiency of process specific time-steps would be higher for either a longer simulation period or a larger model domain.

Comparison of the snowmelt and evapotranspiration process in Tests 1-4 demonstrate the complexity of the process simulated is proportional to computational time. This is specifically evident when comparing the snowmelt results from Test 2 (Energy Balance method, requiring seven function calls) and Test 4 (Degree-day method, requiring one function call). The computational difference between these two methods, for these two simulations, is nearly 9%.

The format of the input data result in a slight difference in the total computational time (comparing Tests 1 & 5 and Tests 3 & 6), with the time series data format slightly slower than the grid sequence format. The difference in computational time is reflected exclusively in the precipitation and stream flow processes. The input variables of the stream flow process are identical for Tests 1-6, meaning the format of the precipitation data has a direct impact on the computational efficiency of the stream flow process. This is in part due to the fact variable precipitation durations are allowed in the time-series input method.

Table 4.2. Summary of the TopoFlow process analysis. Simulation characteristics are represented in the following order: Process time interval (PS= process specific, U = uniform), Process complexity (> = high complexity, < = low complexity), and Input data format (G = variable grid sequence, T = ASCII string, uniform spatial properties).

| | **Test 1** PS,>,G | **Test 2** U,>,G | **Test 3** PS,<,G | **Test 4** U,<,G | **Test 5** PS,>,T | **Test 6** PS,<,T |
|---|---|---|---|---|---|---|
| **Process** | Time (min) [%] | Time (min) [%] | Time (min) [%] | Time (min) [%] | Time (min) [%] | Time (min) [%] |
| Precipitation | 0.01 [0.47] | 0.02 [0.1] | 0.01 [0.47] | 0.02 [0.12] | 0.15 3.96 | 0.14 [3.62] |
| Stream flow | 1.65 [51.96] | 2.53 [14.7] | 1.65 [51.86] | 2.45 [16.8] | 2.12 [55.62] | 2.1 [55.94] |
| Snowmelt | 0.02 [0.62] | 2.28 [13.21] | 0.01 [0.38] | 0.64 [4.4] | 0.02 [0.42] | 0.01 [0.28] |
| Evapotrans-piration | 0.02 [0.51] | 1.36 [7.91] | 0.01 [0.44] | 1.21 [8.28] | 0.01 [0.33] | 0.01 [0.34] |
| Infiltration | 0.05 [1.5] | 0.06 [0.34] | 0.05 [1.52] | 0.06 [0.4] | 0.05 [1.27] | 0.05 [1.28] |
| Groundwater flow | 0.01 [0.3] | 9.34 [54.18] | 0.02 [0.62] | 8.55 [58.7] | 0.01 [0.28] | 0.01 [0.27] |
| Soil moisture | 0.01 [0.24] | 0.08 [0.47] | 0.01 [0.26] | 0.08 [0.55] | 0.01 [0.2] | 0.01 [0.2] |
| Effective rain rate | 0.06 [1.92] | 0.08 [0.44] | 0.06 [1.89] | 0.08 [0.52] | 0.06 [1.62] | 0.06 [1.66] |
| Update flow volume | 0.2 [6.2] | 0.23 [1.36] | 0.2 [6.19] | 0.23 [1.59] | 0.19 [5.09] | 0.19 [5.11] |
| Update flow depth | 0.8 [25.21] | 0.88 [5.09] | 0.8 [25.19] | 0.88 [6.05] | 0.83 [21.85] | 0.82 [21.9] |
| Output | 0.04 [1.09] | 0.04 [0.23] | 0.04 [1.12] | 0.04 [0.26] | 0.03 [0.91] | 0.03 [0.93] |
| Display progress | 0.03 [0.88] | 0.02 [0.12] | 0.03 [0.98] | 0.02 [0.13] | 0.03 [0.89] | 0.03 [0.87] |
| Total simu-lation | 3.17 | 17.23 | 3.19 | 14.56 | 3.81 | 3.75 |
| Total process | 2.88 [90.91] | 16.91 [98.14] | 2.9 [90.91] | 14.24 [97.79] | 3.52 [92.44] | 3.47 [92.39] |

**Notes:** PS: Stream flow - 20 secs.; Precipitation, Snow melt, Evapotranspiration, and Soil moisture - 1 hour; Groundwater flow - 24 hours. U: All processes - 20 secs. > : Energy Balance method used for both the Snow melt and Evapotranspiration processes. < : Degree-day method and Priestley-Taylor used for the Snow melt and evapotranspiration processes, respectively. G: Grid sequence (spatial and temporal variation) files used as input data format. T:Time series (temporal variation) files are used as input data format. Soil properties in the Groundwater process are input from a table. Total simulation and Total process represent the total time required to complete each test simulation and simulated hydrologic processes, respectively.

Table 4.3. TopoFlow Calculations Available for Output.

| Hydrologic Process | Output Available |
|---|---|
| Snowmelt | Snowdepth |
| | Snow water equivalent |
| | Snowmelt rate |
| Evapotranspiration | Evapotranspiration rate |
| Infiltration | Infiltration rate |
| | Total infiltrated depth |
| Subsurface flow | Water table elevation |
| | Volumetric soil moisture content |
| Surface flow | Discharge |
| | Flow velocity |
| | Flow depth |
| | Drag coefficient |

When this method is used, a precipitation function call occurs at each time-step to check for changes in the precipitation rate. Conversion of ASCII data into binary format and spatial distribution of point data may , in part, account for a lower computational efficiency.

The computational efficiency is largely dependent upon process time-step used, the size of the model domain, the length of simulation, method complexity, and format of the precipitation input data. Additional computational time is required in passing data between model components. The difference between the total simulation time and the total process time is 0.30 minutes (range 0.28 - 0.32 minutes) and is independent of process complexity, process time-step, and input data format.

### 4.2.4 Model output

For each hydrologic process simulated, TopoFlow is able to output a number of parameters calculated during the simulation. TopoFlow has two types of output. The first type of output is a time series at a specified element(s). The second is spatially distributed values for each element within the model domain. The time interval for both types of output is user specified for each hydrologic process. Table 4.3 shows the calculations available for output.

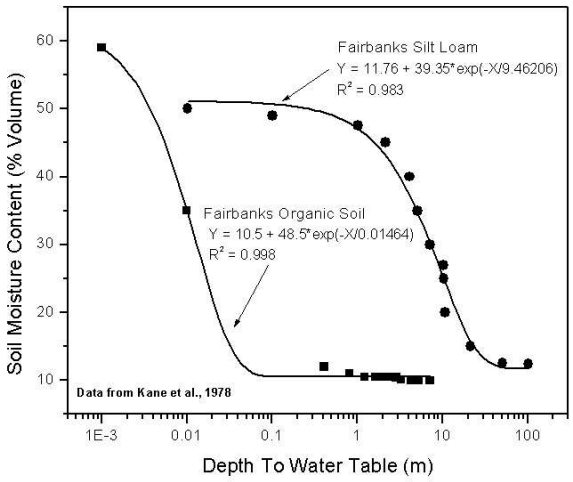


Figure 4.8. Soil moisture characteristic curves for Fairbanks Organic soil and Fairbanks Silt Loam. A first-order exponential decay equation (with the form $Y = y0 + A1exp(-X/t1)$)) is used to fit the soil moisture characteristic curve data. Soil data from *Kane et al.* [1978].

**Soil moisture content from soil moisture characteristic curves**

The volumetric soil moisture content may be obtained from the position of the water table and a soil moisture characteristic curve for each soil layer. A first-order exponential decay equation (with the form $Y = y0 + A1 \cdot \exp(-X/t1)$, is used to fit the soil moisture characteristic curve data (Figure 4.8). For each soil layer, the coefficients $y0$, $A1$, and $t1$, are input into TopoFlow. The soil moisture content is calculated, at the specified time interval, based on the distance between the top of each soil layer and the water table. In order to reduce the computational time, the soil moisture content is only calculated for soil layers which output is specified.

Near surface soil moisture dynamics to rapid wetting and drying events are not captured using this method. However, this appears to be an viable and efficient method of determining the long-term moisture content of deeper soil layers or in areas of continuous permafrost, as the water table typically is located at or near the land surface.

**TopoFlow output tools**

TopoFlow has two post-processing tools that provide immediate graphical feedback of simulation output files. The first tool displays the time series output from a single specified element. The upper panel of Figure 4.9 shows an example of this tool. The second tool displays, in animation form, spatially distributed output for the entire model domain. The lower series of images in Figure 4.9 display example snapshots from a grid sequence output file of water velocity. The color scheme of the animation tool is defined such that low output values correspond to 'cool' or darker colors, while high output values correspond to 'hot' lighter colors. Particle tracking is also possible as red pixels are randomly placed in the animation track the position throughout the duration of the animation. The particle tracking feature is most useful for output variables where lateral exchange of water from element to element take place (overland/channel flow volume, overland/channel velocity, groundwater flow, etc.) The TopoFlow dialog box provides additional information including the largest and smallest values displayed in the animation. With these tools, rapid visualization and analysis of simulation results is possible without the use of external programs.

## 4.3 Model Discussion and Conclusions

The sub-arctic ecosystem represents an important transitional region between the temperate and arctic environments. Many of the observed and predicted changes in the arctic hydrologic system will occur in this region first, as the permafrost conditions are very warm and unstable. Soil moisture is an important variable in most hydrologic and thermal processes in the (sub-)Arctic including permafrost distribution, stream flow, carbon flux, and energy balance processes. Soil moisture is also the common link between the terrestrial and atmospheric systems. In this environment, accurate prediction of the soil moisture and streamflow regimes, at the watershed scale, is essential in developing a more complete understanding of local and regional scale climatic processes.

In every environment, accurate prediction of hydrologic processes requires addressing a number of challenges distinct to the system. The sub-arctic environment is no exception. In this paper, a number of challenges to hydrologic modeling in the sub-arctic environment are identified. The challenges identified include the discontinuous distribution of

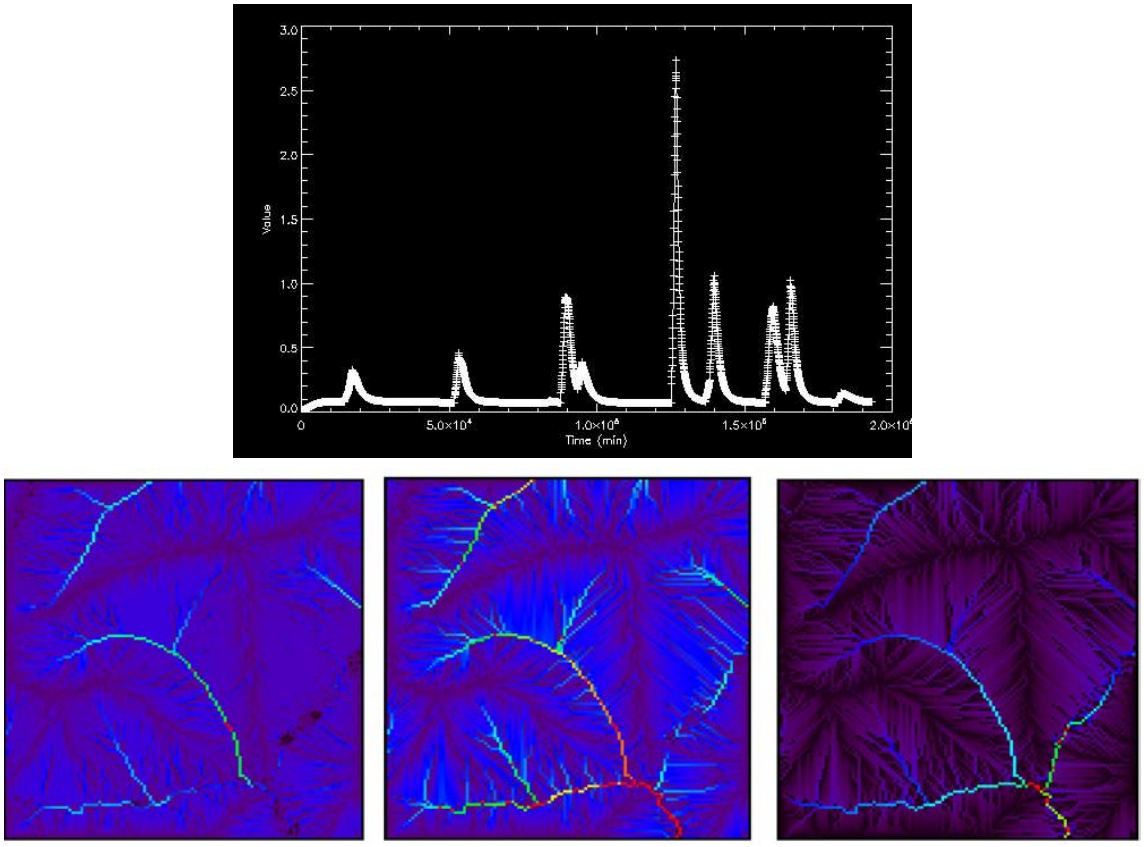


Figure 4.9. TopoFlow output tools. TopoFlow has two tools providing immediate graphical feedback of simulation output files. The upper panel shows an example, in this case discharge, of simulated output from a single specified element at a specified interval. The lower series of images are from an TopoFlow animation tool which displays spatially distributed output at a specified interval. The animation utility displays 'high' values with 'warm' light colors and 'low' values with 'cold' darker colors. Particle tracking is also possible with red pixels that are randomly placed in the animation. The TopoFlow dialog box provides additional information including the range of values displayed throughout the animation.

permafrost resulting in an environment where the hydraulic conductivity and storage capacity of the soil can vary greatly over short spatial (x-, y-, and z-directions) and temporal (short- and long-term) scales. Additional challenges include multiple, distinct groundwater systems, hydrologic processes which operate on different time scales, and a limited number of meteorologic data collection stations. The hydrologic model described in this paper, TopoFlow, is designed to address each of these challenges.

The structure and execution of TopoFlow is very flexible. A number of methods, ranging from the relatively simple to the complex, are available for every hydrologic process simulated (including the option 'None'). As every hydrologic in the sub-arctic operates on different time scales, each hydrologic process is simulated on user specified time-steps. For nearly every input variable, four separate data formats are allowed (scalar, time series, grid, and grid sequence). Finally, a number of hydrologic variables are available for output. Output variables, from either specified elements or the entire model domain, are also produced at user specified time-steps. TopoFlow is able to handle each of these features without changing the source code.

TopoFlow is also designed to be a user friendly, community-based hydrologic model. With the hydrologic community/modeler in mind, TopoFlow incorporates a wizard-style GUI; on-line help dialogs; open source code which is well documented; and a number of pre- and post-processing tools. The modular design of TopoFlow allows members of the hydrologic community to add additional processes or methods without altering the overall functionality and structure of the model. With these features, TopoFlow is designed to evolve and serve the broad hydrologic community as new challenges arise.

The performance of TopoFlow is dependent upon a number of factors such as the size of the model domain and duration of the simulation period. Additional factors include method complexity, process time-step, and format of the input data. The complexity of the hydrologic method simulated is proportional to the simulation time. As the time-step used by TopoFlow is limited by the Courant condition, it is important that for each hydrologic processes simulated, an appropriate time-step is used. The availability of meteorologic data may or may not warrant creating spatial and temporal input data sets. However, the computational efficiency of TopoFlow increases if grid sequence files are utilized. Creating grid sequence files is a simple task using the available pre-processing tools.

TopoFlow simulates the major components of water balance (precipitation, snowmelt, evapotranspiration, groundwater flow, and overland/channel flow) and some storage processes (snow accumulation and Richards Equation soil moisture). Significant improvements in the model design and processes simulated have been made since the release of the ARHYTHM model. The overland/channel flow process has significantly improved by defining characteristic channel properties by order number and incorporating a robust flow routing mechanism. Process specific time-steps and multiple data formats make possible a hydrologic model flexible enough to handle spatial and temporal created by the discontinuous permafrost condition.

A number of storage processes, important in the sub-arctic environment, are not currently incorporated into TopoFlow. Storage processes such as aufeis accumulation and melt, precipitation interception, and surface storage (lakes or ponds), have not been addressed. Active layer development is based upon a simple $\alpha\sqrt{Time}$ formulation. This simple formulation of the active layer provides a reasonable estimate of the active layer depth. However, as the position of the active layer impacts many of the hydrologic processes, including stream flow and soil moisture dynamics, this process should be treated in a more robust manner.

Future plans for TopoFlow development include enhancements to both the model structure and incorporation of additional hydrologic processes. The basic structure of TopoFlow will be examined and modified to allow simulations from a 'batch' file (multiple simulations completed using one instruction file) and to run on multiple computer processors (high performance computing platform). Additional hydrologic processes such as nutrient, contaminant, and sediment transport, landform evolution, and lake storage are also being planned for future releases. In order to accurately assess the hydrologic impact of a changing permafrost condition, a spatially distributed thermal model which describes the presence or absence of permafrost and active layer depth as a function of soil properties, soil moisture, and climate, will be incorporated into TopoFlow.

### 4.4 Acknowledgments

Support for this research was provided by the U.S. National Science Foundation Arctic System Science Program (OPP-0229705), the U.S. National Science Foundation Division of

Environmental Biology under the Long Term Ecological Research Program (Grant number DEB-9211769), a fellowship from the Inland Northwest Research Alliance (U.S. Dept. of Energy contract DE-FG07-021D14277), and a grant from the Center of Global Change - University of Alaska Fairbanks.

The TopoFlow source code and executables may be downloaded from http:// instaar. colorado.edu/topoflow. TopoFlow maybe used for free but is subject to the GNU license agreement (found on the TopoFlow website). You are permitted to use, study or modify it for your own needs but you may not publish, sell or distribute it in any form without the written permission of the authors. You may not remove the copyright notices or use the TopoFlow name for another program. It you use results from TopoFlow for a publication, the authors would greatly appreciate an acknowledgment and a reprint. The purpose of freely sharing this source code is to encourage further developments and code sharing by a user community of hydrologists.

## 4.5 Appendix

Table 4.4: Simulated processes and formulation used in TopoFlow. A listing of the symbols used in this table are found in Table 4.5.

| Process | Method | Formula | Equation |
|---|---|---|---|
| Snowmelt | Energy Balance | Energy Balance of the Snowpack | $Q_m = Q_{net} + Q_h + Q_e + Q_a + Q_c - Q_{cc}$ |
| | | Sensible Heat Flux | $Q_h = \rho_a \cdot C_{pa} \cdot K_h \cdot dT/dz$ $= \rho_a \cdot C_{pa} \cdot D_h \cdot (T_a - T_s)$ |
| | | Latent Heat Flux | $Q_e = \rho_a \cdot L_v \cdot K_e \cdot dq/dz$ $= \rho_a \cdot L_v \cdot D_e \cdot (0.622/p) \cdot (e_a - e_s)$ |
| | | Bulk Exchange Coefficient for Atmospheric Stability ($T_a = T_s$) | $D_n = \kappa^2(u_z)/[\ln((z-h)/z_0)]^2$ |
| | | Bulk Exchange Coefficient for Unstable Atmosphere ($T_a < T_s$) | $D_{(u)} = D_n/(1 + 10 \cdot R_i)$ |
| | | Bulk Exchange Coefficient for Stable Atmosphere ($T_a > T_s$) | $D_{(s)} = D_n \cdot (1 - 10 \cdot R_i)$ |
| | | Richardson Number | $R_i = \frac{gz \cdot (T_a - T_s)}{u_z^2 \cdot (T_a + 273.15)}$ |
| | | Roughness Length | $z_0 = exp \left\lvert \frac{u_2 \ln(z_1) - u_1 \ln(z_2)}{u_2 - u_1} \right\rvert$ |
| | | Cold Content | $Q_{cc} = h_{sn} \cdot \rho_s \cdot C_p \cdot (T_0 - T_{sn})$ |
| | | Snowmelt rate | $M = (1000 \cdot Q_m)/(\rho_w \cdot L_f)$ |
| | Degree-Day | Degree-Day Melt Rate | $M = C_0(T_a - T_0)/S$ |
| Evapotranspiration | Energy Balance | Energy Balance ET | $Q_{ET} = Q_{net} + Q_h + Q_c$ |
| | | Conductive Heat Flux | $Q_c = K_s \cdot \frac{T_x - T_s}{x}$ |
| | | Evapotranspiration Rate | $M_{ET} = \frac{1000 \cdot Q_{ET}}{\rho_w \cdot L_v}$ |

Continued on next page...

Table 4.4 – Continued

| Process | Method | Formula | Equation |
|---|---|---|---|
| | Priestley-Taylor Method | Priestley-Taylor equation | $Q_{ET} = \alpha \cdot \left(\frac{s}{s+\gamma}\right)(Q_{net} - Q_c)$ |
| | | Stewart & Rouse Approximation | $\frac{s}{s+\gamma} = 0.406 + 0.011 T_a$ |
| Infiltration & Percolation | Richards Equation | Richards Infiltration Rate | $\frac{\partial \theta}{\partial t} = \frac{\partial}{\partial z}\left[K\frac{\partial \psi}{\partial z} - K\right]$ |
| | | Finite Difference Solution Richard Equation | $\frac{\theta^j - \theta^{j-1}}{\Delta t} = \frac{-2}{(z_{i+1} - z_{i-1})} \cdot \left[\overline{K}_{i,i+1}\left(\frac{\psi_{i+1} - \psi_i}{\Delta z_{i,i+1}} - 1.0\right) - \overline{K}_{i,i+1}\left(\frac{\psi_i - \psi_{i-1}}{\Delta z_{i,i-1} - 1.0}\right)^{j-1}\right]$ |
| | | Brooks - Corey Relationship | $\psi(\theta) = \psi_b \cdot \theta_e^{1.0/\lambda}$ |
| | | Transitional Brooks-Corey Relationship | $\theta_e = \left[1 + \left(\frac{\psi + \psi_a}{\psi_b}\right)^c\right]^{-\frac{\lambda}{c}}$ |
| | | Unsaturated Hydraulic Conductivity | $K(\psi) = K_s \cdot K_r$ |
| | | Relative Hydraulic Conductivity | $K_r = \left[1 + \left(\frac{\psi + \psi_a}{\psi_b}\right)^c\right]^{-\frac{\eta}{c}}$ |
| | | Conductivity exponent Parameter | $\eta = 2.0 + (3.0 \cdot \lambda)$ |
| | | Wetting Front Velocity | $u_s(\theta_u, \theta_l) = \frac{K(\theta_u) - K(\theta_l)}{\theta_u - \theta_l}$ |
| | Green-Ampt, Single Event | Green-Apmt Infiltration Rate | $IN = \frac{(K_s - K_i)(G \cdot (\theta_s - \theta_i) + I')}{I'} + K_i$ |

Continued on next page...

Table 4.4 – Continued

| Process | Method | Formula | Equation |
|---|---|---|---|
| | | Capillary Drive Parameter | $G = \frac{2 \cdot b+3}{2 \cdot b+6} \cdot \psi_b$ |
| | | Incremented Soil Moisture Depth | $I' = \frac{G \cdot (\theta_s - \theta_i) \cdot (K_s - K_i)}{IN - K_s}$ |
| | Smith-Parlange 3-Parameter Infiltration | Smith-Parlange Infiltration Rate | $IN = K_s + \frac{\gamma \cdot (K_s - K - i)}{exp\left(\frac{\gamma \cdot I'}{G \cdot (\theta_s - \theta_i)}\right)}$ |
| | Instantaneous Infiltration | Instantaneous Rate | $IN = (P + SM)$ |
| Subsurface Flow | Darcy's Law | Darcy Flow | $Q = K \cdot Sh \cdot dw \cdot y$ |
| | | Total Darcy Flow | $Q_T = \sum_{i=1}^{n} (K_i \cdot Sh_i \cdot dw_i \cdot y_i)$ |
| Overland & Channel Flow | Manning's Equation | Manning Formula | $Q_c = R^{2/3} \cdot A_c \cdot \sqrt{S}/N$ |
| | | Hyrdaulic Radius | $R_H = A_C/PW$ |
| | | Cross-Sectional Area | $A_C = d \cdot (wb + (d \cdot tan(\theta_{rad})))$ |
| | | Wetted Perimeter | $PW = wb + (2.0 \cdot d/cos(\theta_{rad})$ |

Table 4.5: List of symbols used.

| Symbol | Meaning | Unit |
|---|---|---|
| $A_c$ | Cross sectional area of stream channel | $m^2$ |
| $a$ | Area draining through a point upslope | $m^2$ |
| $b$ | Pore size distribution index | |
| $c$ | Curvature parameter | |
| $C_o$ | Degree-day melt factor | $mm/^oCday$ |
| $C_p$ | Heat capacity of snow | $J/kg^oC$ |
| $C_{pa}$ | Specific heat of air | $J/kg/^C$ |
| $D_e$ | Bulk exchange coefficient for vapor | $m/s$ |
| $D_h$ | Bulk exchange coefficient for heat | $m/s$ |
| $d$ | Channel flow depth | $m$ |
| $dx$ | Element width | $m$ |
| $ET$ | Evapotranspiration rate | $m/s$ |
| $e_a$ | Air vapor pressure | $mbar$ |
| $e_s$ | Surface vapor pressure | $mbar$ |
| $f$ | Drag coefficient | |
| $G$ | Capillary drive parameter | $m$ |
| $GW$ | Ground water flow rate | $m/s$ |
| $g$ | Gravitational constant | $m/s$ |
| $h$ | Free surface height | $m$ |
| $h_{sn}$ | Snow depth | $m$ |
| $I$ | Cumulative infiltration depth | $m$ |
| $IN$ | Infiltration rate | $m/s$ |
| $i$ | Element in TopoFlow flow grid | |
| $I'$ | Incremented infiltration depth | $m$ |
| $j$ | Reference time step | |
| $K$ | Hydraulic conductivity | $m/s$ |

Continued on next page...

Table 4.5 – Continued

| Symbol | Meaning | Unit |
|---|---|---|
| $\overline{K}$ | Mean hydraulic conductivity | $m/s$ |
| $K_e$ | Eddy diffusivity for water vapor | $m^2/s$ |
| $K_h$ | Eddy diffusivity for heat | $m^2/s$ |
| $K_i$ | Initial hydraulic conductivity | $m/s$ |
| $K_r$ | Relative hydraulic conductivity | $m/s$ |
| $K_s$ | Thermal conductivity of soil | $W/m^oC$ |
| $K_{sat}$ | Saturated hydraulic conductivity | $m/s$ |
| $k$ | Reference to 'kid' element | |
| $L_f$ | Latent heat of fusion | $J/kg$ |
| $L_v$ | Latent heat of vaporization | $J/kg$ |
| $l$ | Subscript to indicate lower boundary of soil layer | |
| $M$ | Snow water equivalent | $m$ |
| $M_{ET}$ | Water loss through evapotranspiration | $m$ |
| $N$ | Set of elements that have element 'i' as their parent | |
| $n$ | Manning roughness coefficient | |
| $P$ | Rainfall rate | $m/s$ |
| $P_T$ | Precipitation (rain and/or snow) rate | $m/s$ |
| $PW$ | Wetted perimeter of channel | $m$ |
| $p$ | Atmospheric pressure | $mbar$ |
| $p_g$ | Gravitational coefficient | |
| $Q_{CH}$ | Overland or stream flow | $m^3/s$ |
| $Q_a$ | Advective heat flux | $W/m^2$ |
| $Q_c$ | Conductive heat flux | $W/m^2$ |
| $Q_{cc}$ | Cold content of the snowpack | $W/m^2$ |
| $Q_{ET}$ | Energy utilized to evaporate water | $W/m^2$ |
| $Q_e$ | Latent heat flux | $W/m^2$ |
| $Q_h$ | Sensible heat flux | $W/m^2$ |
| $Q_m$ | Energy utilized to melt snow | $W/m^2$ |

Continued on next page...

Table 4.5 – Continued

| Symbol | Meaning | Unit |
|---|---|---|
| $Q_{net}$ | Net radiation | $W/m^2$ |
| $q$ | Rate of lateral flow per unit length | $m^2/s$ |
| $R$ | Effective rainrate | $m/s$ |
| $R_H$ | Hydraulic radius | $m$ |
| $R_i$ | Richardson number | |
| $S$ | Number of time-steps per day | |
| $Sh$ | Slope of the groundwater surface in an element | |
| $SM$ | Snowmelt rate | $m/s$ |
| $s$ | Slope of the specific humidity and temperature curve | $^oC^{-1}$ |
| $S_f$ | Friction slope | |
| $S_{FS}$ | Free-surface slope between elements | |
| $S_o$ | Bed slope | |
| $T$ | Average snow temperature | $^oC$ |
| $T_a$ | Air temperature | $^oC$ |
| $T_o$ | Temperature when snow reaches isothermal condition for melting | $^oC$ |
| $T_s$ | Surface temperature | $^oC$ |
| $T_sn$ | Snow temperature | $^oC$ |
| $T_x$ | Soil temperature at depth $x$ | $^oC$ |
| $t$ | Time | $sec$ |
| $u$ | Subscript to indicate upper boundary of soil layer | |
| $u_s$ | Kinematic shock velocity | $m/s$ |
| $u_{1,2}$ | Wind speed at height $z_{1,2}$ | $m/s$ |
| $\langle u \rangle$ | Vertically-averaged downstream velocity | $m/s$ |
| $v$ | Fluid velocity | $m/s$ |
| $vmax$ | Estimated maximum velocity a particle of water can travel | $m/s$ |

Continued on next page...

Table 4.5 – Continued

| Symbol | Meaning | Unit |
|---|---|---|
| $vmax_{chan}$ | Maximum velocity of a particle of water travels within a channel segment | $m/s$ |
| $wb$ | Characteristic bed width | $m$ |
| $x$ | Vertical depth into soil | $m$ |
| $y$ | Saturated depth of an element | $m$ |
| $z$ | Vertical height above ground surface | $m$ |
| $z_o$ | Roughness parameter or length | $m$ |
| $\alpha$ | Priestley-Taylor coefficient | |
| $\beta$ | Local slope angle | *radians* |
| $\eta$ | Conductivity exponent parameter | |
| $\Delta Storage$ | Change in water storage (all forms) | $m^3$ |
| $\Delta t$ | Model time step | *sec* |
| $\Delta w(i)$ | 'Differential' width of flow away from an element | $m$ |
| $\Delta x$ | Spatial distance between nodes | $m$ |
| $\Delta x$ | Element dimension in x-direction | $m$ |
| $\Delta y$ | Element dimension in y-direction | $m$ |
| $\Delta x$ | Spatial distance between nodes | $m$ |
| $\gamma$ | Psychrometric constant in terms of specific humidity | $^oC^{-1}$ |
| $\iota$ | Reference location used in Richard Equation | |
| $\kappa$ | von Karmon's constant | 0.408 |
| $\lambda$ | Pore-size distribution coefficient | |
| $\mu$ | Kinematic velocity of soil moisture wave | $m/s$ |
| $\omega$ | Weighting factor | |
| $\varpi$ | Integration constant | 0.476 |
| $\psi$ | Soil water capillary head | $m$ |
| $\psi_a$ | Small shift parameter used to approximate hysteresis | $m$ |
| $\psi_b$ | Air entry or 'bubbling' tension | $m$ |
| $\rho_a$ | Density of air | $kg/m^3$ |

Continued on next page...

Table 4.5 – Continued

| Symbol | Meaning | Unit |
|---|---|---|
| $\rho_s$ | Density of snow | $kg/m^3$ |
| $\rho_w$ | Density of water | $kg/m^3$ |
| $\tau_b$ | Shear stress of the channel bed | $N/m^2$ |
| $\theta$ | Volumetric soil water content | |
| $\theta_e$ | Effective saturation | |
| $\theta_i$ | Initial soil moisture content | |
| $\theta_r$ | Retained soil moisture content | |
| $\theta_s$ | Saturated soil moisture content | |
| $\theta_{rad}$ | Characteristic channel bank angle | *degrees* |
| $\xi$ | Weighting factor | |
| $\zeta$ | Weighting factor using in Smith-Parlange Infiltration | 0.8 -0.85 |

**Bibliography**

Abbott, M., J. Bathurst, J. Counge, P. O'Connell, and J. Rasmussen (1986), An introduction to the European Hydrological System - Systéme Hydrologique Européen 'SHE', 2: Structure of the physically based, distributed modeling system., *Journal of Hydrology*, *87*, 61–77.

ACIA (2005), *Impacts of a warming Arctic: Arctic Climate Impact Assessment*, 1046 pp., Cambridge University Press.

Alley, W., and P. Smith (1982), Distributed Routing Rainfall-Runoff Model - Version II, *Open File Report 82-344*, United States Geological Survey. 233 pp.

Anisimov, O., and F. E. Nelson (1997), Permafrost zonation and climate change: Results from transient general circulation models, *Climatic Change*, *35*, 241–258.

Arnell, N. (2005), Implications of climate change for freshwater inflows to the Arctic Ocean, *Journal of Geophysical Research*, *110*.

Arnold, J., P. Allen, and G. Bernhardt (1993), A comprehensive surface-groundwater flow model, *Journal of Hydrology*, *142*, 47–69.

Baldocchi, D., F. M. Kelliher, T. Black, and P. Jarvis (2000), Climate and vegetation controls on boreal zone energy exchange, *Global Change Biology*, *6*(Supplement 1), 69–83.

Bevin, K., and J. Freer (2001), Dynamic TOPMODEL, *Hydrologic Processes*, *15*(10), 1993–2011.

Bevin, K., and M. Kirkby (1979), A physically based variable contributing area model of catchment hydrology, *Hydrologic Science Bulletin*, *24*, 43–69.

Bicknell, B., J. Imhoff, J. Kittle, A. Donigian, and R. Johanson (1997), Hydrological simulation program - fortran, Users manual for version 11, *EPA/600/R-97/090*, United States Environmental Protection Agency. 755 p.

Boike, J., K. Roth, and P. Overduin (1998), Thermal and hydrologic dynamics of the active layer at a continuous permafrost site (Taymyr Peninsula, Siberia), *Water Resources Research*, *34*(3), 355–363.

Bolton, W., L. Hinzman, and K. Yoshikawa (2000), Stream flow studies in a watershed underlain by discontinuous permafrost, in *Proceedings Water Resources in Extreme Environments*, edited by D. Kane, pp. 31–36.

Bolton, W., L. Hinzman, and K. Yoshikawa (2004), Water balance dynamics of three small catchments in a sub-arctic boreal forest, in *Northern Research Basins Water Balance (Proceedings of a workshop held at Victoria, Canada, March 2004)*, edited by D. L. Kane and D. Yang, IAHS Series of Proceedings and Reports Number 290, pp. 213 – 223.

Brakensiek, D., R. Engelman, and W. Rawls (1981), Variation within texture classes of soil water parameters, *Transaction of the American Society of Agricultural Engineers*, *24*, 335–339.

Brooks, R., and A. Corey (1964), Hydraulic properties of porous media, *Hydrology Paper 3*, Civil Engineering Department, Colorado State University.

Brown, R. (1973), Influence of climate and terrain factors on ground temperatures at three locations in the permafrost region of Canada, in *The North American Contribution to the Second International Conference on Permafrost, Yakutsk*, pp. 27–34, National Academy of Sciences, Washington, D.C.

Burt, T., and P. Williams (1976), Hydraulic conductivity in frozen soils, *Earth Surficial Processes*, *1*, 349–360.

Callaghan, T., and S. Jonasson (1996), Arctic terrestrial ecosystems and environmental change, in *The Arctic and Environmental Change*, edited by P. Wadhams, J. Dowdeswell, and A. Schofield, pp. 59–76, Gordon and Breach.

Carsel, R., and R. Parrish (1988), Developing joint probability distributions of soil water retention characteristics, *Water Resources Research*, *24*, 755–769.

Chacho, J., E.F., and S. Bredthauer (1983), Runoff from a small subarctic watershed, in *Proceedings of the Fourth International Conference on Permafrost*, pp. 115–120, National Academy of Sciences, Washington D.C.

Chapman, W., and J. Walsh (1993), Recent variations in sea ice and air temperature in high latitudes, *Bulletin American Meteorology Society*, *74*, 33–47.

Clapp, R., and G. Hornberger (1978), Empirical equations for some soil hydraulic properties, *Water Resources Research*, *14*, 601–604.

DHI (1998), MIKE-SHE water movement - user guide and technical reference, *Edition 1.1*, Danish Hydraulic Institute.

Dickman, R. (2004), Fractal rain distributions and chaotic advection, *Brazilian Journal of Physics*, *34*(2), 337–345, doi:10.1590/S0103-97332004000300002.

Dingman, S. (1973), Effects of permafrost on stream flow characteristics in the discontinuous permafrost zone of central Alaska., in *Permafrost: North American Contribution to the Second International Conference*, pp. 447–453, National Academy of Sciences, Washington D.C.

Dingman, S. (1975), Hydrologic effects of frozen ground, *Special Report 218*, U.S. Army Cold Regional Research and Engineering Laboratory. 55 pp.

Dingman, S. L. (2002), *Physical Hydrology*, 2 ed., 646 pp., Prentice Hall, New Jersey.

Dingman, S. L., and F. R. Koutz (1974), Relations among vegetation, permafrost, and potential insolation in central Alaska, *Arctic and Alpine Research*, *6*(1), 37–42.

Freeze, R. A., and J. A. Cherry (1979), *Groundwater*, Prentice-Hall.

French, N., E. Kasischke, J. Michalek, and L. Bourgeau-Chavez (1997), Monitoring the effects of fire on soil temperature and moisture in boreal forest ecosystems using satellite imagery, in *Proceedings of the International Symposium on Physics, Chemistry, and Ecology in Seasonally Frozen Soils*, edited by I. Iskandar, E. Wright, J. Radke, B. Sharratt, P. Groenevelt, and L. Hinzman, pp. 551–557, Fairbanks, Alaska.

Friborg, T., H. Soegaard, T. Christensen, C. Lloyd, and N. Panikov (2003), Siberian wetlands: Where a sink is a source, *Geophysical Research Letters*, *30*(21), 2129.

Garbrecht, J., and L. Martz (1997), The assignment of drainage direction over flat surfaces in raster digital elevation models, *Journal of Hydrology*, *193*, 204–213.

Goodrich, D., C. Unkrich, R. Smith, and D. Woolhiser (2000), KINEROS2 - a distributed runoff and erosion model, in *Proceedings of the 2nd Federal Interagency Hydrologic Modeling Conference*, July 28- August 1, Las Vegas, NV. p. 14.

Grayson, R., and G. Blöschel (2000), *Spatial Patterns in Catchment Hydrology*, chap. Spatial Modelling of Catchment Dynamics, pp. 51–81, Cambridge University Press.

Green, W., and G. Ampt (1911), Studies on soil physics: 1. the flow of air and water through soils, *Journal of Agricultural Science*, *4*, 1–24.

Haugen, R., C. Slaughter, K. Howe, and S. Dingman (1982), Hydrology and climatology of the Caribou-Poker Creeks Research Watershed, Alaska, *CRREL Report 82-26*, US Army Corps of Engineers Cold Regions Research and Engineering Laboratory.

Hinzman, L., and D. Kane (1991), Snow hydrology of a headwater arctic basin, 2. Conceptual analysis and computer modeling, *Water Resources Research*, *27*(6), 95–100.

Hinzman, L., D. Kane, R. Gieck, and K. Everett (1991), Hydrologic and thermal properties of the active layer in the Alaskan Arctic, *Cold Regions Science and Technology*, *19*, 95–110.

Hinzman, L., D. Kane, and Z. Zhang (1995), A spatially distributed hydrologic model for arctic regions, in *International GEWEX Workshop on Cold-Season/Region Hydrometeorology. Summary Report and Proceedings*, no. 15 in Int. GEWEX Project Office Publication, pp. 236–239.

Hinzman, L., D. Goering, and D. Kane (1998), A distributed thermal model for calculating soil temperature profiles and depth of thaw in permafrost regions, *Journal of Geophysical Research*, *103*(D22), 28,975–28,991.

Hinzman, L., R. Johnson, D. Kane, A. Farris, and G. Light (2000), *Contaminant Hydrology: Cold Regions Modeling*, chap. Measurements and modeling of benzene transport in a discontinuous permafrost region, pp. 175–237, Lews Publishers.

Hinzman, L., W. Bolton, K. Petrone, J. Jones, and P. Adams (2006), Watershed hydrology and chemistry in Alaska's boreal forest: The central role of permafrost, in *Alaska's Changing Boreal Forest*, edited by F. C. III, M. Oswood, K. V. Cleve, L. Viereck, and D. Verbyla, Oxford University Press, Oxford.

Hinzman, L., N.D. Bettez, W.R. Bolton, F.S. Chapin, M.B. Dyurgerov, C.L. Fastie, B. Griffith, R.D. Hollister, A. Hope, H.P. Huntington, A.M. Jensen, G.J. Jia, T. Jorgenson, D.L. Kane, D.R. Klein, G. Kofinas, A.H. Lynch, A.H. Lloyd, A.D. McGuire, F.E. Nelson, W.C. Oechel, T.E. Osterkamp, C.H. Racine, V.E. Romanovsky, R.S. Stone, D.A. Stow, M. Sturm, C.E. Tweedie, G.L. Vourlitis, M.D. Walker, D.A. Walker, P.J. Webber, J.M. Welker, K.S. Winker, and K.Yoshikawa (2005), Evidence and implications of recent climatic change in northern Alaska and other arctic regions, *Climatic Change*, *72*, 251–298.

Horton, R. (1945), Erosional development of streams and their drainage basins: hydrophysical approach to quantitative morphology, *Geologic Society of American Bulletin*, *56*, 275–370.

IPCC (2001), Climate change 2001: Synthesis report. Summary for policymakers., *Tech. rep.*, Intergovernmental Panel on Climate Change.

Jonch-Clausen, T. (1979), SHE, Systéme Hydrologique Européen, a short description, Danish Hydraulic Institute, Hørsholm, Denmark.

Jones, J., K. Petrone, J. Finlay, L. Hinzman, and W. Bolton (2005), Nitrogen loss from watersheds of interior Alaska underlain with discontinuous permafrost, *Geophysical Research Letters*, *32*(10.1029/2004GL021734), L02,401.

Jorgenson, M., C. Racine, J. Walters, and T. Osterkamp (2001), Permafrost degradation and ecological changes associated with a warming climate in central Alaska, *Climate Change*, *48*, 551–571.

Julian, P., and B. Saghafian (1991), CASC2D: A two-dimensional watershed rainfall-runoff model, CASC2D user's manual, *Report CER90-91PYJ-BJ-12*, Colorado State University, Colorado State University, Fort Collins, Colorado. 66 pp.

Kane, D., and L. Hinzman (2004), Monitoring extreme environments: Arctic hydrology in transition, *Water Resources Impact*, *6*(1), 24–27.

Kane, D., and J. Stein (1983a), Water movement into seasonally frozen soils, *Water Resources Research*, (6), 1547–1557.

Kane, D., and J. Stein (1983b), Field evidence of groundwater recharge in interior Alaska, in *Proceedings of the Fourth International Conference on Permafrost*, pp. 572–577, National Academy Press.

Kane, D., L. Hinzman, and J. Zarling (1991), Thermal response of the active layer to climatic warming in a permafrost environment, *Cold Regions Science and Technology*, *19*(2), 111–122.

Kane, D. L., and D. Yang (2004), Overview of water balance determinations for high latitude watersheds, in *Northern Research Basins Water Balance*, edited by D. L. Kane and D. Yang, 290, pp. 1–12, International Association of Hydrologic Sciences.

Kane, D. L., R. D. Seifert, and G. S. Taylor (1978), Hydrologic properties of subarctic organic soils, *Tech. Rep. IWR-88*, Institute of Water Resources, University of Alaska Fairbanks.

Kite, G. (1978), Development of a hydrologic model for a Canadian watershed, *Canadian Journal of Civil Engineering*, *5*, 126–134.

Kite, G. (1989), Hydrologic modelling with remotely sensed data, in *Proceedings of the 5th Annual Western Snow Conference*, pp. 1–8, Fort Collins, Colorado.

Leavesley, G., R. Lichty, B. Troutman, and L. Saindon (1983), Precipitation-runoff modeling system, *Water Resources Investigations Report 83-4238*, United States Geological Survey. 207 p.

Liang, X., D. Lettenmair, E. Wood, and S. Burges (1994), A simple hydrologically based model of land surface water, energy, fluxes for general circulation models, *Journal of Geophysical Research*, *99*(D7), 14,415–14,428.

Magnuson, J., D. Robertson, B. Benson, R. Wynne, D. Livingstone, T. Arai, R. Assel, R. Barry, V. Card, E. Kuusisto, N. Granin, T. Prowse, K. Steward, and V. Vuglinski (2000), Historical trends in lake and river ice cover in the northern hemisphere, *Science*, *289*, 1743–1746.

McGuire, A., J. Melillo, D. Kicklighter, and L. Joyce (1995), Equilibrium responses of soil carbon to climate change: Empirical and process-based estimates, *Journal of Biogeography*, *22*, 785–796.

McNamara, J., D. Kane, and L. Hinzman (1998), An analysis of streamflow hydrology in the Kuparuk River basin, Arctic Alaska: a nested watershed approach, *Journal of Hydrology*, *206*, 39–57.

Moore, I., R. Grayson, and A. Ladson (1993), Digital terrain modelling: A review of hydrological, geomorphological, and biological applications, in *Terrain Analysis and Distributed Modelling in Hydrology*, edited by K. Beven and I. Moore, pp. 7–34.

Moore, T., N. Roulet, and J. Waddington (1998), Uncertainty in predicting the effect of climatic change on the carbon cycling of Canadian peatlands, *Climatic Change*, *40*, 229–245.

Nelson, G. (1978), Hydrologic information for land-use planning, Fairbanks vicinity, Alaska, *Open-File Report 78-959*, U.S. Geological Society.

O'Callaghan, J., and D. Mark (1984), The extraction of drainage networks from digital elevation data, *Computer Vision, Graphics, and Image Processing*, *28*(3), 323–344.

Osterkamp, T. (2003), A thermal history of permafrost in Alaska, in *Proceedings of the Eighth International Conference on Permafrost, 21-25 July 2003*, pp. 863–868, Balkema Publishers.

Osterkamp, T., and V. Romanovsky (1999), Evidence for warming and thawing of discontinuous permafrost in Alaska, *Permafrost and Periglacial Processes*, *10*, 17–37.

Osterkamp, T., L. Viereck, Y. Shur, M. Jorgenson, C. Racine, A. Doyle, and R. Boone (2000), Observations of thermokarst and its impact on boreal forests in Alaska, USA, *Arctic, Antarctic and Alpine Research*, *32*, 303 – 315.

Panian, T. (1987), Unsaturated flow properties data catalog, volume ii, *DOE/NV/10384-20 45061*, Water Resources Center, Desert Research Institute.

Peckham, S. D. (1995), New results for self-similar trees with applications to river networks, *Water Resources Research*, *31*(4), 1023–1029.

Peterson, B., R. Holmes, J. McClelland, C. Vörösmarty, R. Lammers, A. Shiklomanov, I. Skiklomanov, and S. Rahmstort (2002), Increasing river discharge to the Arctic Ocean, *Science*, *298*, 2171–2173.

Petrone, K., L. Hinzman, and R. Boone (2000), Nitrogen and carbon dynamics of storm runoff in three sub-arctic streams, in *Water Resources of Extreme Environments*, edited by D. Kane, pp. 167–172, American Water Resources Association.

Ravi, V., and J. R. Williams (1998), Estimation of infiltration rate in the vadose zone: *Tech. Rep. EPA/600/R-97/128a*, U.S. Environmental Protection Agency.

Rawls, W., L. Ahuja, . D. Brakensiek, and A. Shirmohammadi (1992), Infiltration and soil water movement, in *Handbook of Hydrology*, edited by D. Maidment, McGraw-Hill, New York.

Richards, L. (1931), Capillary conduction of liquids through porous media, *Physics*, *1*, 316–333.

Romanovsky, V., M. Burgess, S. Smith, K. Yoshikawa, and J. Brown (2002), Permafrost temperature records: Indicators of climate change, *EOS Transactions of the American Geophysical Union*, *83*(50), 589–594.

Serreze, M., D. Bromwich, M. Clark, A. Etringer, T. Zhang, and R. Lammers (2002), Large-scale hydro-climatology of the terrestrial arctic drainage system, *Journal Geophysical Research*, *108*(D2), D01,108.

Serreze, M., et al. (2000), Observational evidence of recent change in the northern high latitude environment, *Climate Change*, *46*, 159–207.

Shiklomanov, A., R. Lammers, and C. Vörösmarty (2002), Widespread decline in hydrological monitoring threatens pan-arctic research, *EOS, Transactions, American Geophysical Union*, *83*(2), 13–17.

Slaughter, C., and D. Kane (1979), Hydrologic role of shallow organic soils in cold climates, in *Canadian Hydrology Symposium: Proceedings, 79-Cold Climate Hydrology*, pp. 380–389.

Slaughter, C., J. Hilgert, and E. Culp (1983), Summer streamflow and sediment yield from discontinuous-permafrost headwater catchments, in *Proceedings of the Fourth International Permafrost Conference*, pp. 1172–1177, National Academy Press.

Smith, L., Y. Sheng, G. MacDonald, and L. Hinzman (2005), Disappearing arctic lakes, *Science*, *308*, 1429.

Smith, R. (1990), Analysis of infiltration through a two-layer soil profile, *Soil Science Society*, *54*(5), 1219–1227.

Smith, R., and J.-Y. Parlange (1978), A parameter-efficient hydrologic infiltration model, *Water Resources Research*, *14*(3), 533–538.

Smith, R., C. Corradini, and F. Melone (1993), Modeling infiltration for multistorm runoff events, *Water Resources Research*, *29*(1), 133–144.

Smith, R. E. (2002), *Infiltration Theory for Hydrologic Applications*, Water Resources Monograph 15, American Geophysical Union.

Strahler, A. (1957), Quantitative analysis of watershed geomorphology, *American Geophysical Union Transactions*, *38*(6), 913–920.

Vörösmarty, C., W. Gutowski, M. Person, T.-C. Chen, and D. Case (1993), Linked atmosphere-hydrology models at the macroscale, in *Macroscale Modeling of the Hydrosphere*, edited by W. Wilkinson, no. 214 in International Association of Hydrological Sciences, pp. 3–27.

Walter, M. T., T. S. Steenhuis, V. K. Mehta, D. Thongs, M. Zion, and E. Schneiderman (2002), Refined conceptualization of TOPMODEL for shallow subsurface flows, *Hydrological Processes*, *16*, 2041–2045.

Walsh, J. E., O. Anisimov, J.O.M. Hagen, T. Jakobsson, J. Oerlemans, T.D. Prowse, V. Romanovsky, N. Savelieva, M. Serreze, A. Shiklomanov, I. Shiklomanov, S. Solomon, A. Arendt, D. Atkinson, M.N. Demuth, J. Dowdeswell, M. Dyurgerov, A. Glazovsky, R.M. Koerner, M. Meier, N. Reeh, O. Sigurosson, K. Steffen, and M. Truffer (2005) Cryosphere and hydrology, in *Arctic Climate Impact Assessment*, edited by C. Symon, L. Arris, and B. Heal, Chap. 6, pp. 184–242, Cambridge University Press.

Washburn, A. (1979), *Geocryology: A survey of Periglacial Processes and Environments*, Wiley.

Wigmosta, M. S., L. W. Vail, and D. Lettenmair (1994), A distributed hydrology - vegetation model for complex terrain, *Water Resources Research*, *30*(6), 1665–1679.

Williams, J. R., Y. Ouyang, and J.-S. Chen (1998), Estimation of infiltration rate in vadoze zone: Application ii, *Tech. Rep. EPA/600/R-97/128b*, U.S. Environmental Protection Agency.

Woo, M., and P. Steer (1983), Slope hydrology as influenced by thawing of the active layer, *Canadian Journal of Earth Science*, *20*, 978–986.

Woo, M.-k. (1986), Permafrost hydrology in North America, *Atmosphere-Ocean*, *24*(3), 201–234.

Woo, M. K. (1990), Permafrost hydrology, in *Northern Hydrology, Canadian Perspectives. Proceedings of the Northern Hydrology Symposium*, edited by T. Prowse, C. Ommanney, and M. Woo, no. 1 in Canadian National Hydrology Research Institute Science Report, pp. 63–76.

Woo, M.-K. (2000), *The Arctic: Environment, People, Policy*, chap. Permafrost and Hydrology, pp. 57–96, Harwood Academic Publications.

Yoshikawa, K., W. Bolton, V. Romanovsky, M. Fukuda, and L. Hinzman (2002), Impacts of wildfire on the permafrost in the boreal forest of interior Alaska, *Journal of Geophysical Research*, *107*(8148: doe:10.1029/2001JD000438), printed 108(D1), 2003.

Zhang, T. (2005), Spatial and temporal variability in active layer thickness over the Russian Arctic drainage basin, *Journal of Geophysical Research*, *110*, D16,101.

Zhang, Z., D. Kane, and L. Hinzman (2000), Development and application of a spatially-distributed arctic hydrological and thermal process model (ARHYTHM), *Hydrological Processes*, *14*, 1017–1044.

# Chapter 5
# Evaluating the Hydrologic Response to Changing Watershed Characteristics and Climate in the Subarctic*

**Abstract**

The Arctic region is currently experiencing rapid environmental change, with increases in both air temperature and precipitation. These changes in the climate system are expected to continue well into the century. The TopoFlow model is used to test the sensitivity of the stream flow process due to these expected environmental changes in an area underlain with discontinuous permafrost. Simulation of the hydrologic processes in the sub-arctic environment is challenging due to rapidly changing thermal (permafrost versus non-permafrost, thaw depth development) and hydrologic (hydraulic conductivity and storage capacity) in both time and space. By spatial and temporal variation of the hydraulic conductivity (proxy for permafrost distribution) and porosity (proxy for storage capacity) with active layer thaw depth, the sub-arctic hydrologic environment can be adequately represented. Sensitivity results indicate that changes in rainfall is the dominant control on the stream flow process. Permafrost, which is the dominant control on soil moisture dynamics, plays an important secondary role in its control on contributing area, storage processes, and vegetation distribution. With the exception of increased rainfall, all expected environmental changes result in a decrease in summer runoff. Simulation results indicate the only changes in stream flow occur with changes within the contributing area of the watershed. If the expected changes in the permafrost regime are realized (decrease in areal extent of permafrost and an increase in active layer depth), the contributing area of the watershed will decrease, reducing the area of influence to which hydrologic processes respond.

KEY WORDS: Permafrost; Active layer; Modeling; Computational hydrology; Climate Impacts.

*W.R. Bolton, L.D. Hinzman, and D.L. Kane, in Preparation to be submitted to the *Journal of Geophysical Research – Biogeosciences*.

## 5.1 Introduction

The Arctic, including Alaska, is currently experiencing an unprecedented degree of environmental change [*Chapman and Walsh*, 1993; *Serreze et al.*, 2000; *IPCC*, 2001; *ACIA*, 2005; *Hinzman et al.*, 2005]. Increases in both the mean annual surface temperature (2-3$^o$C) and annual precipitation have been observed [*Chapman and Walsh*, 1993; *Serreze et al.*, 2000; *ACIA*, 2005; *Hinzman et al.*, 2005]. In Interior Alaska, the combination of the recent increase in air and an unstable permafrost condition [*Yoshikawa et al.*, 2002] has resulted in a reduction in areal permafrost coverage and an increase in active layer depth [*Jorgenson et al.*, 2001; *Yoshikawa et al.*, 2003]. Recent studies have documented a variety of hydrologic responses associated with the shifting climatic and permafrost regimes, including later freeze-up and earlier break-up dates of rivers [*Magnuson et al.*, 2000], increased arctic river discharge [*Peterson et al.*, 2002], shrinking lakes [*Smith et al.*, 2005], and thermokarst development [*Osterkamp and Romanovsky*, 1999; *Osterkamp et al.*, 2000; *Jorgenson et al.*, 2001].

The observed climatic changes are expected to continue into the next century [*IPCC*, 2001; *ACIA*, 2005]. The sub-arctic environment can be characterized as being located in the zone of discontinuous permafrost. As such, most of the current or expected changes (such as increased temperature and precipitation, decreased permafrost extent, increased active layer depth, tree line expansion and vegetation composition), will be experienced first in this region. In light of the observed and expected changes, it is important to understand and predict the feedback mechanisms of the water cycle [*Kane and Hinzman*, 2004], where small changes in the natural system may result in dramatic, threshold changes in the hydrology, ecology, and surface energy balance, with subsequent climatological impacts on local and regional scales.

### 5.1.1 Objectives

The objectives of this study are to (1) examine the viability of representing the discontinuous permafrost condition through spatial and temporal variation of the hydraulic conductivity and porosity within a spatially-distributed, process-based hydrologic model; and (2) assess the sensitivity of the sub-arctic hydrologic regime to changes in the permafrost regime (permafrost distribution and active layer depth), climate conditions (temperature and precipitation), and vegetation distribution, in order to better understand potential hy-

drologic feedbacks expected in a changing climate.

### 5.1.2 Previous Modeling Studies

A number of hydrologic modeling studies, each focusing on a specific process, have been conducted in the sub-arctic environment of Interior Alaska. *Carlson* [1972] developed and applied a simple conceptual reservoir-type rainfall-runoff model, describing the interactions between the surface storage, channel storage, groundwater storage, and soil moisture storage in the Caribou-Poker Creeks Research Watershed (CPCRW), located in Central Alaska. The conceptualization of this model did not account for discontinuous permafrost. *Carlson* [1972] notes the model was designed as a first step conceptualization and was intended to help guide future research efforts. *Kane et al.* [1978] developed a two-dimensional, two-layer shallow groundwater flow model that accounted for the hydraulic properties of both permafrost and seasonally-frozen soils found in Interior Alaska. The HBV (Hydrologiska Byråns Vattenbalansavdelńing, [*Bergström*, 1976, 1992]) has been applied successfully in areas of discontinuous permafrost [*Sand and Kane*, 1986; *Knudson and Hinzman*, 2000; *Carr*, 2003]. In the *Sand and Kane* [1986] study, simulation results initially underestimate the snowmelt runoff and overestimate the rainfall runoff, indicating the importance of the active layer development on soil storage on the runoff process. *Sand and Kane* [1986] adjusted the soil parameterization such that a set of soil parameters was used for the snowmelt period and a second set for the summer (rainfall) period. It should be noted that the timing of the switch between the two sets of soil parameters was based upon visual inspection of the simulation hydrograph. *Farris* [1996] and *Youcha* [2003], respectively, applied a groundwater model to an alluvial aquifer and an upland dome, both located near Fairbanks, Alaska. In these ground water studies, permafrost soils are represented with a very low hydraulic conductivity. *Farris* [1996] applied a weighted hydraulic conductivity for model elements which included both frozen and thawed soils.

## 5.2 Study Area

The Caribou-Poker Creeks Research Watershed (CPCRW) is located 48 km north of Fairbanks, Alaska ($65^o10'$N, $147^o30'$W) and encompasses an area of 101.5 km$^2$. Hydrologic and climatological data collection began immediately following the 1969 establishment of

CPCRW. The three headwater catchments selected for this study are the C2 (5.2 $km^2$), C3 (5.7 $km^2$) and the C4 (11.4 $km^2$) sub-watersheds of CPCRW (Figure 5.1).

### 5.2.1 Permafrost distribution

CPCRW is located in the zone of discontinuous permafrost. Permafrost in CPCRW is generally found along north facing slopes and valley bottoms [*Haugen et al.*, 1982; *Nelson*, 1978]. Soils free of permafrost are generally found on south to southwest facing slopes. The C2, C3, and C4 sub-watersheds are underlain with approximately 3, 53, and 18% permafrost, respectively [*Haugen et al.*, 1982; *Yoshikawa et al.*, 1998]. In CPCRW, the thermal condition of the permafrost is unstable, varying from -3.0 to -0.5$^oC$ [*Yoshikawa et al.*, 2003]. Permafrost thickness ranges from 0 - 120 meters [*Yoshikawa et al.*, 2003]. The maximum active layer thickness, measured at the CRREL meteorological station, averaged 0.52 m (2000-2002). The C2, C3, and C4 sub-watersheds are underlain with approximately 3, 53, and 18% permafrost, respectively (Figure 5.1) [*Haugen et al.*, 1982; *Yoshikawa et al.*, 1998].

### 5.2.2 Climate

The climate in CPCRW is classified as continental sub-arctic [*Strahler*, 1969], characterized by large diurnal and annual temperature extremes and low annual precipitation [*Slaughter et al.*, 1983]. The mean annual air temperature is $-1.2^oC$ on Caribou Peak and $-4.9^oC$ at the Caribou Main sites [*Haugen et al.*, 1982]. A strong winter temperature inversion results in warmer winter air temperatures with elevation (the estimated January temperature is $-17.0^oC$ for Caribou Peak and $-22.9^oC$ at Caribou Main [*Haugen et al.*, 1982]) is reflected in the mean annual temperature. Summer air temperature is slightly cooler with elevation (estimated July air temperature $12.5^oC$ at Caribou Peak and $13.0^oC$ at Caribou Main).

The average (1978-2003) annual precipitation (combined rain and snow) is 411.6 mm (635.1 mm maximum, 310.5 mm minimum, 80.3 SD), of which approximately 2/3 occurs as rain [*Bolton et al.*, 2004]. The average snowpack is 130.7 mm (342.1 mm maximum, 53.2 mm minimum, 69.5 mm SD) The average rainfall is 280.9 mm (381.6 mm maximum, 150.4 mm minimum, 52.6 mm SD). The snowpack throughout most of CPCRW is fairly uniform and is classified as 'taiga snow,' with a density of about 0.2 $g/cm^3$ [*Slaughter and Benson*,

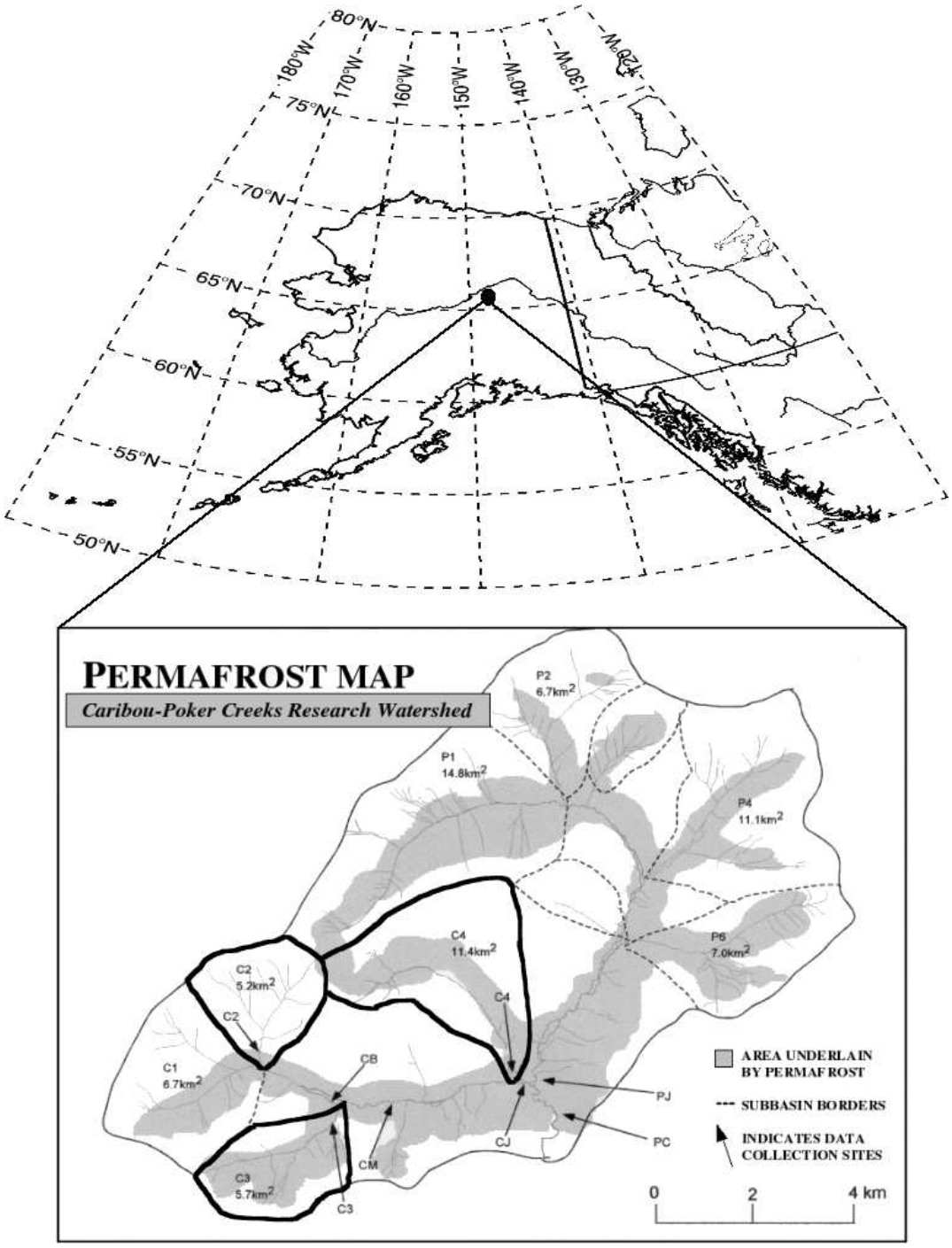


Figure 5.1. Study location and permafrost distribution map. The C2, C3, and C4 subwatershed boundaries are indicated with heavy lines. Permafrost distribution map modified from *Haugen et al.* [1982].

1986; *Bolton et al.*, 2004]. Snow on exposed ridge tops is redistributed resulting in a slightly higher snow density of about 0.3 g/cm$^3$ and is classified as 'tundra snow.'

### 5.2.3 Vegetation

The most common tree species in CPCRW is black spruce (*Picea mariana*), found on north facing slopes and in stunted stands in valley bottoms. Paper birch (*Betula papyrifera*), quaking aspen (*Populus tremuloides*), and occasional stands of alder (*Alnus crispa*) are found along south facing slopes. White spruce (*Picea glauca*) are also found on south facing slopes adjacent to stream drainages. Willow (*Salicaceae*), Arctic dwarf birch (*Betula nana L.*), tussock tundra (*Carex aquatilis*), feather moss (*Hylocomium spp.*), and sphagnum mosses (*Sphagnum*) are also found in valley bottoms [*Troth et al.*, 1975].

### 5.2.4 Geology and soils

CPCRW is part of the Yukon-Tanana Uplands that consist of metamorphic Precambrian mica schists of the Birch Creek formation, mantled with Quaternary aeolian silts of varying thickness [*Wahrhafting*, 1965; *Rieger et al.*, 1972]. The soils are poorly developed silts loams, containing varying amounts of sand and gravel [*Koutz and Slaughter*, 1972; *Haugen et al.*, 1982]. Overlying the silt loams are organic soils. In areas overlain with permafrost, low ground temperature reduces the rate of decomposition, resulting in an organic soil cover between 20-50 cm thick [*Slaughter and Kane*, 1979]. In the warmer non-permafrost areas, the organic soils are no more than 15 cm thick [*Slaughter and Kane*, 1979].

## 5.3 Field Studies

**Stream flow**

Calibrated Parshall flumes were installed in the C2, C3 and C4 sub-basins in 1977, 1978, and 1979, respectively [*Slaughter*, 1981]. Stage measurements are recorded at regular intervals using a Micro-switch 5-psi pressure transducer and Campbell Scientific data loggers. The recorded stage measurements are used to generate a continuous discharge record. Periodic manual discharge measurements are collected at various stage levels to verify the

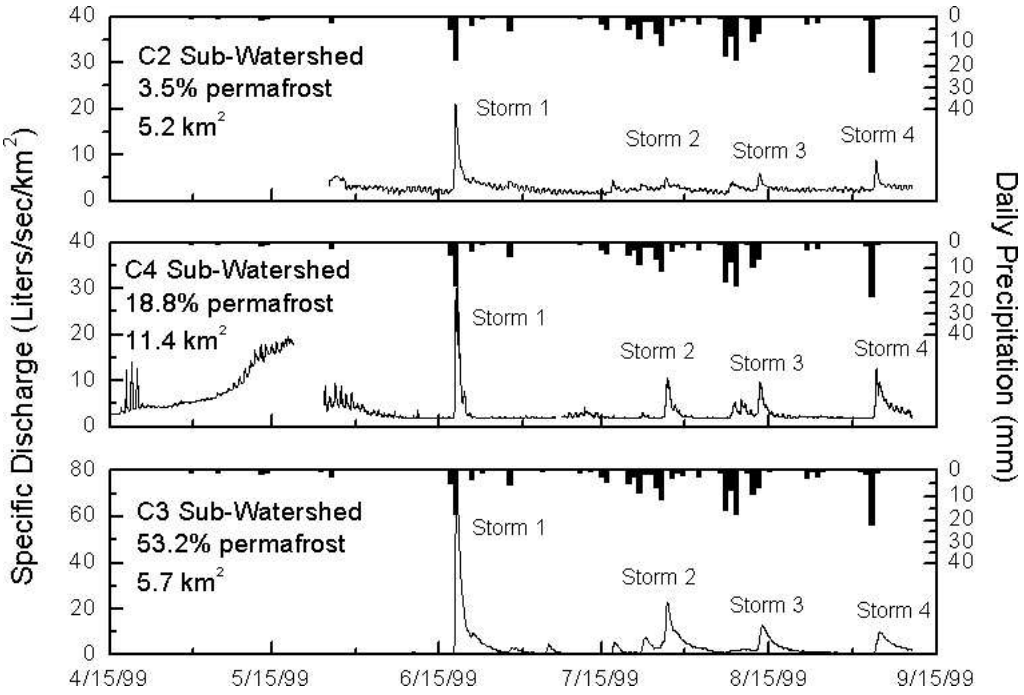


Figure 5.2. Specific discharge of the 1999 C2, C3, and C4 sub-basins of the Caribou-Poker Creeks Research Watershed.

calculated discharge data. Streamflow measurements are collected from the initiation of spring snowmelt until late fall, when freeze-up occurs.

The differences in stream flow between these three sub-basins are dependent upon the areal extent of permafrost. Comparison of the specific discharge (measured stream flow normalized by basin area) indicate that during precipitation events, peak specific discharge, response time, and recession period all increase with permafrost extent. Between precipitation events, a lower specific discharge is observed in basins with greater permafrost coverage (Figure 5.2).

**Soil moisture**

Soil moisture content was measured at four locations in CPCRW. At each site, Campbell Scientific CS615 soil moisture probes were installed horizontally into small soil pits and connected to a Campbell Scientific data logger. The soil moisture sites are located in a valley bottom underlain by permafrost (C4 Bottom), a deciduous stand (C4 Birch), a conifer-

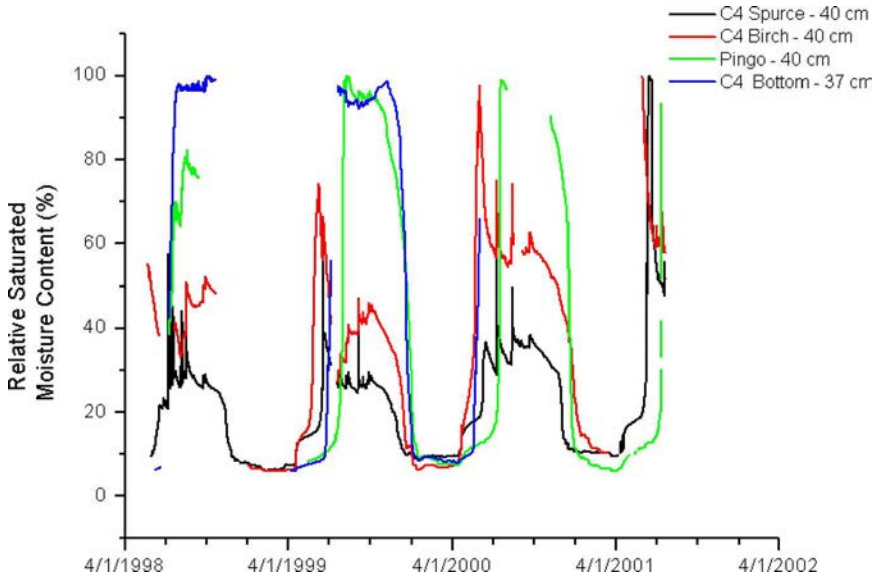


Figure 5.3. Soil moisture content from the C4 Bottom, C4 Spruce, C4 Birch, and Pingo soil moisture sites. Results are shown from near surface mineral soils of comparable depth.

ous stand (C4 Spruce), and in a mixed hardwood/spruce stand underlain with permafrost (Pingo). The C4 Spruce, C4 Birch, and Pingo sites are all located on gentle slopes, while the C4 Bottom site is located in a relatively flat valley bottom. The data obtained from the CS615 probes were used to calculate the dielectric constant of the soil. The *Topp et al.* [1980] equation for mineral soils and the *Stein and Kane* [1983] equation for organic soils were then applied to obtain the volumetric soil moisture content (Figure 5.3). The volumetric soil moisture content is normalized to a 'saturated' soil moisture content by scaling the highest measured value to 100% (assumed to be saturated) and the lowest value to 6% (the soil moisture content when the soil is frozen [*Stein and Kane*, 1983]).

The presence or absence of permafrost significantly impacts the soil moisture content in the sub-arctic. In areas free of permafrost, the soils are relatively well-drained, allowing percolation of surface waters to the deep sub-surface system. In areas underlain with permafrost, ice-rich conditions at the permafrost table inhibit percolation of surface waters to the sub-surface soils, resulting in relatively wetter soils (Figure 5.4).

The effects of wildfire on soil moisture content are seen in comparing the C4 Spruce with the C4 Birch sites (Figure 5.5). These sites are located within 500 meters of each

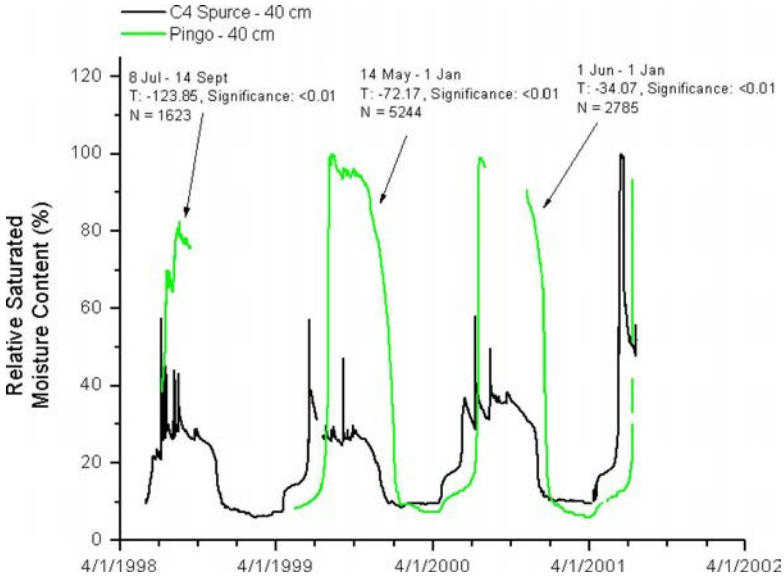


Figure 5.4. Mineral soil moisture content in an area underlain with permafrost and an area free of permafrost.

other on the same hillslope. In 1999, the C4 Birch site was burned during the FROSTFIRE experiment [*Hinzman et al.*, 2003]. Following the fire, the large increase in soil moisture at the C4 Birch site is most likely due to a reduction in evapotranspiration.

The effects of slope on the soil moisture content are seen when comparing the C4 Bottom with the Pingo soil moisture sites. The relatively high hydraulic gradient on the hillslope allows the near surface waters to drain quickly compared to the low gradient valley bottom (Figure 5.6).

## 5.4 Conceptual Model

A number of studies have focused on runoff generation mechanisms in the sub-arctic. *Dingman* [1973] used the variable source area concept to describe the runoff generation as originating from the valley bottoms. *Dingman* [1973] stated the size of the source area (or contributing area) during precipitation events is dictated by the the position of the water table in the valley bottoms, which is in turn dependent upon the antecedent conditions of the watershed. *Carey and Woo* [2001] expanded upon the variable source concept by including a two-layer flow system, described by *Kane et al.* [1978], due to the sharp change

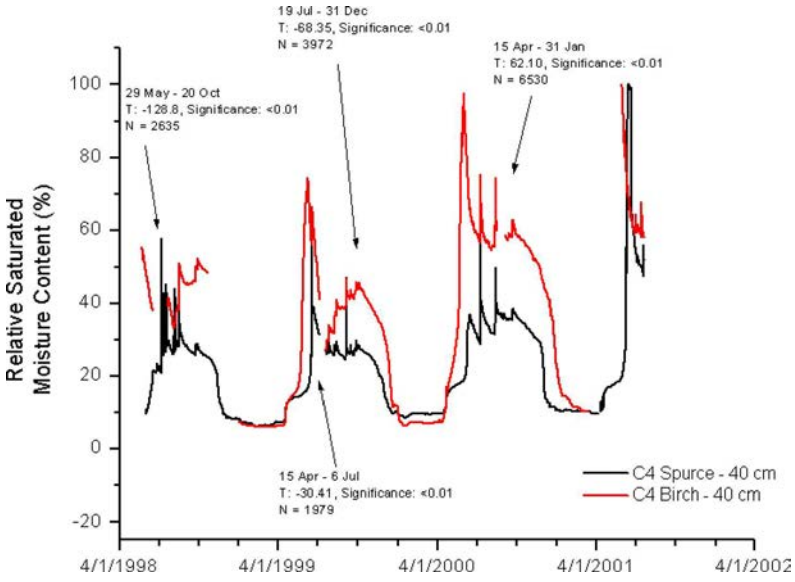


Figure 5.5. Soil moisture content from the C4 Spruce and C4 Birch sites. In July 1999, the C4 Birch site was burned as part of the FROSTFIRE [*Hinzman et al.*, 2003] experimental burn. Following the fire, the large increase in the soil moisture content of the C4 Birch is most likely due to the reduction of evapotranspiration.

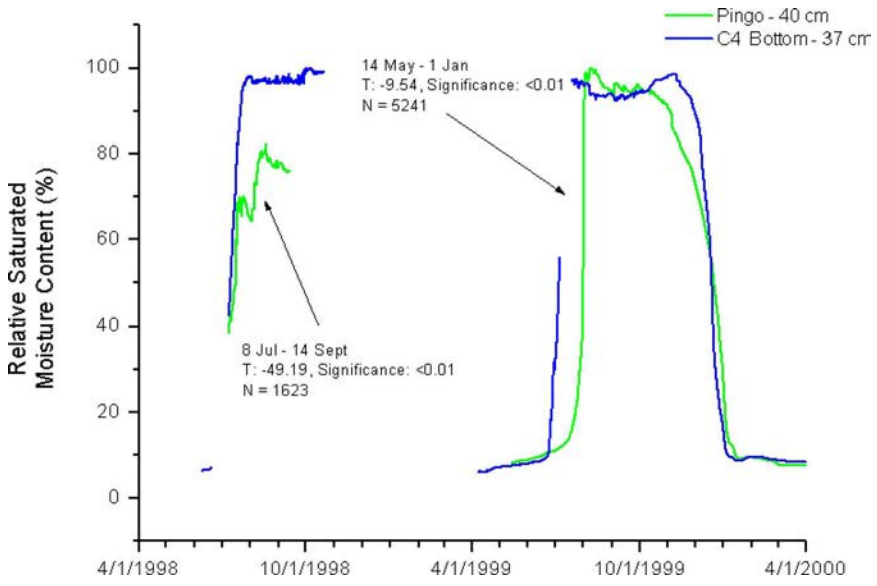


Figure 5.6. Soil moisture content from the C4 Bottom and Pingo soil moisture sites.

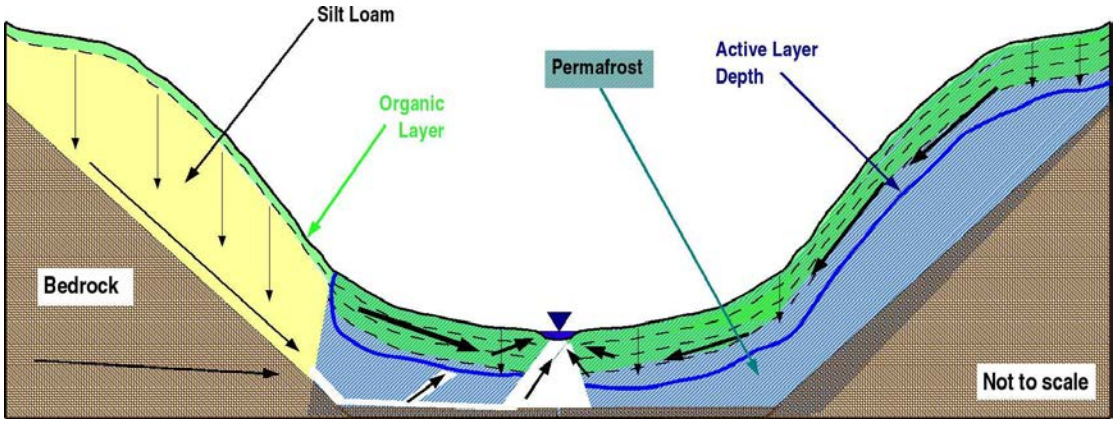


Figure 5.7. Conceptual model the water flow paths in areas of discontinuous permafrost. The direction and magnitude of flow paths are indicated by the arrows.

in hydraulic conductivity between the organic and mineral soils.

The conceptual model used in this study incorporates the above concepts. In areas underlain with permafrost, a relatively thick organic layer (of high hydraulic conductivity and porosity) overlies an ice-rich mineral soil (of very low hydraulic conductivity and porosity). A near-surface ground water table is located above the permafrost table, due to the impermeable nature of the ice-rich mineral soil. During precipitation events, the ice-rich conditions inhibit percolation to the deeper subsurface, allowing surface waters to travel relatively quickly through the organic mat and active layer to the stream (Figure 5.7).

Permafrost-free areas consist of a relatively thin organic layer (of high hydraulic conductivity and porosity) overlying a well-drained mineral soil (with relatively a high hydraulic conductivity and porosity). The ground water table is located in the deeper subsurface (within a bedrock aquifer or along the contact between the mineral soil and bedrock surface). During precipitation events, surface waters are allowed to rapid percolation to the deep groundwater system occurs. In these non-permafrost areas, the infiltration capacity of the soils must be exceeded before runoff generation can occur. The deep groundwater system contributes a steady source of base flow to stream flow.

## 5.5 Choice of Model

The process-based, spatially-distributed hydrologic model, TopoFlow, is selected for use in this study. The TopoFlow structure is described in Chapter 4. This model has been successfully applied in an arctic environment [*Schramm*, 2005]. TopoFlow is well suited to the sub-arctic environment as input variables are allowed to change through both time and space. This feature is particularly important in the sub-arctic environment where the thermal and hydraulic properties of the soils vary rapidly in both the spatial and temporal dimensions.

## 5.6 Adaptation of TopoFlow

Hydrologically speaking, the main difference between frozen (permafrost) soils and thawed (non-permafrost) soils is the difference in hydraulic conductivity [*Kane et al.*, 1978; *Kane and Stein*, 1983; *Burt and Williams*, 1976; *Freeze and Cherry*, 1979] and storage capacity (due to ice-rich pores) [*Woo*, 1986]. In our conceptualization of the sub-arctic hydrologic regime, permafrost soils are represented with a very low hydraulic conductivity and a low porosity. Non-permafrost soils (or thawed soils in the active layer) are represented by an appropriate (larger) hydraulic conductivity and porosity for the soil.

Development of the thaw depth begins immediately at conclusion of snowmelt [*Boike et al.*, 1998] and progresses throughout the summer season. The thaw depth is approximated by step function (Equation 5.1) that is proportional to the square root of time since the beginning of the thaw depth development [*Terzaghi*, 1952; *Woo*, 1986].

$$X[t] = \Gamma\sqrt{t} \tag{5.1}$$

Where X is the depth of thaw from the surface, [$m$], $\Gamma$ is the characteristic thaw coefficient [$m^2/day$], and $t$ is the time from the completion of snowmelt [*days*].

For each layer, the frozen and thawed hydraulic conductivity and porosity of the soil are defined. In permafrost areas, the location of the thaw depth (Equation 5.1) is determined relative to the soil layers following the completion of snowmelt. Prior to the completion of snowmelt, the frozen hydraulic conductivity and porosity are used for each soil layer. If an entire soil layer(s) is in the area above the thaw depth, the thawed hydraulic

conductivity and porosity value is used for that time step. If the entire soil layer(s) is areas below the thaw depth, the frozen hydraulic conductivity and porosity value is used for that time step. If the thaw depth is located within a soil layer, the hydraulic conductivity and porosity are determined using simple weighting functions:

$$K_X = \frac{K_F d_F + K_T d_T}{D} \tag{5.2}$$

and

$$P_X = \frac{P_F d_F + P_T d_T}{D} \tag{5.3}$$

Where $K_{F,T}$ are the frozen and thawed hydraulic conductivity, $[m/s]$; $P_{F,T}$ are the frozen and thawed porosity, [*unitless*]; $d_{F,T}$ are the thickness of the frozen and thawed portion of the soil layer in question, $[m]$; and $D$ is the total depth of the soil layer, $X$, $[m]$; (note: $D = d_F + d_T$).

In the model formulation, the hydraulic conductivity and porosity of the non-permafrost soil layers is prescribed based upon the presence or absence of snow. In the timesteps prior to the completion of snowmelt, the frozen hydraulic conductivity and porosity is defined for all soil layers. Following the completion of snowmelt, it is assumed the ground thaws instantaneously and the corresponding thawed hydraulic conductivity and porosity is used for all soil layers. This assumption is based upon the work of *Carey and Woo* [1998] that show on a south-facing (permafrost free) slope, the seasonal frost layer is completely thawed at the completion of snowmelt. The rapid thawing of the frost layer is attributed to the release of latent heat by infiltrating snowmelt water during the melt period, and two-sided thawing of the frost layer from the ground surface and below the frost layer [*Carey and Woo*, 1998].

The mathematical representation of the discontinuous permafrost condition was tested using the C2 sub-basin of CPCRW. In this test, the areal extent of permafrost is assumed to be 17, 50, and 80%. Each soil layer is assumed to have the same frozen and thawed hydraulic properties (and varies only with permafrost extent). Simulations last 120 days, with a large (uniform) precipitation event lasting 1 day occurring on Day 0, 30, 60, and 90. The thaw depth is initialized at 0.0 meters and begins to develop at the beginning of the

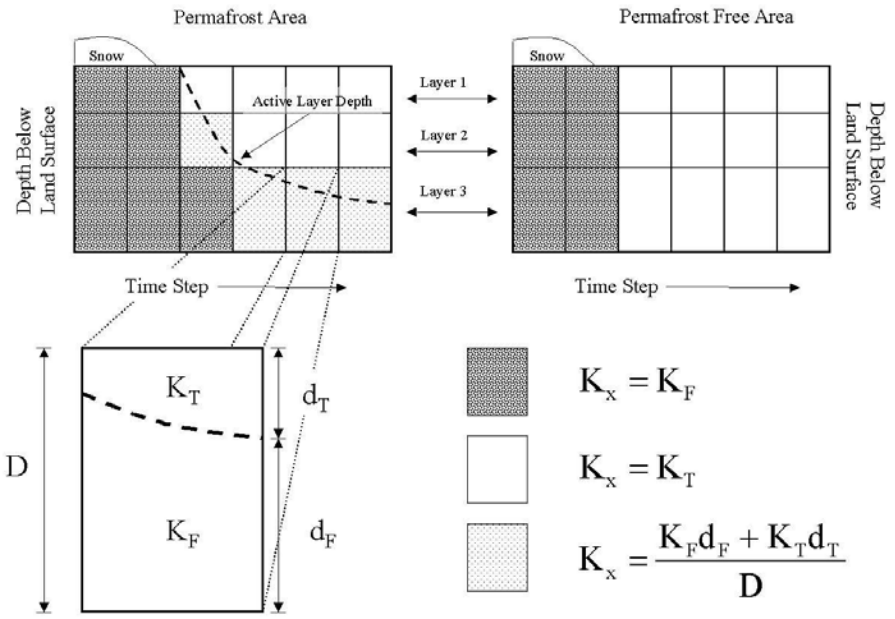


Figure 5.8. Mathematical representation of discontinuous permafrost and thaw depth development. The porosity of each soil layer is determined in the same manner.

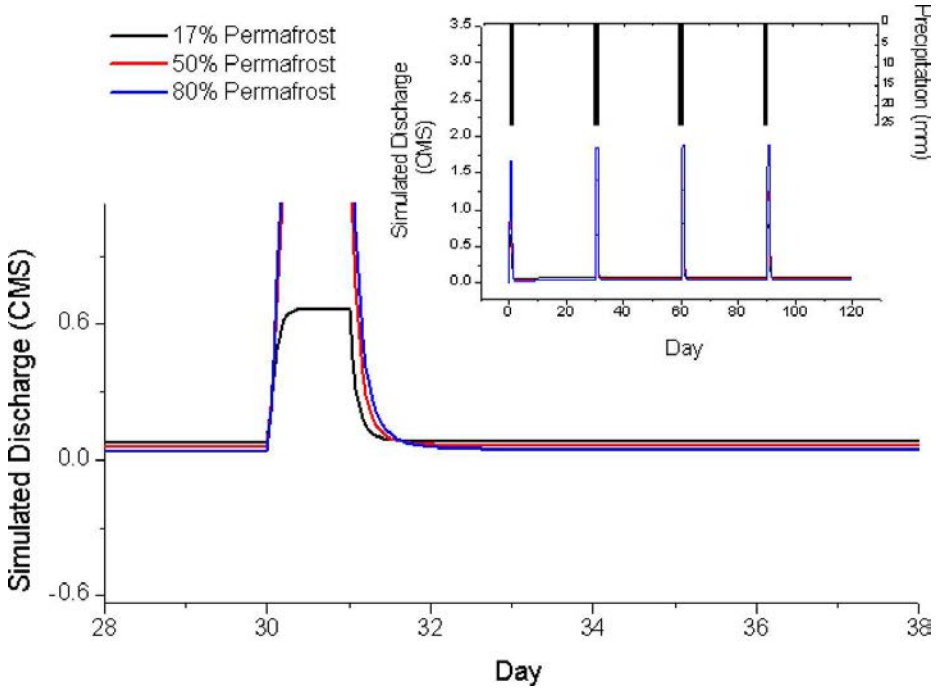


Figure 5.9. Comparison of simulated hydrographs for varying representation of permafrost extent.

simulations. The thaw depth at the end of the 120 days is 0.5 meters. The snowmelt and evaporation processes were not represented in these simulations.

Comparison of the simulation hydrographs show that increasing permafrost extent results in a larger peak discharge, a lower base flow between precipitation events, and a longer recession period following each precipitation event (Figure 5.9). These results give us confidence in the mathematical conceptualization of the sub-arctic hydrologic system.

### 5.7 Assessing the Potential Hydrologic Response to a Changing Climate

A number of possible scenarios are simulated in order to assess the influence of expected climatic changes to stream flow system through the use of the 'virtual control watershed' concept [*Andreassian et al.*, 2003]. Using this technique, the sensitivity of potential changes in the sub-arctic system can be assessed. The scenarios explored include changing permafrost extent, active layer depth, distribution of vegetation, equilibrium evapotranspiration rates, precipitation, and temperature (air, ground, and soil). Simulation scenarios are

listed Table 5.1.

The reference scenario (0% change) for these simulations is the C2 sub-basin of CPCRW with the following conditions: 1) The areal extent of permafrost is 50% (Figure 5.10); 2) the maximum active layer depth at the end of the simulation is 0.54 meters; 3) vegetation is distributed by permafrost distribution, with coniferous vegetation (40% equilibrium evapotranspiration rate) occupying the permafrost region and deciduous vegetation (100% equilibrium evapotranspiration rate) in the permafrost free region; 4) with the exception of precipitation, the model simulation is driven by climatic data measured in 2000, beginning on 1 May and over a period of 120 days; and 5) realistic soil properties and channel properties, obtained from field measurements are used. Soil properties fall within the range of values listed in *Kane et al.* [1978]; *Beringer et al.* [2001]; *Mölders et al.* [2005]. Table 5.2 shows the soil and channel properties used for each simulation.

### 5.7.1 Changes in Permafrost Condition

The ground water process in TopoFlow is very sensitive to the location of the water table [*Schramm*, 2005]. The large differences in hydraulic properties between the organic and mineral soil amplifies this sensitivity. In these scenarios, the water table is set at a depth of 0.15 meters below land surface in permafrost regions and 3.5 meters in non-permafrost regions. Each scenario is run twice. In the first simulation, the water table location is output every 2 days. The last output water table from the first simulation is used as the initial water table condition for the second simulation.

Results from the permafrost distribution scenario are similar to the conceptual model test simulations with higher peak flows, lower baseflows, and longer recessions in the higher permafrost simulations (Figure 5.11). The +80% and +100% permafrost simulations are similar due to the fact the 80% permafrost boundary is very close to the natural 'watershed' boundary (Figure 5.10).

The scenarios of different active layer depths also include a water table that is initialized from a previous simulation (solid lines in Figure 5.12) as the water table input for the second simulation (dashed lines in Figure 5.12). It can be seen that as the active layer increases, the peak flows decrease throughout the simulation period. As the active layer develops, the soil storage increases, resulting in lower peak flows during precipitation

Table 5.1. Simulation Scenarios Used in Sensitivity Analysis

| Reference Simulation | | | | | | |
|---|---|---|---|---|---|---|
| **Scenario** | **Permafrost Distribution** | **Active Layer Depth** | **Conifer Distribution** | **Equilibrium Evapotranspiration** | **Precipitation** | **Average Temperature** |
| Reference | 50% | 0.545 | 50% | 0.4 C, 1.0 D | 6.25 mm | 10.06$^o$C AT<br>4.77$^o$C Surface<br>0.87$^o$C Ground |
| **Change (%) from Reference Simulation** | | | | | | |
| **Scenario** | **Permafrost Distribution** | **Active Layer Depth** | **Conifer Distribution** | **Equilibrium Evapotranspiration** | **Precipitation** | **Average Temperature** |
| Permafrost | -100, -66<br>+60, +100 | 0 | 0 | 0 | 0 | 0 |
| Active Layer Depth | 0 | -100, -66<br>+60, +100 | 0 | 0 | 0 | 0 |
| Conifer Distribution | 0<br>0 | 0<br>0 | -100, -66<br>+60, +100 | 0<br>0 | 0<br>0 | 0<br>0 |
| Equilibrium ET Rate | 0 | 0 | 0 | -100, -66<br>+60, +100 | 0<br>0 | 0<br>0 |
| Precipitation | 0 | 0 | 0 | 0 | -100, -66<br>+60, +100 | 0<br>0 |
| Temperature | 0 | 0 | 0 | 0 | 0 | -100, -66<br>+60, +100 |

Symbols Used: C: Conifer Vegetation; D: Deciduous Vegetation; AT: Air Temperature; 0: No change from the reference conditions.

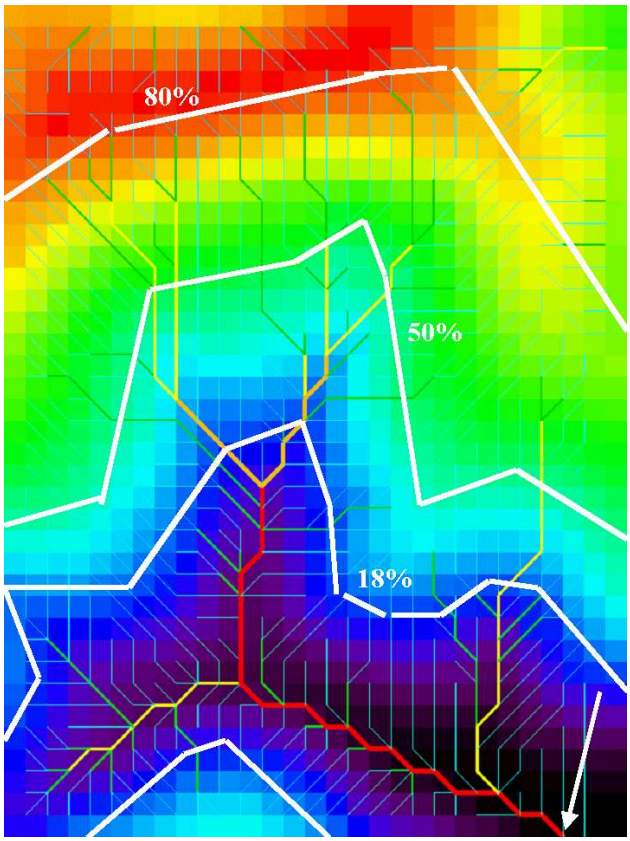


Figure 5.10. Model domain, channel network, and permafrost distribution of the 'virtual watershed.' The heavy white lines indicate the approximate permafrost/no permafrost boundary for the 18, 50, and 80% spatial distributions. The white arrow indicates the location of simulation output. The channel network for the entire model domain is displayed, with heavier lines indicating higher order channel segments.

Table 5.2. Soil and channel variables used in the model simulations.

| **Soil Properties** | | | | | |
|---|---|---|---|---|---|
| | | **Permafrost** | | | |
| **Layer** | **Thickness [m]** | $K_T$ **[m/s]** | $K_F$ **[m/s]** | $P_T$ | $P_F$ |
| 1 | 0.10 | 1.5e-4 | 1.5e-5 | 0.9 | 0.7 |
| 2 | 0.15 | 2.0e-5 | 2.0e-7 | 0.9 | 0.3 |
| 3 | 5.0 | 2.83e-7 | 2.83e-9 | 0.48 | 0.25 |
| 4 | 0.50 | 1.0e-10 | 1.0e-10 | 0.5 | 0.5 |
| | | **Non-Permafrost** | | | |
| **Layer** | **Thickness [m]** | $K_T$ **[m/s]** | $K_F$ **[m/s]** | $P_T$ | $P_F$ |
| 1 | 0.10 | 1.5e-4 | 1.5e-5 | 0.9 | 0.7 |
| 2 | 0.15 | 2.83e-7 | 2.83e-10 | 0.5 | 0.5 |
| 3 | 5.0 | 2.83e-7 | 2.83e-9 | 0.5 | 0.5 |
| 4 | 0.50 | 5.0e-6 | 5.0e-6 | 0.5 | 0.5 |
| | | **Channel Properties** | | | |
| | | **Order** | **Manning's 'N'** | **Width [m]** | **Bank Angle [Degrees]** |
| | | 1 | 0.3 | 100 | 89 |
| | | 2 | 0.3 | 100 | 89 |
| | | 3 | 0.16 | 0.15 | 33 |
| | | 4 | 0.16 | 0.30 | 33 |
| | | 5 | 0.16 | 0.48 | 33 |

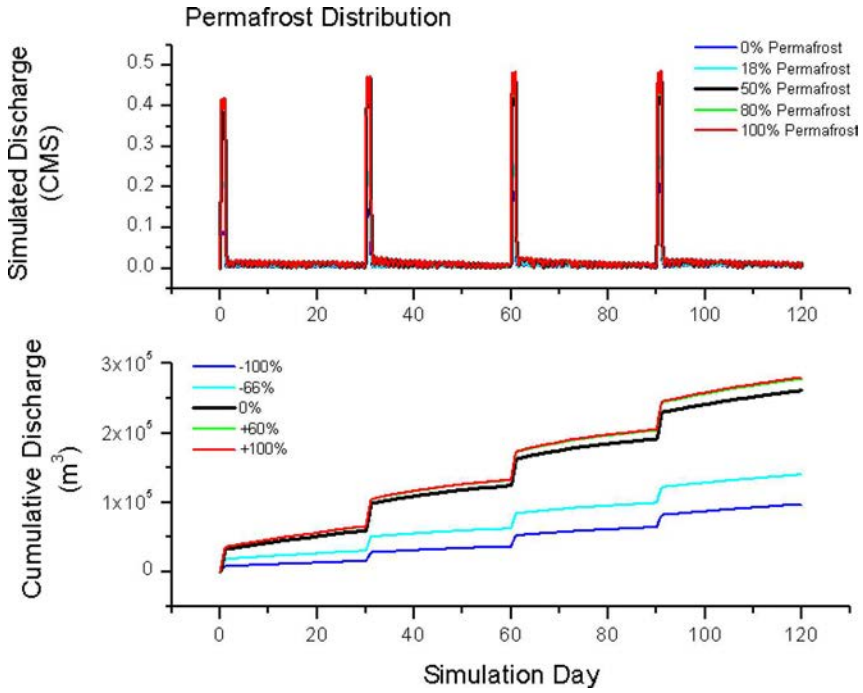


Figure 5.11. Stream flow variation with changes in permafrost distribution.

events. In the situation where the active layer does not develop (maximum active layer depth = 0.0 meters), the storage capacity is limited to the highly conductive near surface organic soils, resulting in high runoff generation.

### 5.7.2 Changes in Vegetation

In the boreal forest, deciduous vegetation show evaporative losses that approach the equilibrium rate, while only 25-50% of the equilibrium rate is realized in coniferous vegetation [*Baldocchi et al.*, 2000; *Eugster et al.*, 2000]. Vegetation in Figure 5.13 is distributed with coniferous vegetation located in the valley bottoms, while deciduous vegetation is distributed in the uplands. During the precipitation events, the contributing area (Total Discharge [$m^3$] / Total Precipitation [$m$]) is calculated to be approximately 43%. Simulation results indicate the only changes in model output occur when the vegetation type is altered within the contributing area. This is confirmed by reversing the vegetation distribution (i.e. deciduous vegetation located in the valley bottoms and coniferous vegetation being located in the

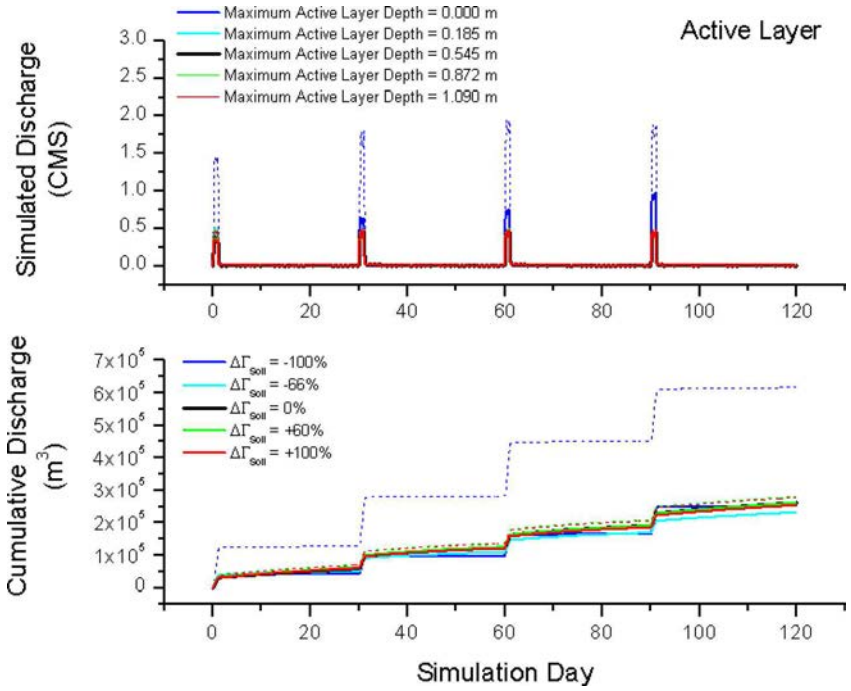


Figure 5.12. Stream flow variation with changes in active layer depth.

higher elevations) (Figure 5.14). The evapotranspiration scenarios indicate the simulated discharge is inversely proportional to the rate of evapotranspiration (Figure 5.15).

### 5.7.3 Changes in the Climate System

Changes in temperature (air, surface, and ground) are calculated by adding or subtracting the appropriate percentage of the average measured temperature, measured over the simulation period, to the measured value. The average measured air, surface, and ground temperatures used in these scenarios are 10.06, 4.77, and 0.87$^{o}$C, respectively. In these scenarios, the only hydrologic process in which temperature is used as an input variable is evapotranspiration, which is simulated with the energy balance method (Table 4.4).

Increasing the temperature by 60 and 100% of average temperatures results in a disproportionately strong temperature gradients between all the temperature variables. Increasing the temperature by 60 and 100% of the average temperature also results in predominately stable atmospheric conditions ($T_{air} > T_{surface}$). The bulk exchange coefficient,

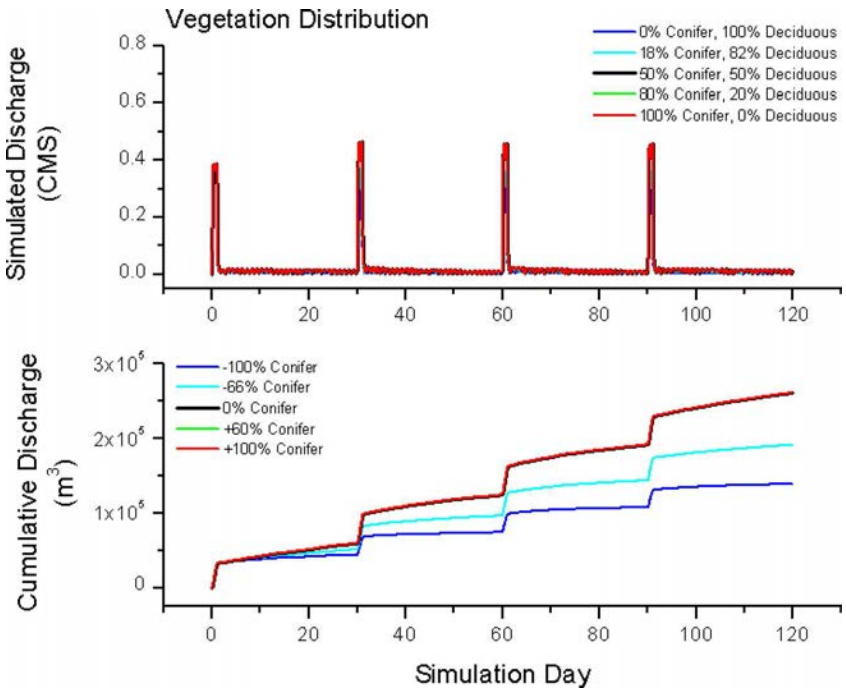


Figure 5.13. Stream flow variation with changes in vegetation distribution. In these simulations, coniferous vegetation is located in valley bottoms. Deciduous vegetation is located in the uplands.

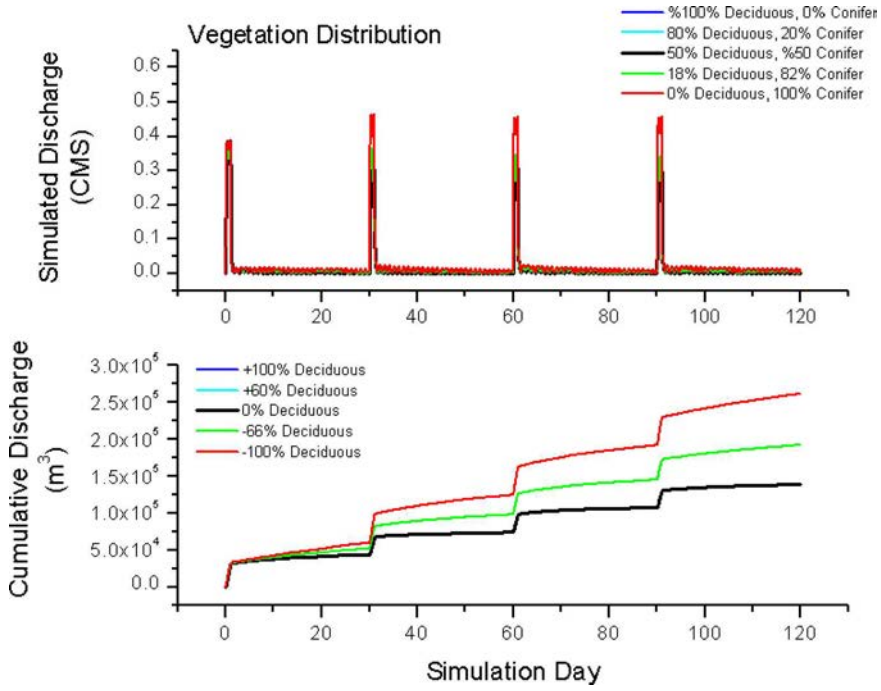


Figure 5.14. Stream flow variation with changes in vegetation distribution. In these simulations, deciduous vegetation is located in valley bottoms and coniferous vegetation is located in the uplands.

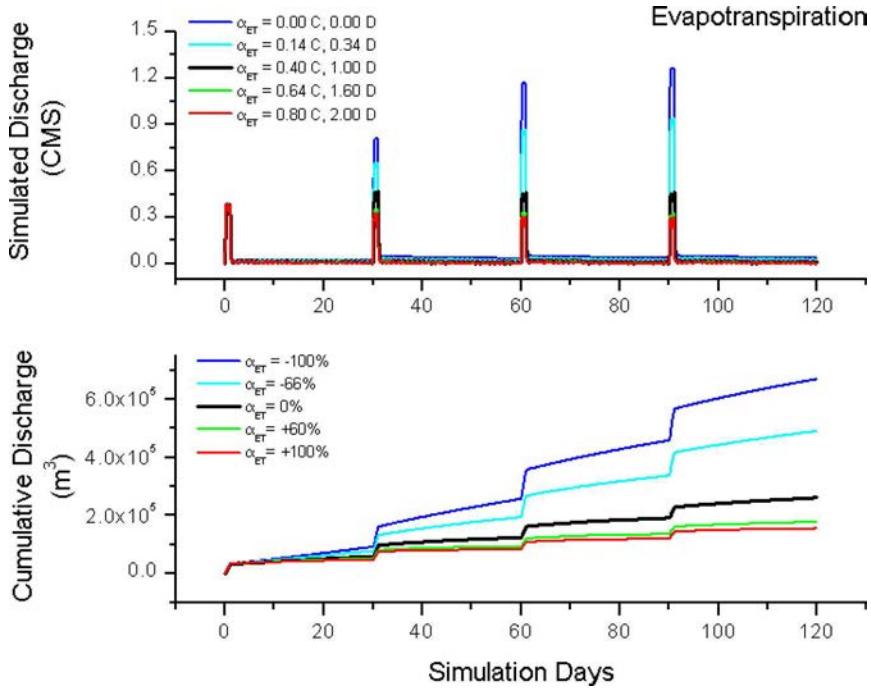


Figure 5.15. Stream flow variation with changes in evaporation rate.

$D_s$ for a stable atmosphere is given by $D_s = D_n \cdot (1 - 10 \cdot Ri)$. $D_n$ is the bulk exchange coefficient for atmospheric stability and $Ri$ is the Richardson number. The Richardson number is proportional to the temperature gradient between the air and surface temperature (the stronger the temperature gradient, the higher the Richardson number) and is always positive when $T_{air} > T_{surface}$. By increasing the temperature gradient, the amount of energy available for evapotranspiration is decreased. Similarly, the conductive heat flux is a function of the temperature gradient between the ground and surface temperatures. Similar to the sensible heat flux, increasing the temperature gradient between the ground and surface results in a reduced amount of energy available for evapotranspiration. The overall net result of this is that temperature increases result in a decreased evapotranspiration rate and increased stream flow (Figure 5.16). A second temperature change scenario is based upon the expected $3 - 6^oC$ range of temperature increase reported by the *ACIA* [2005]. In this scenario, a uniform temperature increase or decrease is specified for each temperature variable ($\pm 3^o$, $\pm 6^o$C), maintaining the reference simulation temperature gradients. In this scenario, increases in temperature result in increased evapotranspiration and decreased

streamflow. The range in difference from the reference simulation is $\pm 0.08\%$(*Figure*5.18).

The temperature change scenarios are also simulated using the Priestley-Taylor method of evapotranspiration. The Priestley-Taylor equation for evapotranspiration used in Topo-Flow is:

$$Q_{ET} = \alpha \cdot (0.406 + 0.011 T_{air}) \cdot (Q_{net} - Q_c) \tag{5.4}$$

where: $\alpha$ is the coefficient relating potential to actual evapotranpiration, $T_{air}$ is the air temperature, $Q_{net}$ is the net radiation, and $Q_c$ is the conductive heat flux. While increases in the conductive heat flux, $Q_c$, will reduce the evapotranspiration rate, it can be seen that evapotranspiration rate is proportional to the air temperature. Using this method, increases in air temperature results in a decreased stream flow (Figure 5.16).

The precipitation change scenarios results indicate that the simulated discharge is proportional to change in precipitation rate (Figure 5.17).

### 5.8 Discussion and Conclusions

Simulation of the hydrologic processes in the sub-arctic environment is challenging due to the rapidly changing thermal (permafrost verses non-permafrost, active layer development) and hydrologic (hydraulic conductivity and storage capacity) conditions in both time and space (x, y, and z-directions). By spatially and temporally varying the hydraulic conductivity (proxy for permafrost distribution) and porosity (proxy for storage capacity) with thaw depth development, stream flow patterns observed in the field are simulated.

The importance of soil storage and contributing area on the stream flow process is illustrated by the sensitivity analysis. As permafrost extent was decreased, the size of the contributing area was proportionately reduced, reducing the cumulative discharge. This is consistent with field observations made between the C2 and C3 sub-basins, which are underlain with 3 and 53% permafrost. *Dingman* [1973] observed the hydrologic response to precipitation events is proportional to the antecedent conditions of the watershed. The second active layer scenario, in which subsurface storage is limited within the contributing area by a near surface water table, resulted in a greater simulated discharge. This result is consistent with the findings of *Dingman* [1973]. The fact that evaportranspiration is an important process in the sub-arctic is not a suprise. *Gieck and Kane* [1986] and [*Bolton*

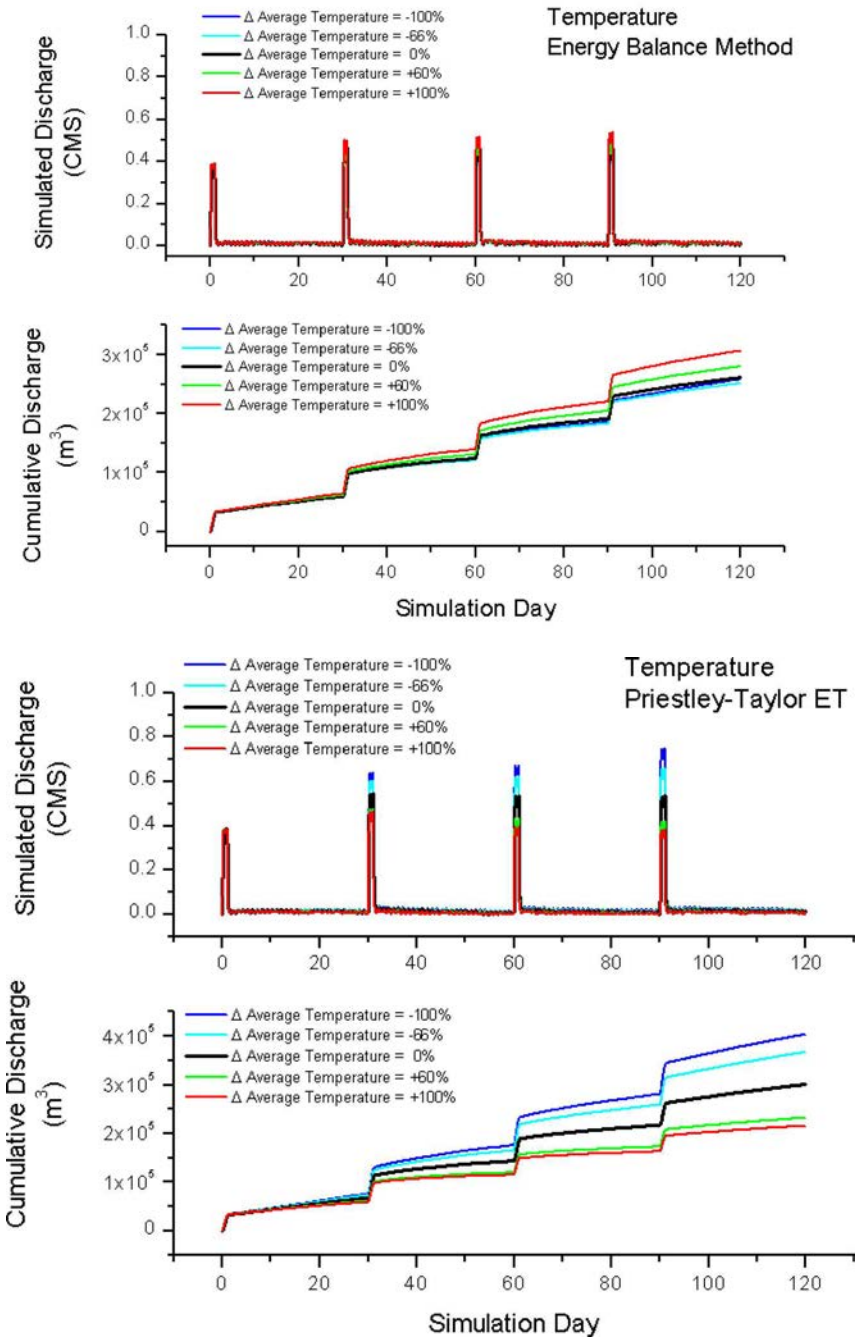


Figure 5.16. Stream flow variation with changes in temperature using the energy balance method (top panel) and the Priestley-Taylor method (bottom panel).

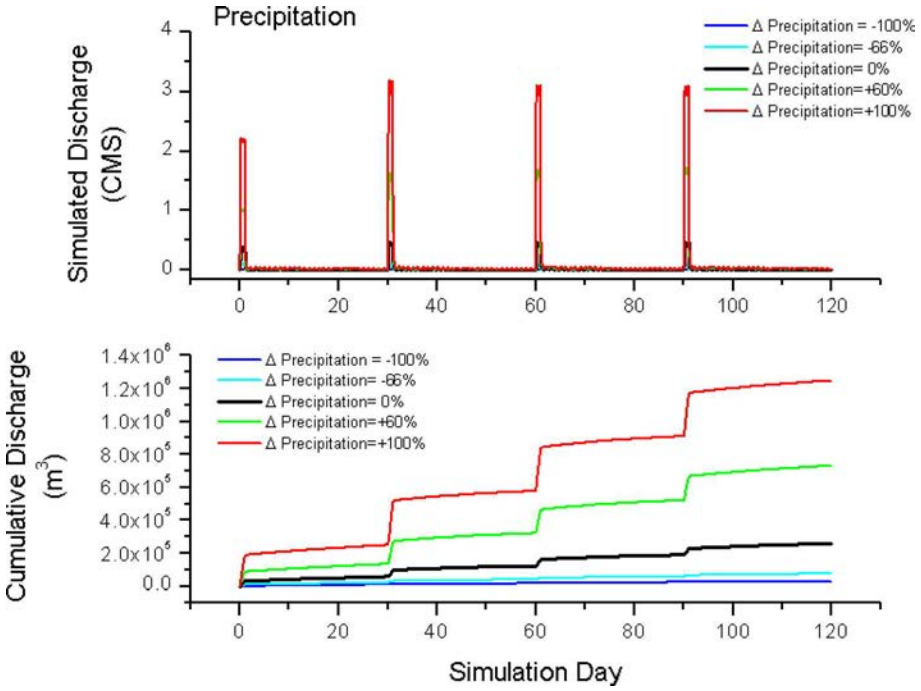


Figure 5.17. Stream flow variation with changes in precipitation.

*et al.*, 2004] report evapotranspiration can account for nearly all the summer precipitation. However, the magnitude of evapotranspiration should be viewed with care. In the current formulation of TopoFlow, the water evaporated from the system is removed directly from the top of the water table. Given the known sensitivity to water table position, it is not suprising the difference in cumulative discharge between the -100% and +100% evapotranspiration rates is large. While the evapotranspiration changes due temperature (air, surface, and soil) variation are mathematically accurate, the realized hydrologic response is not correct. The singular influence of temperature on evapotranspiration must also be viewed with caution.

The model assessment of climate sensitivity indicate that if the climate continues to change as expected, every process tested, with the important exception of increased precipitation, will result in decreased summer runoff. This by extention will lead to an increase the winter runoff. Furthermore, if the observed changes in the permafrost regime (decrease in areal extent, increase in active layer depth) continue, the contributing area of the watersheds will decrease, reducing the area of influence to which hydrologic processes

respond.

Although rainfall has the largest influence on stream flow dynamics (Figure 5.18), permafrost plays an important secondary role through its strong influence on the size of the watershed contributing area, groundwater flow, soil moisture, soil storage, and distribution of vegetation. The presence or absence of permafrost has the primary influence on the soil moisture dynamics in this region.

The design of TopoFlow is well suited to the sub-arctic environment. By using a spatially distributed model, important hydrologic processes, such as the influence of vegetation in the contributing area or the impact of varying thaw depths, can be readily identified. This is not possible using typical rainfall-runoff or 'black box' models. In the subarctic, the hydrologic and thermal processes are tightly coupled. Incorporating a thermal model (either directly or by coupling to an independent model), which defines the presence or absence of permafrost and thaw depth in a physically-based manner is a logical next step in the TopoFlow development.

### 5.9 Acknowledgements

Support for this research was provided by the U.S. National Science Foundation Arctic System Science Program (OPP-0229705), the U.S. National Science Foundation Division of Environmental Biology under the Long Term Ecological Research Program (Grant number DEB-9211769), a fellowship from the Inland Northwest Research Alliance (U.S. Dept. of Energy contract DE-FG07-021D14277), and a grant from the Center of Global Change - University of Alaska Fairbanks.

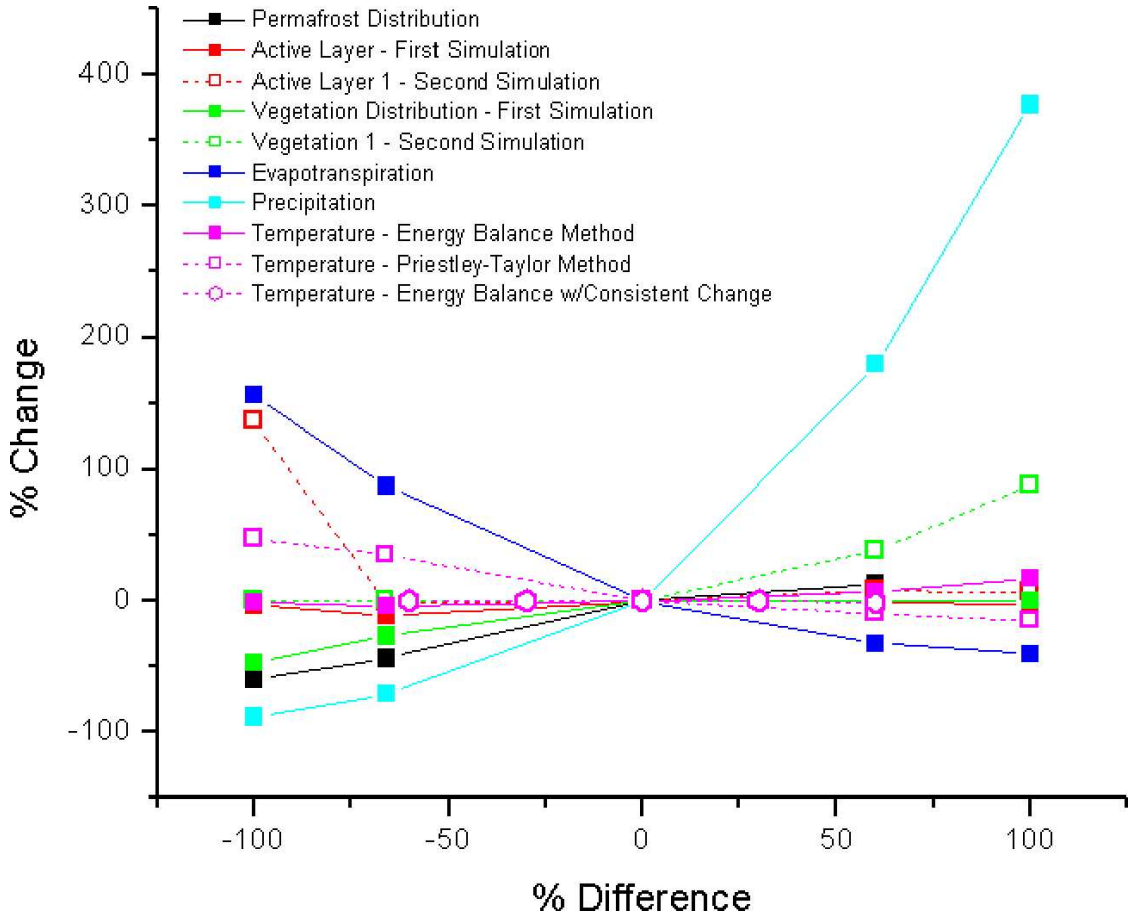


Figure 5.18. Results of sensitivity analysis. Notes: Temperature - Energy Balance with Consistent Change: Simulation scenarios in which the change is temperature is uniform ($\pm 3^o$C, $\pm 6^o$C) for $T_{air}$, $T_{surface}$ and $T_{soil}$ input variables and are plotted relative to the difference in air temperature.

**Bibliography**

ACIA (2005), *Impacts of a warming Arctic: Arctic Climate Impact Assessment*, 1046 pp., Cambridge University Press.

Andreassian, V., E. Parent, and C. Michel (2003), A distribution-free test to detect gradual changes in watershed behavior, *Water Resources Research*, *39*(9), 10–1–11.

Baldocchi, D., F. M. Kelliher, T. Black, and P. Jarvis (2000), Climate and vegetation controls on boreal zone energy exchange, *Global Change Biology*, *6*(Supplement 1), 69–83.

Bergström, S. (1976), Development and application of a conceptual runoff model for Scandinavian catchments, *SMHI Reports RHO 7*, Swedish Meteorological and Hydrological Institute, Norrköping, Sweden.

Bergström, S. (1992), The HBV model - it's structure and applications, *SMHI Reports RHO 7*, Swedish Meteorological and Hydrological Institute, Norrköping, Sweden.

Beringer, J., A. H. Lynch, F. S. Chapin, M. Mack, and G. B. Bonan (2001), The representation of Arctic soils in the land surface model: The importance of mosses, *Journal of Climate*, *14*, 3324–3335.

Boike, J., K. Roth, and P. Overduin (1998), Thermal and hydrologic dynamics of the active layer at a continuous permafrost site (Taymyr Peninsula, Siberia), *Water Resources Research*, *34*(3), 355–363.

Bolton, W., L. Hinzman, and K. Yoshikawa (2004), Water balance dynamics of three small catchments in a sub-arctic boreal forest, in *Northern Research Basins Water Balance (Proceedings of a workshop held at Victoria, Canada, March 2004)*, edited by D. L. Kane and D. Yang, IAHS Series of Proceedings and Reports Number 290, pp. 213 – 223.

Burt, T., and P. Williams (1976), Hydraulic conductivity in frozen soils, *Earth Surficial Processes*, *1*, 349–360.

Carey, S. K., and M.-k. Woo (1998), Snowmelt hydrology of two Subarctic slopes, Southern Yukon, Canada, *Nordic Hydrology*, *29*(4/5), 331–346.

Carey, S. K., and M.-k. Woo (2001), Slope runoff processes and flow generation in a subarctic, subalpine catchment, *Journal of Hydrology*, *253*, 110–129.

Carlson, R. (1972), Development of a conceptual hydrologic model for a sub-arctic watershed, *Report IWR-28*, Institute of Water Resources, University of Alaska Fairbanks.

Carr, A. T. (2003), Hydrologic comparisons and model simulations of subarctic watersheds containing continuous and discontinuous permafrost, Seward Peninsula, Alaska, Master's thesis, University of Alaska Fairbanks.

Chapman, W., and J. Walsh (1993), Recent variations in sea ice and air temperature in high latitudes, *Bulletin American Meteorology Society*, *74*, 33–47.

Dingman, S. (1973), Effects of permafrost on stream flow characteristics in the discontinuous permafrost zone of central Alaska., in *Permafrost: North American Contribution to the Second International Conference*, pp. 447–453, National Academy of Sciences, Washington D.C.

Eugster, W., W.R. Rouse, R.A. Pielke, J.P. McFadden, D.D. Baldocchi, T.G.F. Kittel, F.S. Chapin, G.E. Liston, P.L. Vidale, E.Vaganov, and S. Chambers (2000), Land-atmosphere energy exchange in arctic tundra and boreal forest: available data and feedbacks to climate, *Global Change Biology*, *6*(Supplement 1), 84–115.

Farris, A. M. (1996), Numerical modeling of contaminant transport in discontinuous permafrost - FT. Wainwright, Alaska, Master's thesis, University of Alaska Fairbanks.

Freeze, R. A., and J. A. Cherry (1979), *Groundwater*, Prentice-Hall.

Gieck, R. J., and D. Kane (1986), Hydrology of two subarctic watersheds, in *Proceedings of the Cold Regions Hydrology Symposium*, edited by D. Kane, pp. 283–291, American Water Resources Association.

Haugen, R., C. Slaughter, K. Howe, and S. Dingman (1982), Hydrology and climatology of the Caribou-Poker Creeks Research Watershed, Alaska, *CRREL Report 82-26*, US Army Corps of Engineers Cold Regions Research and Engineering Laboratory.

Hinzman, L., D. Kane, K. Yoshikawa, A. Carr, W. Bolton, and M. Fraver (2003), Hydrological variations along watersheds with varying degrees of permafrost, in *Proceedings of the 8th International Conference on Permafrost*, pp. 407–411.
*72*, 251–298.

Hinzman, L., N.D. Bettez, F.S. Chapin, M.B. Dyurgerov, C.L.Fastie, B. Griffith, R.D. Hollister, A. Hope, H.P. Huntington, A.M. Jensen, G.J. Jia, T. Jorgenson, D.L. Kane, D.R. Klein, G. Kofinas, A.H. Lynch, A.H. Lloyd, A.D. McGuire, F.E. Nelson, W.C. Oechel, T.E. Osterkamp, C.H. Racine, V.E. Romanovsky, R.S. Stone, D.A.Stow, M. Sturm, C.E. Tweedie, G.L. Vourlitis, M.D. Walker, D.A. Walker, P.J. Webber, J.M. Welker, K.S. Winker, and K. Yoshikawa (2005), Evidence and implications of recent climatic change in northern Alaska and other arctic regions, *Climatic Change*, *72*, 251–298.

IPCC (2001), Climate change 2001: Synthesis report. summary for policymakers., *Tech. rep.*, Intergovernmental Panel on Climate Change.

Jorgenson, M., C. Racine, J. Walters, and T. Osterkamp (2001), Permafrost degradation and ecological changes associated with a warming climate in Central Alaska, *Climate Change*, *48*, 551–571.

Kane, D., and L. Hinzman (2004), Monitoring extreme environments: Arctic hydrology in transition, *Water Resources Impact*, *6*(1), 24–27.

Kane, D., and J. Stein (1983), Field evidence of groundwater recharge in Interior Alaska, in *Proceedings of the Fourth International Conference on Permafrost*, pp. 572–577, National Academy Press.

Kane, D. L., R. D. Seifert, and G. S. Taylor (1978), Hydrologic properties of Subarctic organic soils, *Tech. Rep. IWR-88*, Institute of Water Resources, University of Alaska Fairbanks.

Knudson, J., and L. D. Hinzman (2000), Prediction of streamflow in an Alaskan watershed underlain by permafrost, in *Water Resources in Extreme Environments*, edited by D. L. Kane, pp. 309–313, American Water Resources Association.

Koutz, F., and C. Slaughter (1972), Geological setting of the Caribou-Poker Creeks Research Watershed, Interior Alaska, *Technical note*, U.S. Army Cold Regions Research and Engineering Laboratory.

Magnuson, J., D. Robertson, B. Benson, R. Wynne, D. Livingstone, T. Arai, R. Assel, R. Barry, V. Card, E. Kuusisto, N. Granin, T. Prowse, K. Steward, and V. Vuglinski (2000), Historical trends in lake and river ice cover in the northern hemisphere, *Science*, *289*, 1743–1746.

Mölders, N., M. Jankov, and G. Kramm (2005), Application of gaussian error propagation principals for theoretical assessment of model uncertainty in simulated soil processes caused by thermal and hydraulic parameters, *Journal of Hydrometeorology*, *6*, 1046–1062.

Nelson, G. (1978), Hydrologic information for land-use planning, Fairbanks vicinity, Alaska, *Open-File Report 78-959*, U.S. Geological Society.

Osterkamp, T., and V. Romanovsky (1999), Evidence for warming and thawing of discontinuous permafrost in Alaska, *Permafrost and Periglacial Processes*, *10*, 17–37.

Osterkamp, T., L. Viereck, Y. Shur, M. Jorgenson, C. Racine, A. Doyle, and R. Boone (2000), Observations of thermokarst and its impact on boreal forests in Alaska, USA, *Arctic, Antarctic and Alpine Research*, *32*, 303 – 315.

Peterson, B., R. Holmes, J. McClelland, C. Vörösmarty, R. Lammers, A. Shiklomanov, I. Skiklomanov, and S. Rahmstort (2002), Increasing river discharge to the Arctic Ocean, *Science*, *298*, 2171–2173.

Rieger, S., C. E. Furbush, D. B. Schoephorster, H. Summerfield, and L. C. Geiger (1972), Soils of the Caribou-Poker Creeks Research Watershed Interior Alaska, *Tech. rep.*, Cold Regions Research and Engineering Laboratory.

Sand, K., and D. L. Kane (1986), Effects of seasonally frozen ground on snowmelt modeling, in *Proceedings of the Symposium: Cold Regions Hydrology*, edited by D. L. Kane, pp. 321–327, American Water Resources Association.

Schramm, I. (2005), Hydrologic modeling of an Arctic watershed, Alaska, Master's thesis, Universität Potsdam, Potsdam, Germany.

Serreze, M., et al. (2000), Observational evidence of recent change in the northern high latitude environment, *Climate Change*, *46*, 159–207.

Slaughter, C. (1981), Streamflow measurement with pre-fabricated partial flumes in a permafrost dominated watershed., *Research Note 382*, USDA Forest Service PNW Forest and Range Experimental Station.

Slaughter, C., and C. Benson (1986), Seasonal snow cover and aufeis in Alaska's taiga, in *Cold Regions Hydrology Symposium*, pp. 101–109, American Water Resources Association.

Slaughter, C., and D. Kane (1979), Hydrologic role of shallow organic soils in cold climates, in *Canadian Hydrology Symposium: Proceedings, 79-Cold Climate Hydrology*, pp. 380–389.

Slaughter, C., J. Hilgert, and E. Culp (1983), Summer streamflow and sediment yield from discontinuous-permafrost headwater catchments, in *Proceedings of the Fourth International Permafrost Conference*, pp. 1172–1177, National Academy Press.

Smith, L., Y. Sheng, G. MacDonald, and L. Hinzman (2005), Disappearing Arctic lakes, *Science*, *308*, 1429.

Stein, J., and D. Kane (1983), Monitoring the unfrozen water content of soil and snow using time domain reflectometry, *Water Resources Research*, *19*(6), 1537–1584.

Strahler, A. (1969), *Physical Geography*, 3rd ed., Wiley.

Terzaghi, K. (1952), Permafrost, *Journal of the Boston Society of of Civil Engineers*, *39*(1), 1–50.

Topp, G., J. Davis, and A. Annan (1980), Electromagnetic determination of soil water content: measurements in coaxial transmission lines, *Water Resources Research*, *16*(3), 574–582.

Troth, J. L., F. J. Deneki, and L. M. Brown (1975), Subarctic plant communities and associated litter and soil profiles in the Caribou Creek Research Watershed, Interior Alaska, *Research Report 330*, Cold Regions Research and Engineering Laboratory.

Wahrhafting, C. (1965), Physiographic divisions of Alaska, *Professional Paper 482*, U.S. Geological Survey.

Woo, M.-k. (1986), Permafrost hydrology in North America, *Atmosphere-Ocean*, *24*(3), 201–234.

Yoshikawa, K., L. Hinzman, N. Ishikawa, C. Collins, and V. Lunardini (1998), Air and ground temperature models at Caribou-Poker Creeks Research Watershed, in *Proceedings of the 49th AAAS Arctic Science Conference*, Fairbanks, Alaska.

Yoshikawa, K., W. Bolton, V. Romanovsky, M. Fukuda, and L. Hinzman (2002), Impacts of wildfire on the permafrost in the boreal forest of Interior Alaska, *Journal of Geophysical Research*, *107*(8148: doe:10.1029/2001JD000438), printed 108(D1), 2003.

Yoshikawa, K., D. White, L. Hinzman, D. Goering, K. Petrone, W. Bolton, and N. Ishikawa (2003), Water in permafrost: Case study of aufeis and pingo hydrology in discontinuous permafrost, in *International Conference on Permafrost, Proceedings 8*, vol. 2, edited by M. Phillips, S. Springman, and L. Arenson, pp. 1259–1264.

Youcha, E. K. (2003), A geohydrologic analysis of an upland-bedrock aquifer system: Applications to Interior Alaska, Master's thesis, University of Alaska Fairbanks.

# Chapter 6
# Conclusions

Hydrologically speaking, the presence or absence of permafrost, is the defining characteristic of the sub-arctic environment. Although the distribution of permafrost is site specific in this environment, it impacts most of the hydrologic processes including stream flow, soil moisture dynamics, ground water flow, and water storage processes. The overarching hypothesis for this research is **'in the sub-arctic environment, the presence or absence of permafrost is the dominant influence on the soil moisture regime and stream flow patterns.'** A series of research objectives and questions, presented in Chapter 1 were formulated in order to test this hypothesis. These research objectives and questions, presented in Chapter 1, are approached through a combination of field study and computer simulation. Results from the field studies show that the presence or absence of permafrost is the dominant influence on soil moisture dynamics. Results from the computer simulations suggest that rainfall has the largest influence on the stream flow regime. The distristribution of permafrost and the depth of thaw play an important, but secondary, role. This research expands upon the current knowledge of the hydrologic processes, with emphasis on the stream flow and soil moisture processes, which operate in the sub-arctic environment. Results from the field and computer studies are discussed below.

## 6.1 Field Study

In Chapters 2 and 5, the soil moisture regime in areas of discontinuous permafrost is analyzed. Based upon field measurements in the Caribou-Poker Creeks Research Watershed (CPCRW), it was found that large differences in soil moisture exist in areas underlain by permafrost and those which are free of permafrost. In areas underlain by permafrost, ice-rich pores at the permafrost table impedes movement of near surface water to the subsurface, resulting in soils which are at or near saturation throughout the summer period, showing little response to precipitation events. In non-permafrost areas, soils tend to be well-drained and tend to be drier, having a greater response to precipitation events. Significant soil moisture differences were found in between in vegetation type (deciduous versus coniferous), permafrost condition (permafrost verses no-permafrost), and topography (hillside verses valley bottom), with the largest difference occurring between the

permafrost and non-permafrost sites. In Chapter 2, the stream flow hydrographs are analyzed. In permafrost dominated watersheds display slower response times and a higher peak specific discharge during precipitation events, a longer recession period following a precipitation event, and lower specific baseflow between precipitation events. Using hydrograph separation analysis, it is shown that as the thaw depth develops throughout the summer, the sub-surface water contribution ('old water' held in storage) to storm hydrographs increases significantly (from approximately 20-60%) in the permafrost dominated watersheds. In the C2 sub-basin, which is underlain by about 3%, the sub-surface contribution to storm events is fairly constant at about 70%.

In Chapter 3, the relative importance of hydrologic processes in the sub-Arctic environment is addressed. In this chapter, a water balance in three sub-basins of CPCRW of varying permafrost extent, was conducted over the 1978-2003 time period. For every year of the study period, the water balance was calculated from the time of maximum snow water equivalent (mid-March to early-April) to the time of winter freeze-up (late-September to mid-October). The approach we took to solving the water balance equation was to set the change in storage term, ($\Delta S$ in Equation 3.1), as the residual. In taking this approach, all associated measurement errors are lumped into this term, limiting our ability to determine the degree to which we are able to 'close' the water balance. In terms of a yearly water balance, it is clear significant errors exist as reflected in the reported $\Delta S$ values. The $\Delta S$ term is reported as a positive value for all watersheds over most years of study - an unlikely result. The predominately positive $\Delta S$ values indicate our ability to quantify water sources entering the system is better than our ability to quantify the water sources leaving the system. This is not a surprising result as the winter baseflow and (typically) the snow melt runoff events were not taken into account. Despite the limitations of the method used, some important findings were obtained.

In terms of processes, the snowmelt period is typically the major hydrologic event of the year. Over a 2-3 week period, approximately 1/3 of the annual precipitation (rain + snow), which is held in storage over 7-8 month period, is introduced to the watershed system. The snowmelt period also coincides at the time when the water storage capacity of the permafrost soils is at its lowest as ice-rich mineral soils are completely frozen. However, the snowmelt event was hard to capture due to extensive aufeis buildup leading to

dispersal of snow melt runoff outside the normal channel boundaries. In comparing the stream flow between the watersheds, it was found that the watersheds with lesser amounts of permafrost produce less runoff compared to watersheds with a larger areal extent of permafrost, although the runoff ratios between all the watersheds vary little. Differences in summer runoff between the low and high permafrost watersheds must be offset by a higher winter discharge as water is released from the deep groundwater system. The areal composition of vegetation plays an important role as evaportranspiration was found to consume between 1/3 to nearly all the summer precipitation (depending upon the sub-basin in question). In this study, it became clear the role of the water storage processes is critically important in terms of the water balance, but is the least well quantified. Changes in the water storage processes, in particular the active layer depth (increasing the storage capacity of the soils), may lead to shift in magnitude and timing of runoff.

As part of the FROSTFIRE experiment, I participated in a study which analyzed the role of short- and long-term effects of wildfire on permafrost in Interior Alaska (Appendix A). My role in this study was to examine the short- and long-term effects of wildfire on the soil moisture regime. It was found that in both the short and the long term, the most significant impact on the soil moisture regime was through the removal of vegetation and the surface organic layers. In the short term, the loss of vegetation results in a decreased evapotranspiration demand, resulting in wetter soils than compared to adjacent non-burned sites. The increased moisture content increases the thermal conductivity of the soils. In the moderate (partial, but significant removal of the organic layer) or severe (complete removal of the organic layer) sites surveyed, the increase in thermal conductivity led to a thickening of the active layer, increasing the soil storage capacity. The long-term (>10 years) effect of wildfire in these (moderate or severe) sites were drier soils (at depth) compared to adjacent un- or lightly-burned areas.

### 6.2 Computer simulation

A new spatially-distributed, process-based model hydrologic model, TopoFlow, was developed to simulate the hydrologic processes in the Arctic and sub-Arctic environments. The TopoFlow model is very well suited to simulating the hydrologic processes in the sub-arctic environment. TopoFlow is flexible enough to handle spatial and temporal in-

put files, which is critical in describing the soil properties in the discontinuous permafrost environment. In Chapter 4, the structure of TopoFlow is described. TopoFlow is a second generation hydrologic model, following ARHYTHM, developed by the Water and Environmental Research Center, University of Alaska Fairbanks.

Hydrologic modeling in any environment is challenging due to site specific conditions In the sub-arctic environment, the challenge is presented by the discontinuous permafrost condition, in which rapid changes in thermal properties of the soils (permafrost versus non-permafrost, thaw depth) and hydrologic (hydraulic conductivity, storage capacity) occur over short temporal and spatial scales. In our approach to representing the discontinuous permafrost condition, TopoFlow was modified to allow spatial and temporal variable inputs of hydraulic conductivity and porosity. By continually varying of the hydraulic conductivity (used as a proxy for permafrost distribution and thaw depth) and porosity (used as a proxy for storage capacity), the dynamic changes of the soil properties associated with the discontinuous permafrost environment can be adequately represented. In Chapter 5, we show that by only varying the hydraulic conductivity and porosity over time and space, we are able to reproduce the stream flow patterns observed in watersheds of varying permafrost coverage.

An analysis was conducted to test the hydrologic sensitivity under a variety of climatic conditions. The hydrologic response to changes (both positive and negative) in permafrost distribution, active layer thickness, distribution of vegetation, evapotranspiration rates, precipitation, and temperature were all tested. Results from this study suggest that if the climate system changes as expected, the total amount of summer runoff will be reduced. Every scenario tested, with the very important expection of precipition, resulted (to varying degrees) decreases in runoff under the climate warming scenarios. By extension, an a decrease in summer runoff will (most likely) result in an increased winter runoff. This analysis demonstrates that precipitation has the strongest influence on stream flow regime. The sensitivity test also illustrates the importance of the contributing area. A hydrologic response to spatial changes in vegetation distribution was found only in simulations in which the contributing area was altered.

# Appendix A

## Impacts of wildfire on permafrost in the boreal forests of Interior Alaska*

**Abstract**

The impact to the permafrost during and after wildfire was studied using 11 boreal forest fire sites including two controlled burns. Heat transfer by conduction to the permafrost was not significant during fire. Immediately following fire, ground thermal conductivity may increase 10-fold and the surface albedo can decrease by 50% depending on the extent of burning of the surficial organic soil. The thickness of the remaining organic layer strongly affects permafrost degradation and aggradation. If the organic layer thickness was not reduced during the burn, then the active layer (the layer of soil above permafrost that annually freezes and thaws) did not change after the burn in spite of the surface albedo decrease. Any significant disturbance to the surface organic layer will increase heat flow through the active layer into the permafrost. Approximately 3–5 years after severe disturbance and depending on site conditions, the active layer will increase to a thickness that does not completely refreeze the following winter. This results in formation of a talik (an unfrozen layer below the seasonally frozen soil and above the permafrost). A thawed layer (4.15 m thick ) was observed at the 1983 burned site. Model studies suggest that if an organic layer of mare than 7–12 cm remains following a wildfire then the thermal impact to the permafrost will be minimal in the boreal forests of Interior Alaska.

### A.1 Introduction

The discontinuous permafrost zone is one of the most sensitive areas to climate warming in the world. Throughout the circumpolar north, the boreal forest widely overlaps the area of discontinuous permafrost [*Péwé*, 1975; *Brown et al.*, 1997; *Osterkamp et al.*, 2000]. The thermal condition of permafrost in this region is quite unstable, as it is very close to thawing, often $-1^oC$ or warmer. The distribution of the permafrost is strongly influenced by local factors such as landscape, soil type, and vegetation cover [*Viereck*, 1982; *Haugen et al.*, 1982]. The presence and thickness of the surface organic layer are the most important

*K. Yoshikawa, W.R. Bolton, V.E. Romanovsky, M. Fukuda, and L.D. Hinzman, Impacts of wildfire on the permafrost in the boreal forests of Interior Alaska, *J. Geophys. Res., 107*, 8148, doi:10.1029/2001JD000438, 2002. [printed 108(D1), 2003]

factors controlling degradation or addradation of permafrost [*Viereck*, 1982]. When the organic layer is removed, the surface albedo decreases and the soil thermal conductivity of the surface soil layer increases from about 0.2 to about 1.0 W/m K [*Hinzman et al.*, 1991]. Wildfire is one of the most important agents controlling the thickness of organic layer in the boreal forest.

Wildfires have been a natural part of the boreal forest ecosystems, burning an average of 1 million ha/yr in 1950 increasing to almost 3 million ha/yr in 2000 in the North American boreal forests (B. Stocks et al., The changing fire regime of Western North America submitted to *Journal of Geophysical Research*, 2002) [*Kasischke and Stocks*, 2000]. Fires in boreal forests have both immediate and long-term impacts on the ecosystem due to their effects on surface energy, water balance, and underlying permafrost. The return period for wildfire in the boreal forest is about 29 - 300 years [*Yarie*, 1981; *Kasischke et al.*, 2000; *Dyrness et al.*, 1986] and is strongly influenced by climate and human activities (both as a source of ignition and as an agent of fire control) [*Burn*, 1998a; *Brown and Grave*, 1979; *Fastie and Mann*, 1993].

Short-term studies of the effects of fire on the soil moisture and ground thermal regime in more temperate regions as well as cold regions have been well documented. Soil moisture content increases immediately following fires due to a decrease in evapotranspirations [*Tiedemann et al.*, 1979; *Klock and Helvey*, 1976; *Moore and Keeley*, 2000]. *Klock and Helvey* [1976] also noted a decrease in soil moisture content to prefire levels after a 5 year period. However, *Liang et al.* [1991] reported lower soil moisture contents in a burned area 2 years after a fire. Numerous other studies show increasing soil moisture contents following logging operations [*Klock and Helvey*, 1976; *Croft and Monninger*, 1953; *Zierner*, 1964].

Although the net surface energy balance may not change significantly after fire, the ways in which the incoming energy is partitioned does change substantially. For example, following wildfire, the surface albedo is significantly reduced. The reduced albedo means that soils can absorb incoming shortwave radiation then before the fire, which is then converted to sensible heat, resulting in higher ground surface temperatures. The offset of this is significantly increased outgoing longwave radiation due to these higher ground temperatures. The effect of this is an actual decrease in the net radiation by about 10%, but increased energy conducted into the ground [*Rouse and Mills*, 1977].

Changes in depth to permafrost and active layer thickness are well documented and have been observed in numerous experimental studies. Changes in the surface material and thermal properties allow for increased heat flow. *MacKay* [1970] reported an average 24.1 cm (149%) increase in active layer thickness at the end of the first year and 34.8 cm increase (171%) in the second autumn. *Burn* [1998b] documented more rapid thawing and delayed freeze-back of the active layer compared to unburned areas. *Brown* [1983] noted that each of these effects is directly proportional to the fire severity. In cases of more severe fires, the surface organic layer is entirely combusted exposing the mineral soil beneath. Any disturbance to the surface layer will increase heat flow through the active layer into the permafrost. After approximately 3-5 years (depending on site conditions) the active layer will increase to a thickness that does not completely refreeze the following winter forming a talik. *Viereck* [1982] reported there was no significant difference in the active layer between the burned site and unburned sites in the first summer following the 1971 Wickersham Dome fire, located near Fairbanks, Alaska. However, the time required for the active layer to become completely frozen was delayed by 1 month compared to the unburned site in the first winter after the fire (12 December to 15 January 1971). In the following summer, the active layer was 161% deeper in the burned site as compared to the unburned control area. *Viereck* [1982] also demonstrated that fire lines (mechanically removing vegetation with a bulldozer) had more impact to the active layer than the severely burned site. *Heginbottom* [1971] reported that by the summer after a fire in Northwest Canada, thaw as 9 cm deeper on a burned site as compared to a control. *Lotspeich et al.* [1970] reported that the 1966 Dennison River fire, Eastern Alaska, showed no significant difference in thaw depth between burned and unburned sites. The burn was not severe enough at any site to remove the organic layer, which remained about 20 cm thick at the study burned site. *Wein* [1971] reported the conditions of site burned in 1969 in Interior Alaska. He described the active layer as being 35-50% deeper the next spring following the fire, and 15-20% greater in fall. *Brown et al.* [1969] observed several fire sites along the Alaskan Taylor Highway. The thaw depth was increased 140-160% *Kryuchkov* [1968] observed the active layer was actually thinner several years after a fire in case of Siberian tundra. Before the fire, the active layer was 50-70 cm deep however it was on 40-45 cm a few years after the fire. This decrease in summer thawing was due to higher soil mois-

ture (ice) contents resulting from decreased transpiration. Controlled field experiments achieved more uniform results as compared with observations following wildfires. *Dyrness* [1982] studied differences in active layer thickness under different ground surface treatments (control, lightly burned, heavily burned, half the forest floor organic layer removed, and entire organic layer removed). After the fourth summer, the only treatment that had a statistically significant effect on soil temperature and permafrost depth was the mechanical removal of all or a portion of the forest floor. *Esch* [1982] tested the impact on permafrost of removing vegetation for road construction in Alaska. Three years after treatment he observed the removal of vegetation had increased the depth to permafrost by 300-600%.

Wildfires also impact geomorphological features on small and larger scales. In the first and second years after a fire, mass wasting or landslides frequently occur on hillslopes, being more prone to failure due to increased soil moisture content [*Brown and Grave*, 1979; *Brown*, 1983; *Tiedemann et al.*, 1979]. Several decades later, thermokarst formation may occur as a result of thawing of ice-rich permafrost [*Brown*, 1983; *Viereck*, 1973].

This investigation focused on postfire impacts to the permafrost to quantify the impacts of fire on (1) direct heat conduction and convection to the ground, (2) removing moss as an insulating material, (3) heat budget, (4) soil moisture characteristics, and (5) active layer thickness and talik formation. These agents are the major components of permafrost dynamics. The evaluation of these agents will provide a better understanding of the relationship between burn severity and permafrost response and the effects on the hydrologic regime following wildfire.

### A.2 Methods

Eleven wildfire sites throughout Interior Alaska, with dates of ignition ranging from 1924 to 2000, were selected for this study (Figure A.1). At each of these sites, active layer depth, ground temperature, soil moisture content, thermal conductivity and air temperature were measured. Several historical fires are located near Caribou-Poker Creeks Research Watershed (CPCRW) 48 km north of Fairbanks, Alaska [*Fastie*, 2000; *Fastie and Mann*, 1993]. Four of these wildfire burn areas within or immediately adjacent to CPCRW were selected for study and occurred in 1999 (site 1, control, moderate, severe), 1996 (site 2, moderate, con-

trol), 1990 (site 3, moderate, control), and 1924 (site 4, severe, moderate). The July 1999 controlled burn experiment (FROSTFIRE) took place in a $9.7km^2$ subbasin underlain by discontinuous permafrost [*Hinzman et al.*, 2000]. At the 1996, 1990, and 1924 burn areas, two small pits were dug: one in a burned area and one control. In the 1924 site, one pit was located inside the severely burned area and the other inside the moderately burned area. Locations of the pits were selected to be as physically similar to each other as possible. The total depth of the pits varied between 60 and 80 cm. In each pit, the temperature and soil moisture content were measured. TDR probe and gravimetric samples were collected in the surface duff layer, in the organic layer, and at regular intervals through the mineral soil. A ground temperature transect was established between the burned and the unburned sites. Shallow surface (15-20 cm depth) temperature measurements were collected at 3 m intervals using a thermocouple. A series of thermistors were used to measure the (0-100 cm depth) ground profile temperatures along the transect. Measurements were collected at 10-20 m intervals with additional measurements made near the boundary of the burned and unburned areas. Measurements were made every other month at the 1996 site and in August 1998 at the 1990 and 1926 sites. Seasonal frost depths were also measured. At the 1999 sites (site 1, FROSTFIRE), active layer depth, ground temperature, thermal conductivity, soil moisture content, and meteorological observations were collected.

The Rosie Creek site (Bonanza Creek LTER) was located in a burn that occurred in 1983 (severe, control) located approximately 10 km southwest of Fairbanks, Alaska. The Chena Host Springs Road site was located at a controlled burn that was conducted in August 2000, approximately 25 km east of Fairbanks, Alaska. This controlled burn lasted about 3 hours, during which direct measurements were collected. The purpose of this experiment was to determine the thermal impact from direct heating by the fire. A black spruce stand, 16 $m^2$ X 5 m high, with woody debris on the surface was ignited on a surface of feathermoss (*Hylocumium* spp.) and *Sphagnum*. Soil moisture contents and temperatures were measured below the surface to a depth of 32 cm in 2 cm increments. Type T and type K thermocouples were installed in the organic layer. Type K thermocouoples with silfa silica insulation were used at the surface and in the moss (8 cm). The deeper layers were monitored using copper-constantan (type T) thermocouples with regular polyvinyl chloride (PVC) insulation. Temperature measurements were collected every minute. Soil

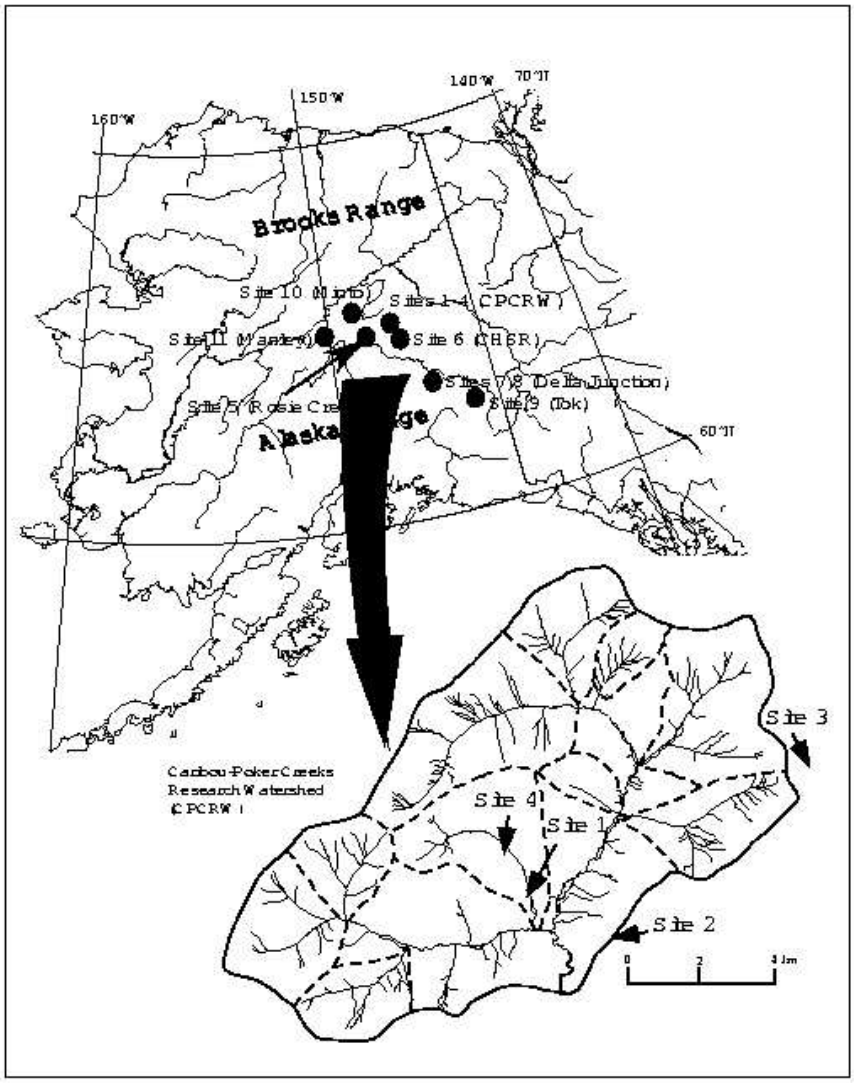


Figure A.1. Map of study sites. Eleven sites are located in Interior Alaska between the Alaska Range and the Brooks Range. Four of the 11 sites were located near CPCRW (insert map).

moisture content was measured using balanced TDR (time domain reflectometery) probes and a Tektronix model 1502B cable tester on 10 min intervals.

Two sites (sites 7 and 8) were located near Delta Junction, Alaska. The 1994 fire at Hajdukovich Creek (severe, control) and the 1999 fire at Donnely Flats (severe, moderate, control). Both fires had a variety of severities in black spruce (*Picea mariana*) with a feathermoss forest floor. The fire at site 9 occurred near Tok, Alaska in 1990 and was classified as a moderate burn with some severe areas. The final two sites are located north of Fairbanks, at Minto (site 10, 1999, moderate, control) and at Manley (site 11, 1963, severe, moderate).

At all sites, the remaining moss thickness, soil moisture content, ground temperature and thermal conductivity were measured (Table A.2). Soil moisture contents were measured using the Hydra soil moisture capacitance probe by Vitel Inc. [*Atkins et al.*, 1998]. The Campbell Scientific CS615 probe [*Bilskie*, 1997] was used to detect changing dielectric permittivity (constant). Electronic measurements were verified by gravimetric sampling and oven drying for 72 hours at $65^oC$. Classification or organic soils and degree of humidification was based on the works of the *Soil Classification Working Group Staff* [1998] and *Pritchett and Fisher* [1987].

Ground temperatures were measured using three different methods. Routine monitoring of active layer temperatures was accomplished using NTC thermistors (Alpha thermistor 14A5001C2) and recorded on Campbell Scientific CR10X data loggers. Type K and T thermocouples with CR10X loggers were used to measure near surface temperatures directly during fire. Three shallow (20-30m) boreholes were installed at the CPCRW 1999 site (site 1) and Rosie Creek 1983 site (site 5) to periodically monitor permafrost temperature profiles. A precision thermistor was lowered slowly down the boreholes to accurately ($< 0.001^oC$ error) record permafrost temperature changes and geothermal gradients.

Thermal conductivity was measured using the heat probe method [*Shiozawa and Campbell*, 1990] made by Kona systems and Thermal Logic. Thermal conductivity was also measured in the laboratory as a function of the water content and temperature on undisturbed samples from all sites.

Incoming and reflected shortwave radiation and incoming and emitted longwave radiation were measured using a pair of calibrated pyranometers (Eppley Black and White Pyranometer Model 8-48) and a calibrated pair of pygeometers (Eppley Precision Infrared

Radiometer Model PIR), respectively. An independent estimation of net radiation was obtained using a calibrated Frischen type net radiometer (REBS Model Q7.1). A wind speed (Met One 014) dependent dome cooling correction was applied to the results. Table A.1 provides a summary of measurements and instruments at each site.

The radiation budget before and after the CPCRW controlled burn was measured using shortwave, longwave and net radiometers. Sensors measuring shortwave and longwave incoming and reflected (emitted) were installed on a 3 m towner (unburned site) and a 1.5 m tower (burned site), both were higher than the black spruce canopy. The radiation balance (Q) is expressed in terms of incoming solar radiation (K↓), surface albedo α, incoming longwave radiation (L↓) and emitted longwave radiation (L↑) in the form:

$$Q = K\downarrow(1-\alpha) + L\downarrow - L\uparrow \tag{A.1}$$

Talik formation was simulated using data from Rosie Creek (site 5). Ground temperature observations and other meteorological, vegetation and soils data were obtained from the data archive of the Bonanza Creek Long-Term Ecological Research (LTER). The thermal models used for these studies were described by *Osterkamp and Romanovsky* [1996] and *Romanovsky et al.* [1997].

### A.3 Results

Five categories of the impacts to the permafrost were evaluated: (1) direct fire affects, (2) removing (burned) moss as an insulating material, (3) heat budget, (4) soil moisture characteristics, and (5) active layer thickness and talik formation. All these impacts are interrelated and cannot be absolutely separated; however, the following is a discussion of the separate mechanisms and the factors that influence them.

#### A.3.1 Impact 1: Direct Fire Affects

Figure A.2 shows the ground temperature at several depths during the fire at 25 km Chena Hot Springs Road (site 6). The increase in temperature at the forest floor during the fire is quite rapid. The temperature of the forest floor (surface of the moss itself) was more than $800^{o}C$ during this experimental burn by using type K thermocouple. Temperature started

Table A.1. Summary of Site Information and Instrumentation

| Site | Location | Latitude | Longitude | Year of ignitiion | Ground temperature | Soil Moisture | Active layer | Profile method | Meteorological observation |
|---|---|---|---|---|---|---|---|---|---|
| Site 1 | CPCRW | 65.1$^o$N | 147.3$^o$W | 1999 | K, Th, Pt | CS, Vt | Thaw probe, MRC | trench, borehole (26 m) | 10 m tower |
| Site 2 | CPCRW | 65.1$^o$N | 147.3$^o$W | 1996 | K, Th | Vt | Thaw probe, MRC | trench | no |
| Site 3 | CPCRW | 65.1$^o$N | 147.3$^o$W | 1990 | K | Vt | Thaw probe | trench | no |
| Site 4 | CPCRW | 65.1$^o$N | 147.3$^o$W | 1924 | K, Th | Vt | Thaw probe | trench | no |
| Site 5 | Rosie Creek (LTER) | 64.7$^o$N | 148.1$^o$W | 1983 | K, Th | CS, Vt | Thaw probe, MRC | trench, borehole (18 m) | 10 m tower |
| Site 6 | 25 km east of Fairbanks | 64.8$^o$N | 147.1$^o$W | 2000 | K, T, Th | CS, Vt, TDR | Thaw probe, T | trench | no |
| Site 7 | Donnely Flats | 64.0$^o$N | 145.7$^o$W | 1994 | K, Th | Cs, Vt | Thaw probe, Th | trench | no |
| Site 8 | Hajdukovich Creek | 64.0$^o$N | 145.7$^o$W | 1999 | K, Th | Cs, Vt | Thaw probe, Th | trench | 10 m tower |
| Site 9 | Tok | 63.3$^o$N | 143.0$^o$W | 1990 | K, Th | CS, Vt | Thaw probe | trench | no |
| Site 10 | Minto | 65.2$^o$N | 149.3$^o$W | 1999 | K | CS, Vt | Thaw probe | trench | no |
| Site 11 | Manley | 65.0$^o$ | 150.6$^o$W | 1963 | K | CS, Vt | Thaw probe | trench | no |

K: Type K Thermocouple, T: Type T Thermocouple, Th: Thermistor (Alpha Thermistor 14A5001C2), Pt: 100 Ohm Platinum Resistor, CS: Campbell Scientific CS615 Probe, Vt: Hydra Soil Moisture Capacitance Probe by Vitel Inc., MRC: MRC Thermistor Ground Temperature Probe, TDR: Time Domain Refractometry

Table A.2. Physical and Thermal Properties of the Organic Layer at Select Study Site

| Site | Year of ignition | Vegetation | Observation date | Density ($g/cm^3$) | SMC (%vol.) | Thermal conductivity (W/m K) | Ground temperature ($^oC$) | Type of layer | Degree of humification | Dielectric constant (100 MHz) |
|---|---|---|---|---|---|---|---|---|---|---|
| Site 1 Birch Stand (3 cm) | 1999 | *Pleurozium schrebrii* | 10 July 2000 | NA | NA | 0.09 | 15.55 | live moss | H1 | 3.1166 |
| Site 1 Birch Stand (10 cm) | 1999 | | 10 July 2000 | NA | NA | 0.15 | 7.84 | Dead moss, litter | NA | 3.5529 |
| Site 1 Birch Stand (15 cm) | 1999 | | 10 July 2000 | NA | NA | NA | NA | mineral, litter | NA | 12.9701 |
| Site 1 Open Spruce (3 cm) | 1999 | *Sphagnum,* | 10 July 2000 | NA | NA | 0.10 | 13.73 | live moss | H1 | 3.4405 |
| Site 1 Open Spruce (12 cm) | 1999 | *Pleurozium schrebrii* | 10 July 2000 | 0.08 | 36.20 | 0.16 | 5.78 | Fibric | H2 | 2.7769 |
| Site 1 Open Spruce (20 cm) | 1999 | | 10 July 2000 | NA | NA | 0.24 | 1.12 | Humic | NA | 28.4742 |
| Site 5 UB (3 cm) | >1900 | *Sphagnum* | 7 July 2000 | 0.05 | 2.96 | 0.03 | 21.98 | live moss | H1 | 2.1634 |
| Site 5 UB (10 cm) | >1900 | *Pleurozium schrebrii* | 7 July 2000 | 0.05 | 10.56 | 0.06 | 7.72 | Dead moss | | 4.7433 |
| Site 5 UB (20 cm) | >1900 | | 7 July 2000 | 0.06 | 19.47 | 0.41 | 0.96 | Humic | | 11.9779 |
| Site 5 B (3 cm) | 1983 | *Hylocomium splendens* | 7 July 2000 | 0.05 | 4.96 | 0.11 | 19.53 | Dead moss | H1 | 2.253 |
| Site 5 B (8 cm) | 1983 | | 7 July 2000 | 0.36 | 41.96 | NA | NA | Humic | NA | 16.7177 |
| Site 5 B (13 cm) | 1983 | | 7 July 2000 | 0.67 | 60.16 | 0.91 | 19.56 | Mineral, charcoal | NA | 36.4338 |
| Site 7 B (3 cm) | 1994 | *Ceratodon purpureum* | 20 June 2000 | 0.79 | 30.58 | 0.49 | 15.0 | live moss, charcoal | NA | 15.94 |
| Site 7 UB (3 cm) | >1860 | *Hylocomium splendens* | 20 June 2000 | 0.09 | 3.27 | 0.05 | 13.3 | Dead moss | H1 | NA |
| Site 7 UB (12–18 cm) | >1860 | | 20 June 2000 | 0.09 | 3.67 | 0.03 | | Fibric | H3 | 2.78 |
| Site 7 UB (25 cm) | >1860 | | 20 June 2000 | 0.71 | | 0.20 | 0.6 | Humic | H7 | 12.60 |
| Site 8 S (3 cm) | 1999 | | 20 June 2000 | 0.88 | 23.76 | 0.39 | 17.8 | Charcoal | H3 | 5.92 |
| Site 8 UB (10 cm) | >1860 | *Polytrichium, lichen* | 20 June 2000 | 0.32 | 24.60 | 0.10 | 10.4 | live moss | H1 | 11.68 |
| Site 8 UB (12 cm) | >1860 | | 20 June 2000 | 1.02 | 71.00 | 0.57 | 1.6 | Humic | H6 | 57.48 |
| Site 8 M (7 cm) | 1999 | | 20 June 2000 | 0.09 | 3.27 | 0.04 | 14.8 | Fibric | H2 | 4.22 |
| Site 8 M (15 cm) | 1999 | | 20 June 2000 | 0.50 | 26.65 | 0.15 | 1.5 | Humic | H4 | 19.20 |
| Site 9_1 (8 cm) | 1990 | *Polytrichium commune,* | 20 June 2000 | 0.45 | 28.34 | 0.13 | | Fibric | H1 | 18.92 |
| Site 9_2 (8 cm) | 1990 | *Polytrichium spp.* | 20 June 2000 | 1.16 | 35.87 | 0.99 | | Humic | H7 | 16.72 |
| Site 10 B (3 cm) | 1999 | | 21 June 2000 | 0.20 | 6.54 | 0.05 | 22.0 | dead moss, charcoal | H3 | 3.13 |
| Site 10 B (15 cm) | 1999 | | 21 June 2000 | 0.86 | 65.19 | 0.58 | 3.1 | fibric | H8 | 55.79 |
| Site 10 UB (5 cm) | 1999 | *Hylocomium splendens* | 21 June 2000 | 0.04 | 1.88 | 0.06 | 15.3 | live moss | H1 | 2.21 |
| Site 10 UB (15 cm) | 1999 | *Pleurozium schrebrii* | 21 June 2000 | 0.09 | 4.50 | NA | 1.4 | fibric | H4 | 3.34 |
| Site 11 M (3 cm) | 1963 | *Drepanocladus sp.* | 21 June 2000 | 0.23 | 16.73 | 0.22 | 6.9 | live moss | H1 | 10.11 |
| Site 11 M (15 cm) | 1963 | *Polytrichium* | 21 June 2000 | 0.44 | 34.23 | 0.44 | 0.3 | Humic | H5 | 41.03 |
| Site 11 S (5 cm) | 1963 | *Polytrichium* | 21 June 2000 | 0.08 | 4.29 | 0.06 | 6.3 | live moss | H1 | 2.50 |
| Site 11 S (15 cm) | 1963 | | 21 June 2000 | 0.07 | 3.89 | 0.11 | 2.0 | Fibric | H2 | 3.85 |
| Site 11 S (23 cm) | 1963 | | 21 June 2000 | 0.97 | 58.10 | 0.58 | 0.5 | Humic | H7 | 20.67 |

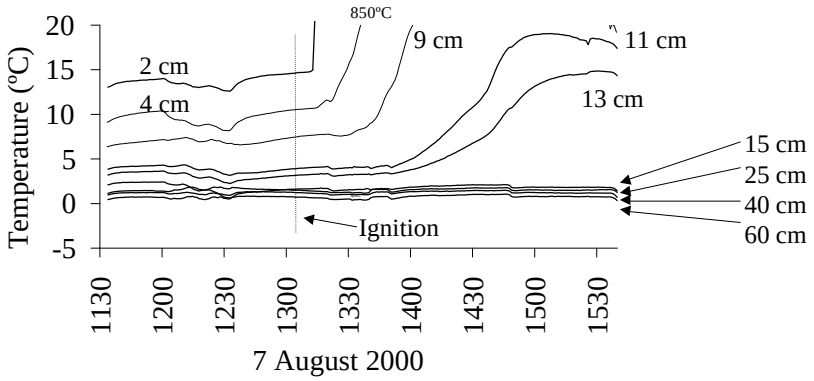


Figure A.2. Ground and surface temperatures during the fire at 25 km Chena Hot Springs Road (site 6) showing the increase in the near surface temperatures shortly after ignition. The ground temperature at this site rose only at the shallow depths(<15 cm). Most of the heat from the wildfire transfers to the ground by conduction, which does not penetrate deeply.

to rise 2 cm below the surface about 10 min after ignition. No significant increase in temperature was recorded below 15 cm at the feathermoss (*Hylocomium* spp.) and *Sphagnum* sites.

Many natural wildfires occur in forests where the floor is dominated by feathermoss (*Hylocomium* spp.) while fires in areas dominated by *Sphagnum* moss are relatively rare. The differences are due primarily to the characteristic moisture conditions both species prefer. Feathermoss (*Hylocomium* spp.) has a much lower moisture field capacity (about 20%) (C.M. Mack, Earth System Science, University of California Irvine, personal communication, 2000) and the typical water content is around 10% by volume in summer months, as compared to *Sphagnum* (40% moisture field capacity and typical levels of 30-40% by volume in summer months). The type of moss is not only an important factor in characterizing burn potential and severity, but also affects the surface thermal properties. About 70% of the volume of the live feathermoss is air and 10% is solid; consequently the thermal conductivity is strongly controlled by the water content. Increasing the water content by 40% increases the thermal conductivity 10-fold (Figure A.3). However, the typical condition of the moisture content of feathermoss is somewhat dry (usually less than 15% by volume). The thermal conductivity of the dry moss is almost the same as air (0.02 W/m K). As a result, under these conditions, fires do not transfer an immediate thermal impact

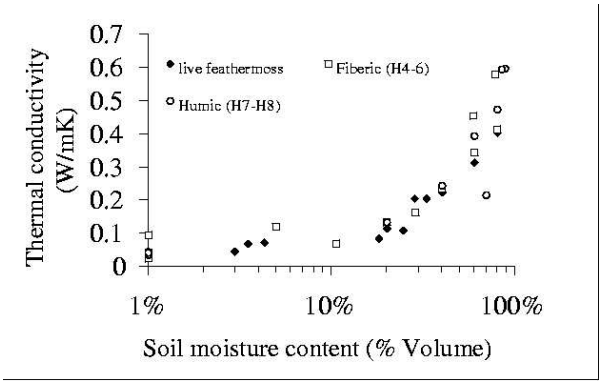


Figure A.3. The thermal conductivity of live feathermoss, fibric, and humic layers are strongly affected by moisture content. The classification of the organic layer was based on the works of *Soil Classification Working Group Staff* [1998] and *Pritchett and Fisher* [1987].

to deeper soil layers during a burn.

### A.3.2 Impact 2: Removing (Burned) Moss as an Insulating Material

Removal of the organic layer exerts a serious impact to the ground thermal regime. In the first year following a fire, *Viereck* [1982] reported the thawing index of the soil surface may reach 1900 days$^o$C in severely burned sites, as compared to 1500 days$^o$C in unburned sites. The Mean Annual Surface Temperature (MAST) can increase by 2-3$^o$C. The thawing index at 10 cm depth was 847 days$^o$C (unburned site), 940 days$^o$C (fire line) and 722 days$^o$C (burned site). These suggest that the burn site is slightly cooler at the ground surface during the summer. However, because of of higher thermal conductivity of the surface soils of the burned site, the thawing index will be larger throughout the soil profile at the burned site as compared to similar depths in an undisturbed site.

At nearly every site we monitored, the summer ground temperatures of the burned areas were substantially warmer (by 1 - 20$^o$C) than the adjacent complementary unburned control sites. The only exception to this trend was site 1 in the 1999 FROSTFIRE burn where the thermistors in the burned site were more shaded from the Sun as compared to the control site (Figure A.4a). In cases of fires that burned within the last 10 years, the ground surface temperature was warmer at the burned sites as compared to control sites during the early freezing period in autumn. This difference was maintained until the

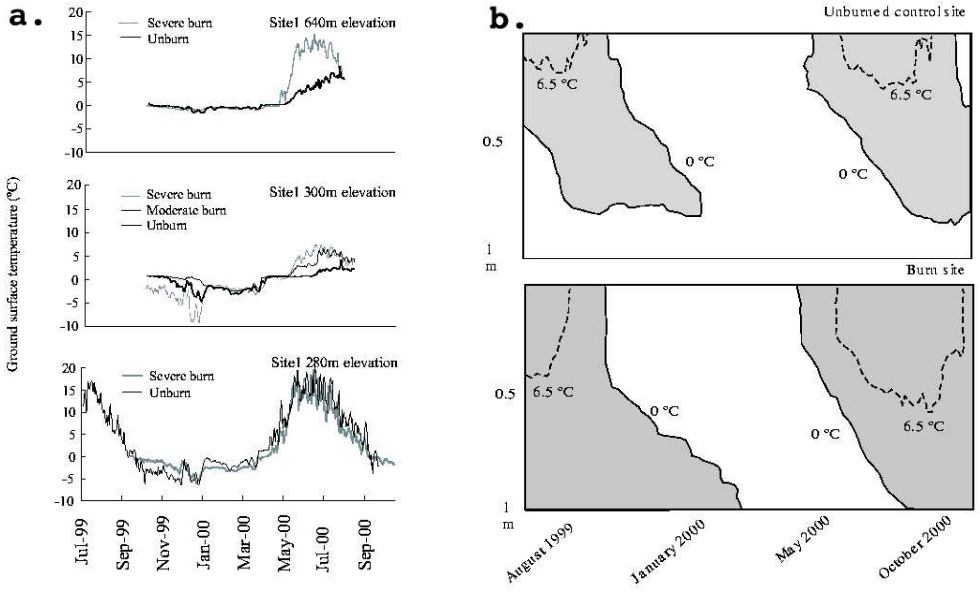


Figure A.4. Ground temperature dynamics at the FROSTFIRE site 1. (a) Annual variation of the near surface temperature in three separate locations showing warmer surface temperatures and delayed freezing in the burned sites. (b) Development of active layer in the unburned site is limited to 80 cm while the active layer in the burned site exceeds 1 m.

active layer became completely frozen. The moisture content of recent fires was higher in the burned sites, probably due to lower transpiration rates, so freezing would take longer due to larger latent heat of fusion requirements. However, in the older fires, the soils of the burned sites were somewhat drier and they would freeze faster in the fall. The depth of snow was not significantly different within sites (except in the Delta Junction area, sites 7 and 8) and is not considered to be a controlling factor for these differences. Sites where the burn severity was classified as moderate or severe also demonstrated an increased thickness in the active layer (Figure A.4b).

The most important factor controlling the active layer thickness is the thermal conductivity of the organic layer. The active layer thickness is not substantially impacted when the thickness of the organic layer is not significantly reduced during burning, even though the surface albedo is lowered. Table A.2 shows field observations of the thermal conductivity of each organic layer. In general, thermal conductivity is mainly a function of density, moisture content, and temperature; water content was particularly important in the post-

fire environment. The type of moss and extent of decomposition of the organic material are important factors in controlling the soil thermal regime (Table A.2). A surficial layer of feathermoss has a lower thermal conductivity than *Sphagnum*, but after burning, feathermoss has a fibric layer that has a higher (or equal) thermal conductivity than *Sphagnum*. The thermal conductivity of the surface layer of *Sphagnum* does not change appreciably with burning, thus feathermoss has potentially larger thermal impacts after burning.

The thickness of the surface organic layer remaining after the fire and the resulting active layer were measured in CPCRW and Delta Junction areas. The active layer thickness is strongly controlled by the moss thickness, its thermal conductivity and moisture content and can be predicted based upon a relatively simple relationship. Sites that were severely burned (all or nearly all organic layer burned) always had deeper active layers than their control or adjacent lightly burned sites. A wildfire did not always affect the underlying permafrost. An organic layer with a thickness of 10 cm provided adequate thermal resistance to protest the frozen mineral soil.

### A.3.3 Impact 3: Heat Budget

After the prescribed burn at the FROSTFIRE site 1, the total net radiation decreased compared to an unburned site (97.7 at a moderate burn site compared to 160.2 $MJ/m^2$ at the control site between 23 July and 10 August 1999) as a result of the increase in the longwave emission (424-438 $W/m^2$). On the other hand, the albedo dramatically decreased from $\sim 0.14$ to $\sim 0.05$ (Figure A.5) yielding greater absorbtion of shortwave radiation at the ground surface. The daily variation of the net radiation (Q) was more variable at the unburned site (max 537 $W/m^2$, min -48.7 $W/m^2$) than the burned site (max 458 $W/m^2$, min -37.6 $W/m^2$). The radiation balance components are given in Table A.3 in terms of 100 units of incoming shortwave.

Radiation efficiency (Re) was calculated as the ratio of incoming shortwave radiation to net radiation, $Re = Q/K_d$. The radiation efficiency of the site 1 (moderately burned) was 50% (at noon) while the control unburned site has a Re of 75%. This indicates that the burned site was 25% less efficient at retaining incoming radiation. *Chambers and Chapin III* [1999] reported somewhat similar results of radiation efficiency being 75% of efficiency at moderate burn site and 78% at an unburned site. The energy absorbed at the ground

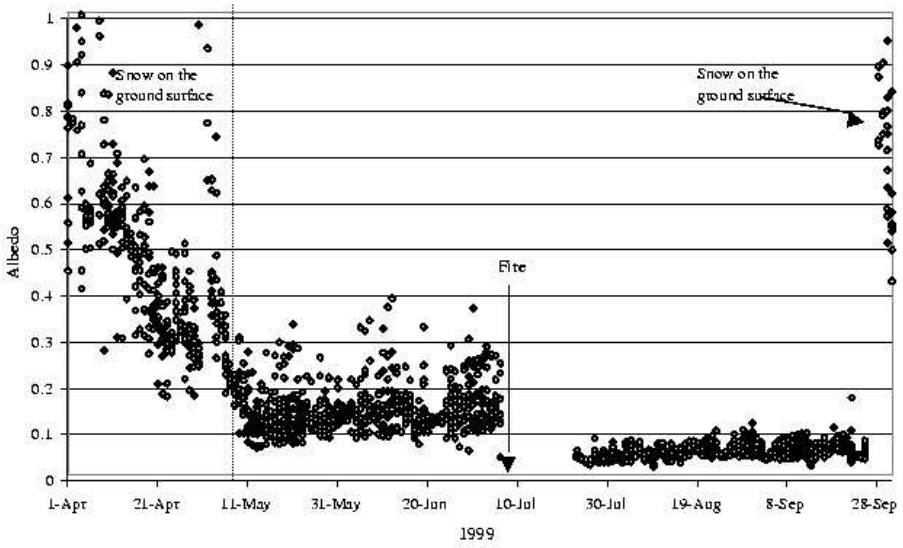


Figure A.5. There are strong differences in albedo before and after wildfire. During snowmelt, the albedo ranges from 0.2 to 0.9 or more, decreasing to about 0.14 on a feathermoss surface prior to the fire. The albedo drops to 0.07 at a moderately burned site after the fire. Plotted data are the daytime (0600–1700 AST) averages.

Table A.3. Radiation Balance of Burned and Control Areas at Site 1 (From 23 July to 10 August 1999 (sensor height 1 m at burned, 1.5 m unburned))

| Radiation | K↓ | K↑ | α (%) | L↓ | L↑ | Re | Q | ∑Q ($MJ/m^2$) | Max. ($W/m^2$) | Min $W/m^2$) |
|---|---|---|---|---|---|---|---|---|---|---|
| Burned (site 1) | 100 | 4.6 | 0.05 | 105 | 122 | 0.47 | 47.43 | 97.7 | 458 | -37.6 |
| Unburned (site 1) | 100 | 13.5 | 0.14 | 105 | 118 | 0.74 | 73.59 | 160.2 | 537 | -48.7 |

Net Radiation Q, Incoming Solar Radiation K↓, Reflected Shortwave Radiation K↑, Surface Albedo (%) α, Incoming Longwave Radiation L↓, Emmitting Longwave Radiation L↑, Radiation Efficiency Re, Total Net Radiation ∑Q

surface divides into sensible, latent, ground heat fluxes and energy storage. The daytime sensible heat flux is large and comprises at least 20% of K↓ (38% according to *Chambers and Chapin III* [1999]). The large sensible heat flux from the fresh burn manifests itself visibly on a sunny day [*Rouse and Mills*, 1977]. The Bowen ratio of a freshly burned site in the FROSTFIRE study was reported at $\beta = 4.5 \pm 3.3$ [*Chambers and Chapin III*, 1999]. Using this value of $\beta$ the ground heat flux and energy storage at our site 1 increased from an unburned area (0.07Q: 18.5 $W/m^2$) at the burned site (0.16Q : 29 $W/m^2$ or more). The ratio of ground heat flux to net radiation increased following fire. The distribution of the energy balance components shifted before and after fire. The increasing sensible heat and ground heat flux was balanced by decreasing the latent heat flux. As a result, ground temperatures were increased and wetter conditions became established despite the total net radiation decrease.

### A.3.4 Impact 4: Soil Moisture Characteristics

During burning, the soil moisture content of the soils becomes drier than an adjacent unburned area (Figure A.6). Burned soils can develop a near surface hydrophobic layer [*DeBano*, 2000] that can resist surface water infiltration. Precipitation occurred during the 2 days following the CHSR Fire (site 6). In the control area, a significant increase in the soil moisture content was observed; while in the burn area, little change was observed. At the end of the observation period, the apparent hydrophobic layer was decreasing and the soil moisture content in the burned soils began to increase. It is unclear if the hydrophobicity effect is very important in the Alaskan soils that are usually somewhat moist to wet.

Prior to the CPCRW fire (site 1), the soil moisture contents at two adjacent sites were nearly the same. However, following the fire, the burned area displayed a noticeable increase in soil moisture content compared to the unburned control area (Figure A.7). However, all of the older fire sits (>10 years) tend to display drier soils as compared to the unburned (or lightly burned) control sites. At several sites, the soil moisture content was measured in burned areas and adjacent unburned areas at the same depth. Figure A.8 shows that the burned sites were always wetter at corresponding depths (active layer 0-50 cm) in the 1996 and 1994 burns. On the other hand, older burn sites were always drier at any depth. At the 1990 burn (site 3) the moisture content was about the same in the burned

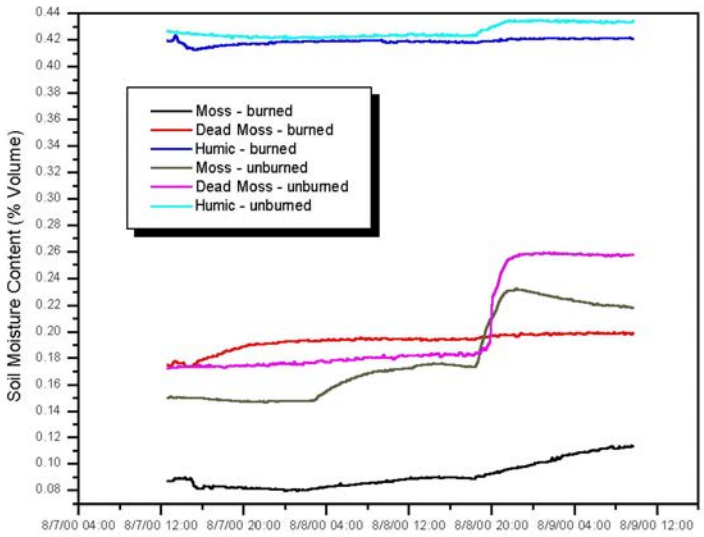


Figure A.6. Soil moisture content during and immediately following fire, 2000 CHSR, site 6

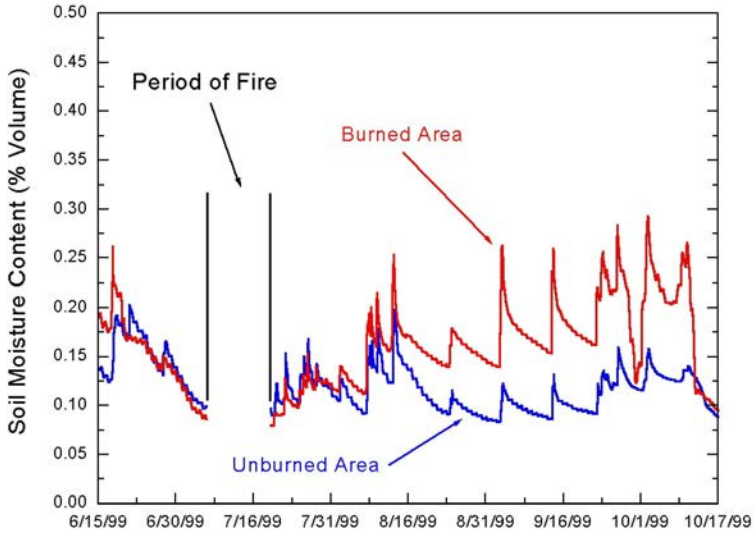


Figure A.7. Short-term near surface soil moisture content following wildfire at FROSTFIRE, site 1

and unburned sites. The results of this study indicate the time required for severely burned soils to transition from having higher soil moisture contents to lower soils moisture contents to be about one decade.

### A.3.5 Impact 5: Active Layer Thickness and Talik Formation

Both increased soil moisture contents as well as soil temperatures affect the active layer at the severe burn sites. Figure A.4b shows the active layer temperature profile for two thaw cycles in the FROSTFIRE severe burn area. There appears to be clear evidence of a change due to the fire in the first summer. The active layer was greater in locations where most of the organic material was burned to mineral soil. At the 1999 Minto fire (site 10), 50 random random active layer depths were measured in both the moderate burned area and unburned areas. The average active layer thickness was virtually identical (29.9 cm burned area versus 29.2 cm unburned area on 21 June 2000). The permafrost has degraded to a depth 4.15 m from the surface at the severe burned area of Rosie Creek (site 5) since

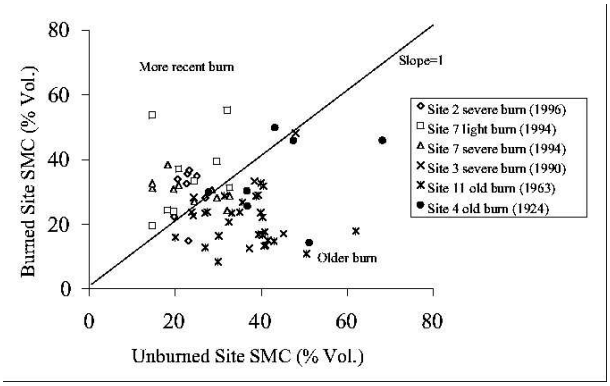


Figure A.8. Comparison of soil moisture contents between burned areas and adjacent unburned areas at fires of various ages (sites 2, 3, 4, 7, and 11) shows that in general more recent fires have higher mineral soil moisture contents in burned areas while older fires have higher mineral soil moisture contents in unburned areas.

1983. The maximum annual depth of seasonally frozen ground is about 2 m, so the layer of unfrozen soil between the seasonally frozen ground and the permafrost is a talik. The thawing of the permafrost seems to have slowed or ceased as evidenced by the year 2000 ground temperature profile being nearly identical (below 4 m) to the year 1996 ground temperature profile (Figure A.9). There are many permafrost-free areas (or deep taliks) in areas where one would expect thick permafrost. Some of these permafrost-free anomalies correspond with fire scars indicating previous disturbances impart long lasting impacts to the permafrost. In light of the recent climatic conditions, we hypothesize that it will be difficult for permafrost to recover once thawed following a severe fire in this area.

### A.4 Discussion

The permafrost distribution and ground surface heat balance are closely related. It is possible to determine a simple heat balance based upon the freezing index ($I_f$) and thawing index ($I_t$) at the ground surface. The freezing and thawing indices are calculated based upon an accumulation of freezing or thawing degree days throughout the positive and negative daily mean temperature periods. $I_t = \Sigma t_s$ when ($t_s > 0$) and $I_f = \Sigma t_s$ when ($t_s < 0$) where $t_s$ is the mean daily ground surface temperature. $I_f$ and $I_t$ were calculated at each burn and control site based on hourly data. The boundary conditions of permafrost presence is calculated using the following formula [*Romanovsky and Osterkamp*, 1995; *Lunardini*,

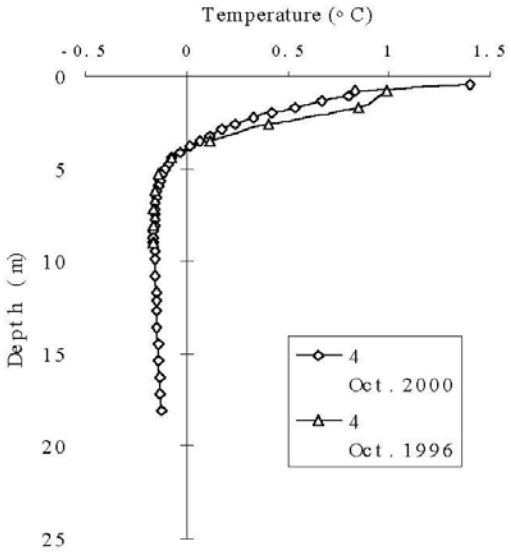


Figure A.9. Ground temperature profile at site 5 borehole. The permafrost starts 4.15 m below the surface (4 October 2000). The permafrost is very warm and close to thawing with the coldest temperature only –0.16$^o$C at 8.6 m.

1981]:

$$I_t \leq (\lambda_f/\lambda_t)I_f \tag{A.2}$$

where $\lambda_f$ and $\lambda_t$ are frozen and thawed thermal conductivities. The ground surface $I_f$ (freezing degree days) ranges between 500 (on south facing slopes) and 3000 (at the base of the north facing slopes) in CPCRW. On the other hand, $I_t$ (thawing degree days) does not vary greatly (Ca. 1400) compared to the freezing degree days [*Yoshikawa et al.*, 1998]. Thus $I_f$ is a key factor in determining the presence or absence or permafrost. *Van Cleve and Viereck* [1983] suggested that $I_t$ measured at 10 cm ground depth is a good indicator of permafrost presence. On a black spruce forest floor, $I_t$ averages about 500-800$^o$C days. Less than 5 years after a fire, $I_t$ increased to 1000-1250. If the organic layer and original trees recover, the active layer may return to its original thickness within 25–50 years [*Van Cleve and Viereck*, 1983].

Wildfire affects frozen ground systems primarily through the removal of vegetation

and the surface organic layer. The loss of vegetation increases the soil moisture content due to reduced evapotranspiration. The thermal conductivity of an organic layer is a function of the moisture content, temperature, and density. If the organic layer remaining after a fire is adequately thick, the active layer thickness will not be depressed, in spite of dramatically lowered albedo. As a result, thickness and type of organic layer are the most important agents influencing the permafrost response to wildfire. Figure A.10 shows the relationship between active layer thickness and a function of the thermal properties of the soil ($\xi$). This function is thermal resistance divided by the local thawing index:

$$\xi = \frac{\sum_i \frac{d^i_{org}}{\lambda_i}}{\sqrt{I_t}} \tag{A.3}$$

where $d^i_{org}$ is the thickness of organic layers (moss and peat, cm), $\lambda_i$ is thermal conductivity of organic layers (W/m K) and $I_t$ is thawing index of the ground surface ($^o$C days). Thermal conductivity is strongly affected by the moisture content of the moss (Figure A.3). The thermal conductivity of moss and peat was determined by field and laboratory measurements [*Burwash*, 1972; *Andersland and Anderson*, 1978; *Farouki*, 1981]. In an unburned forest where permafrost is present, the function of thermal properties of organic soil ($\xi$) is usually greater than one. In areas where the fire severity was rated as low or moderate (organic soil was only lightly burned) such as site 10, the function of thermal properties of organic soils ($\xi$) will be between 0.7 and 1. As the severity of the fire increases, the function of thermal properties of organic soils ($\xi$) decreases. A $\xi$ value of 0.7 or above appears to be a threshold as to when the permafrost will be adversely impacted by a wildfire. In Interior Alaska, the typical patterns of organic soils will yield thermal properties in the range of $\lambda$ = 0.25–0.45 and $I_t$ = 1400. Thus, after wildfire, if more than 7–12 cm of organic soil remain, the active layer thickness in the burned area will not be greater than that in the adjacent unburned area.

Heat transfer processes other than by conduction do occur and have been documented in many studies [*Hinkel and Outcalt*, 1994; *Kane et al.*, 2001; *Outcalt et al.*, 1990, 1997; *Woo*, 1982]. Nonconductive heat transfer processes occur in soils primarily in association with water movement, either in vapor or liquid phase. The processes increase in importance in soils with large pore sizes and large thermal or moisture gradients. Some heat movement

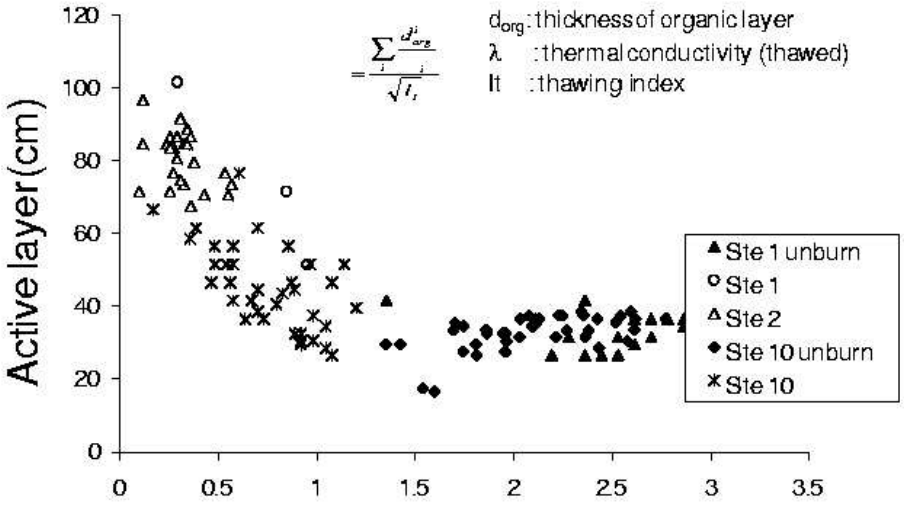


Figure A.10. Active layer thickness is affected by organic (living and dead moss, fibric, humic) layer thickness and composition, its thermal conductivity, and the thawing index. Data from sites 1, 2, and 10 in July 1999 demonstrate increasing active layer thickness with thinner organic layers.

coupled with vapor transport may have occurred in the active layer, decreasing the effective thermal conductivity [*de Vries*, 1974] and lowering the amount of heat transferred by conduction. It is difficult to quantify heat transfer by convection from measurements of soil moisture because the later heat of vaporization is so large (approx. 2.5 MJ/kg), relatively small changes in moisture may accompany significant heat flux. However, we do not believe that convective transport played a major role in accounting for the differences observed among these field sites, except for brief periods when the near surface soils were quite wet and the near surface temperature gradient was quite large (such as on sunny spring days when the active layer was still frozen near the surface). In general the pore size of these soils is quite small following a fire, greatly limiting free convection [*Russell*, 1935]. The most noticeable nonconductive thermal effect is produced by snowmelt water, which during the spring can infiltrate into the upper moss layer and into the frozen soils using the thermal cracks as flow paths. However, the annually averaged effect of this process on permafrost temperatures is minimal because the infiltrating water cannot transport any significant amount of sensible heat due to small differences in temperatures of this wa-

ter and surrounding material. The latent heat of refreezing water can noticeably increase soil temperatures at this time but the same amount of latent heat will be consumed during the melt of this additional ice in the active layer during its thawing. So, the annual heat balance in the active layer will not be changed and the thermal effect on permafrost will be negligible.

### A.5 Modeling

To investigate the effects of forest fire on permafrost temperature regime, we applied numerical modeling of the active layer and permafrost temperature field dynamics at the 1983 Rosie Cree fire (Bonanza Creek LTER, site 5). The models used for these studies were described by *Osterkamp and Romanovsky* [1996] and *Romanovsky et al.* [1997]. Daily air temperatures and snow depth records for the last 46 years from the Fairbanks International Airport meteorological station were used for the upper boundary conditions. The lower boundary was placed at the approximate base of the permafrost at this site (54 m). A constant heat flux of 0.04 $W/m^2$ was used for the lower boundary condition. The models include the effects of latent heat and unfrozen water in the active layer and permafrost since it was found that the thermal response of the active layer and permafrost could not be successfully modeled without doing so [*Riseborough*, 1990; *Burn*, 1992; *Romanovsky and Osterkamp*, 2000]. Time steps in these calculations were 15 min, while the 200 vertical steps were changed from 1 cm within the upper 1 m of soils to 1 m at the lower boundary of the spatial domain (54 m). Site specific calibration of the models was accomplished using annually measured temperature profiles at this site and daily mean temperatures measured at the ground surface and at several depths in the upper meter of soil. Daily air temperatures and snow cover thickness from the Fairbanks International Airport were used to complete the model calibration and to extend the calculations back in time. Drilling records were used to determine the lithology and the initial approximate thermal properties of the soils in the thawed and frozen states. The thermal properties (including unfrozen water content curves) were refined using a trial and error method [*Romanovsky et al.*, 1997]. The results of modeling for the undisturbed site were discussed by *Osterkamp and Romanovsky* [1999]. Here we will compare these results with calculations for the site within the LTER Bonanza Creek research area where a severe forest fire occurred in the summer

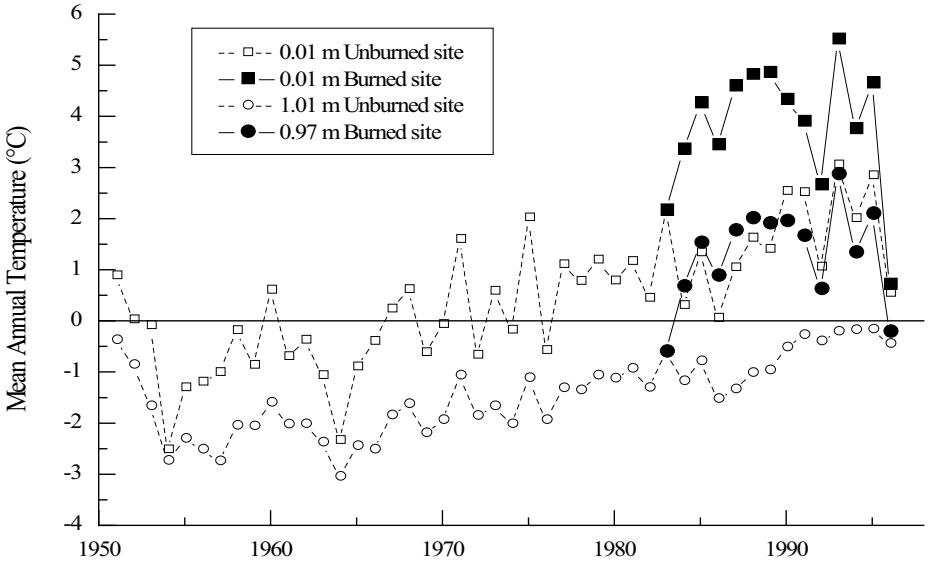


Figure A.11. Modeled mean annual temperature at the ground surface (open and filled squares) and at 1 m depth (open and filled circles) at an unburned site (open symbols) and at burned site 5 (filled symbols).

of 1983 (Rosie Creek fire).

As a result of this fire, the entire moss layer and most of the peat layer were destroyed. The model was modified to reflect these changes in soil properties. Other parameters of the model and driving variables such as air temperature and snow cover thickness were kept the same as in simulations of the undisturbed site. Calculations were started in the summer 1983 and the temperature profile from the no-disturbance simulation at the time of fire ignition were used as initial conditions. The calculation results are shown in Figure A.11. Immediately after the fire, the ground surface and active layer temperatures increased significantly and the long-term permafrost thawing began. As is shown in Figure A.11, the mean annual temperatures at the ground surface and at 1 m depth increased by 3–3.5$^o$C during the first 5 years after the fire. This difference then decreased to 1.5–2$^o$C during the 1990s.

The modeled permafrost thawing progression and a talik development at site 5 are shown in Figure A.12. The thawing of the permafrost was especially rapid during the fire 5 years. By the end of this period, the depth of talik was 3.4 m. During the last 8 years of calculations, the talik increased by only 0.8 m, totaling 4.15 m in depth by 1996. Recent

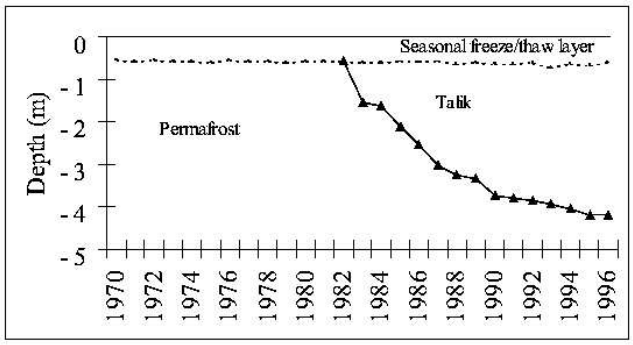


Figure A.12. Simulated active layer dynamics at an undisturbed site (dashed line) and talik formation at a burned site (solid line) at site 5 from 1970 to 1996.

measurements (Figure A.9) show that during the rest of the 1990s, the talik did not increase with the permafrost table position was practically stationary at the 4.15 m depth.

The organic soil was completely burned at site 5 (Table A.2). In the case of a light burn (simulation of a 16 cm moss layer, $\lambda$ = 0.7 W/m K, $\xi$ = 1.2), this model study suggests that maximum active layer reaches only 98 cm instead of 4.15 m observed and simulated following a severe burn (simulation of a 6 cm moss layer, $\xi$ = 0.75). The active layer depth of the area around site 5 is usually 60–70 cm at the unburned control area, while the burned area was about 20 cm deeper. Simulation results indicate at the end of the 1989–1990 winter, the seasonal frost depth did not completely reach the top of the permafrost forming a 10–20 cm thick talik. Model simulations indicate the talik continues to increase in thickness for 5 years. The modeling study suggests that severity of burn (e.g. thickness of remaining organic layer) is an important factor controlling active layer thickness and talik formation. Observations and simulation results of the site 5 area indicate permafrost degradation due to fire is about 10 years in both the lightly and severely burned sites under the current climate conditions.

### A.6 Conclusions

Depending on burn severity, wildfires result in an immediate impact upon the permafrost and ground thermal regime. In permafrost regions, the soils in a burned site will be warmer than in an adjacent unburned site for many decades. In the short term, wild-

fires will decrease rates of transpiration causing increasing soil moisture contents. In the long-term (more than a decade), the increased thickness of the active layer and recovery of vegetation will cause decreases in soil moisture content in burned sites as compared to control sites. However, after a light burn, where most of the fibric layer and some of dead moss remains, the permafrost is not significantly impacted in spite of a decrease in surface albedo to less than half that of an undisturbed forest. The thermal conductivity of the soils is greatly increased by increases in soil moisture content. There appears to be a threshold of organic material remaining after a fire that determines the degree of influence of the wildfire on frozen grounds. This threshold value is a function of the thickness of the moss, thermal conductivity of moss, and thawing index at the ground surface.

In the case of severe fire, the active layer begins to increase immediately following the fire, but heat from the fire itself does not affect the active layer. Formation of talik depends on the thickness of the organic layer. Entirely removing an organic layer would very quickly initiate talik formation in this region. After a talik has formed, it is unlikely that the permafrost will recover under present climate condition. The impact of the wildfires may influence the permafrost on a more global scale as well. With increased global warming (increasing ground surface thawing index), fire frequencies and severities may increase. Since permafrost temperatures in Interior Alaska are at or near $0^{o}$C, the influence of wildfires may have a far-reaching impact on the landscapes, ecological impacts on the vegetation types, and enhanced feedback to global warming.

**Acknowledgments.** The authors are grateful to Tom Osterkamp (University of Alaska Fairbanks) for providing borehole temperature measurement equipment and a wealth of advice and information in support of this work. We also thank Nobuyoshi Ishikawa (Hokkaido University), Eric Kasischke (University of Maryland), Michelle Mack (University of California Irvine), Jennifer Harden (U.S. Geologic Survey), Shawna Laderach, Trevor White, Andrew Monaghan, and Jeremiah Drage (University of Alaska Fairbanks) for providing important suggestions and field assistance. Support for this research was provided by the U.S. National Science Foundation, Division of Environmental Biology, TECO program (DEB-9707461) and NSF LTER program (DEB-9211769) and the Japanese New Energy and Industrial Development Organization.

**Bibliography**

Andersland, O., and D. Anderson (Eds.) (1978), *Geotechnical Engineering for Cold Regions*, McGraw-Hill.

Atkins, T., R. Pangburn, R. Ates, and B. Brockett (1998), Soil moisture determination using capacitance probe methodology, *Special Report 98-2*, CRREL.

Bilskie, J. (1997), Using dielectric properties to measure soil water content, *Sensors*, pp. 26–32.

Brown, J. (1983), *The Role of Fire in Northern Circumpolar Ecosystems*, chap. Effects of fire on permafrost ground thermal regime, pp. 97–100, John Wiley.

Brown, J., and N. Grave (1979), Physical and thermal disturbance and protection of permafrost, *CRREL Report 79-5*.

Brown, J., W. Rickard, and D. Vietor (1969), The effect of disturbance on permafrost terrain, *Special Report 138*, CRREL.

Brown, J., O. Ferrians Jr., J. Heginbottom, and E. Melnikov (1997), Circum-Arctic map of permafrost and ground-ice conditions, *USGS Circum-Pacific Map Series CP-45*, U.S. Geological Survey.

Burn, C. (1992), *Periglacial Geomorphology*, chap. Recent ground warming inferred from the temperature in permafrost near Mayo, Yukon Territory, pp. 327–350, John Wiley.

Burn, C. (1998a), Field investigations of permafrost and climatic change in northwest North America, in *Proceedings of the Seventh International Conference on Permafrost*, vol. 57, edited by A. Lewkowicz and M. Allard, pp. 107–120.

Burn, C. (1998b), The response (1958-1997) of permafrost and near-surface ground temperatures to the forest fire, Takhini River Valley, southern Yukon Territory, *Canadian Journal of Earth Science*, *35*, 184–199.

Burwash, A. (1972), Thermal conductivity of peat, in *Preceedings 4th International Peat Congress*, International Peat Society.

Chambers, S., and F. Chapin III (1999), Fire effects on surface-atmosphere energy exchange in black spruce forests of interior Alaska, in *Proceedings of the 50th AAAS Arctic Science Conference*, American Association for the Advancement of Science.

Croft, A., and L. Monninger (1953), Evapotranspiration and other water losses on some aspen forest types in relation to water available for stream flow, *EOS Transactions of the American Geophysical Union*, *34*.

de Vries, D. (1974), *Heat and Mass Transfer in the Biosphere: Transfer Processes in Plant Environment*, chap. Heat transfer in soils, pp. 5–28, John Wiley.

DeBano, L. (2000), The role of fire and soil heating on water repellency in wildland environments: A review, *Journal of Hydrology*, *231-232*, 195–206.

Dyrness, C. (1982), Control of depth to permafrost and soil temperature by the forest floor in black spruce/feathermoss communities, *Research Note PNW-396*, USDA Forest Service, Pacific Northwest Forest and Range Experiment Station.

Dyrness, C., L. Viereck, and K. Van Cleve (1986), *Forest Ecosystems in the Alaskan Taiga*, chap. Fire in taiga communities of interior Alaska, pp. 74–86, Springer-Verlag.

Esch, D. (1982), Permafrost prethawing by surface modification, *Tech. Rep. FHWA-AK-RD-83-23*, USDT Highway Administration.

Farouki, O. (1981), Thermal properties of soils, *CRREL Monograph 81-1*, Amry Cold Regions Research and Engineering Laboratory.

Fastie, C. (2000), Fire history of the C4 and P6 basins of the Caribou-Poker Creeks Research Watershed, Alaska, in *FROSTFIRE Synthesis Workshop, The Role of Fire in the Boreal Forest and its Impacts on Climatic Processes*, no. 00.03 in INE/WERC Report, pp. 21–23.

Fastie, C., and D. Mann (1993), A preliminary fire history for the Caribou-Poker Creeks Research Watershed, Alaska, unpublished memorandum, 8 pp.

Haugen, R., C. Slaughter, K. Howe, and S. Dingman (1982), Hydrology and climatology of the Caribou-Poker Creeks Research Watershed, Alaska, *CRREL Report 82-26*, US Army Corps of Engineers Cold Regions Research and Engineering Laboratory.

Heginbottom, A. (1971), *Proceedings of a Seminar on the Permafrost Active Layer*, chap. Some effects of a forest fire on the permafrost active layer, pp. 31–36, Technical Memo 103, NRCC.

Hinkel, K., and S. Outcalt (1994), Identification of heat transfer processes during soil cooling, freezing, and thaw in central Alaska, *Permafrost and Periglacial Processes*, *5*, 217–235.

Hinzman, L., D. Kane, R. Gieck, and K. Everett (1991), Hydrologic and thermal properties of the active layer in the Alaskan Arctic, *Cold Regions Science and Technology*, *19*, 95–110.

Hinzman, L., K. Yoshikawa, V. Romanovsky, W. Bolton, and K. Petrone (2000), Effects of forest fires on surface hydrologic and thermal processes, in *FROSTFIRE Synthesis Workshop, The Role of Fire in the Boreal Forest and its Impacts on Climatic Processes*, no. 00.03 in INE/WERC Report.

Kane, D., K. Hinkel, D. Goering, L. Hinzman, and S. Outcalt (2001), Non-conductive heat transfer associated with frozen soils, *Global Plantary Change*, *29*.

Kasischke, E., and B. Stocks (2000), *Fire, Climate Change, and Carbon Cycling in the Boreal Forest*, Springer-Verlag.

Kasischke, E., N. French, K. O'Neill, D. Richter, L. Bourgeau-Chavez, and P. Harrell (2000), *Fire, Climate Change and Carbon Cycling in the Boreal Forest*, chap. Influence of fire on long-term patterns of forest succession in Alaskan boreal forests, pp. 214–238, Springer-Verlag.

Klock, G., and J. Helvey (1976), Soil-water trends following wildfire on the Entiat Experimental Forest, in *Annual Proceedings Tall Timbers Fire Ecologic Conference*, 15, pp. 193–200.

Kryuchkov, V. (1968), Soils of the far north should be conserved (in Russian), *Priroda*, *12*, 72–74, translated and reproduced in Brown et al., 1969.

Liang, L.-H., Y.-W. Zhou, and J. Wang (1991), Changes to the permafrost environment after forest fire, da xi'an ridge, Gu Lian mining area, China, *Permafrost and Periglacial Processes*, *2*, 253–257.

Lotspeich, F., E. Mueller, and P. Frey (1970), Effects of large scale forest fires on water quality in interior Alaska, *Tech. rep.*, US Dept. of Interior, Fed Water Pollu. Control Admin, Alaska Water Lab.

Lunardini, E. (1981), *Heat Transfer in Cold Climates*, Van Nostrand Reinhold.

MacKay, J. (1970), Disturbances to the tundra and forest tundra environment of the western Arctic, *Canadian Geotechnical Journal*, *7*, 420–432.

Moore, C., and J. Keeley (2000), Long-term hydrologic response of a forested catchment to prescribed fire, in *Proceedings Water Resources in Extreme Environments*, edited by D. Kane, pp. 37–42, American Water Resources Association, Anchorage, Alaska.

Osterkamp, T., and V. Romanovsky (1996), Characteristics of changing permafrost temperatures in the Alaskan Arctic, USA, *Arctic Alpine Research*, *28*(3), 267–273.

Osterkamp, T., and V. Romanovsky (1999), Evidence for warming and thawing of discontinuous permafrost in Alaska, *Permafrost and Periglacial Processes*, *10*, 17–37.

Osterkamp, T., L. Viereck, Y. Shur, M. Jorgenson, C. Racine, A. Doyle, and R. Boone (2000), Observations of thermokarst and its impact on boreal forests in Alaska, USA, *Arctic, Antarctic and Alpine Research*, *32*, 303 – 315.

Outcalt, S., F. Nelson, and K. Hinkel (1990), The zero-curtain effect: Heat and mass transfer across an isothermal region in freezing soil, *Water Resources Research*, *26*(7), 2509–2516.

Outcalt, S., K. Hinkel, and L. Miller (1997), *International Symposium on Physics, Chemistry, and Ecology of Seasonally Frozen Soils*, chap. Modeling the magnitude and time dependence of non-conductive heat-transfer effects in taiga and tundra soils, pp. 98–104, Cold Regions Research and Engineering Laboratory.

Péwé, T. (1975), Quaternary geology of Alaska, *Professional Paper 835*, U.S. Geological Survey.

Pritchett, W., and R. Fisher (1987), *Properties and Management of Forest Soils*, 2 ed., John Wiley.

Riseborough, D. (1990), Soil latent heat as a filter of the climate signal, in *Proceedings of the Fifth International Conference on Permafrost*, vol. 54, pp. 199–206.

Romanovsky, V., and T. Osterkamp (1995), Interannual variations of the thermal regime of the active layer and near surface permafrost in northern Alaska, *Permafrost and Periglacial Processes*, *6*, 313–335.

Romanovsky, V., and T. Osterkamp (2000), Effects of unfrozen water on heat and mass transport processes in the active layer and permafrost, *Permafrost and Periglacial Processes*, *11*, 219–239.

Romanovsky, V., T. Osterkamp, and N. Duxbury (1997), An evaluation of three numerical models used in simulations of the active layer and permafrost temperatures, *Cold Regions Science and Technology*, *26*, 195–203.

Rouse, W., and P. Mills (1977), A classification of fire effects on the microclimate of forest and tundra ecosystems, *Tech. Rep. R71-19/2*, Indian and North. Affairs, Ottawa.

Russell, H. (1935), Principals of heat flow in porous insulators, *J. Am. Ceram. Soc.*, *18*(1), 1–5.

Shiozawa, S., and G. Campbell (1990), Soil thermal conductivity, *Remote Sensing Review*, *5*, 301–310.

Soil Classification Working Group Staff (1998), *The Canadian System of Soil Classification*, 3 ed.

Tiedemann, A., C. Conrad, J. Dieterich, J. Hurnbeck, W. Megahan, L. Viereck, and D. Wade (1979), Effects of fire on water – a state-of-knowledge review, *General Technical Report WO-10*, U.S. Department of Agriculture Forest Service, 28 p.

Van Cleve, K., and L. Viereck (1983), A comparison of successional sequences following fire on permafrost-dominated and permafrost-free sites in Interior Alaska, in *Permafrost: Proceedings of the 4th International Conference*, pp. 1286–1291, National Academy Press.

Viereck, L. (1973), Ecological effects of river flooding and forest fires on permafrost in the taiga of Alaska, in *Permafrost: The North American Contribution to the 2nd International Conference*, pp. 60–67, National Academy of Science, Yakutsk, USSR.

Viereck, L. (1982), Effects of fire and firelines on active layer thickness and soil temperatures in Interior Alaska, in *Proceedings of the 4th Canadian Permafrost Conference*, pp. 123–134, Ottawa.

Wein, R. (1971), *Fire in the Northern Environment: A Symposium*, chap. Fire and resources in the subarctic-panel discussion, pp. 251–253, Pacific Northwest Forest and Range Experimental Station.

Woo, M. (1982), Flux of vapor from frozen materials in the high Arctic, *Cold Regions Science and Technology*, *5*, 269–274.

Yarie, J. (1981), Forest fire cycles and life tables: A case study from interior Alaska, *Canadian Journal of Forest Research*, *11*, 554–562.

Yoshikawa, K., L. Hinzman, N. Ishikawa, C. Collins, and V. Lunardini (1998), Air and ground temperature models at Caribou-Poker Creeks Research Watershed, in *Proceedings of the 49th AAAS Arctic Science Conference*, Fairbanks, Alaska.

Zierner, R. (1964), Summer evapotranspiration trends as related to time after logging of forests in Sierra Nevada, *Journal of Geophysical Research*, *69*, 615–620.